Fakultät für Medizin

Lehrstuhl für Molekulare Allergologie und Umweltforschung

The role of IL-22 in kidney disease and regeneration

Dr. med. Marc J. Weidenbusch

Vollständiger Abdruck der von der Fakultät für Medizin der Technischen Universität München zur Erlangung des akademischen Grades eines

Doctor of Philosophy (Ph.D.)

genehmigten Dissertation.

Vorsitzende/r: Prof. Dr. med. Jürgen Ruland

Betreuer/in: Prof. Dr. rer. nat. Carsten Schmidt-Weber

Prüfer der Dissertation:

1. Prof. Dr. med. Hans-Joachim Anders

2. Prof. Dr. med. Dirk Busch

Die Dissertation wurde am 20.08.2018 bei der Fakultät für Medizin der Technischen Universität München eingereicht und durch die Fakultät für Medizin am 12.09.2018 angenommen.

[9] Two *are* better than one,

Because they have a good reward for their labor.

[10] For if they fall, one will lift up his companion.

But woe to him *who is* alone when he falls,

For *he has* no one to help him up.

[11] Again, if two lie down together, they will keep warm;

But how can one be warm *alone?*

[12] Though one may be overpowered by another, two can withstand him.

And a threefold cord is not quickly broken.

Ecclesiastes 4:9-12 ***New King James Version (NKJV)***

The research presented in this thesis was performed between October 2014 and August 2018.

Publications from this work:

Weidenbusch M, Rodler S, Song S, Romoli S, Marschner JA, Kraft F, Holderied A, Kumar S, Mulay SR, Honarpisheh M, Kumar Devarapu S, Lech M, Anders HJ. Gene expression profiling of the Notch-AhR-IL22 axis at homeostasis and in response to tissue injury. Biosci Rep. 2017 Dec 22;37(6). pii: BSR20170099.

Weidenbusch M, Song S, Iwakura T, Shi C, Rodler S, Kobold S, Mulay SR, Honarpisheh M, Anders HJ. IL-22 sustains epithelial integrity in progressive kidney remodeling and fibrosis. Physiological Reports 2018 (6):15,e 13817.

Table of contents

List of Figures and tables

1 Introduction

1.1 Kidney disease

1.1.1 Definition und global burden

Kidney disease, i.e. the objective measure of kidney damage and/or function, is a global health burden [1]. Available data from different country show both a considerably high morbidity of chronic, i.e. irreversible kidney disease (Germany: 25,6%, [2], Ireland: 18,6% [2], Italy: 9,6% [2], Netherlands: 7,6% [2], Norway: 6,3% [2], Spain: 15,2% [2], USA: 10% of the adult population ([3]), as well as significant health-care cost (Germany: 3 billion EUR/year [4]), UK: 1.5 billion GBP/year [5], USA: 60 billion USD/year [6]. Importantly, the pathogenesis of kidney disease is manifold, so there exist various ways to categorize it. For this work, two axes of distinction are important: a) the spatial axis (i.e. glomerular vs. tubular kidney disease, see Fig. 1a) and b) the temporal axis (i.e. acute kidney injury, AKI, vs. chronic kidney disease, CKD, see Fig. 1b). Of note, these distinctions mainly serve educational purposes, as in reality substantial overlap between the poles on each axis exist: every primary glomerular kidney disease induces secondary tubular injury (and vice versa) and equally, there is a complex interplay between AKI and CKD, leading to clinical entities such as acute-on-chronic [7] as wells as chronic-on-acute kidney injury [8],[9]. Nevertheless, those categories are used both for diagnostic as well as therapeutic purposes and hence will be briefly introduced here.

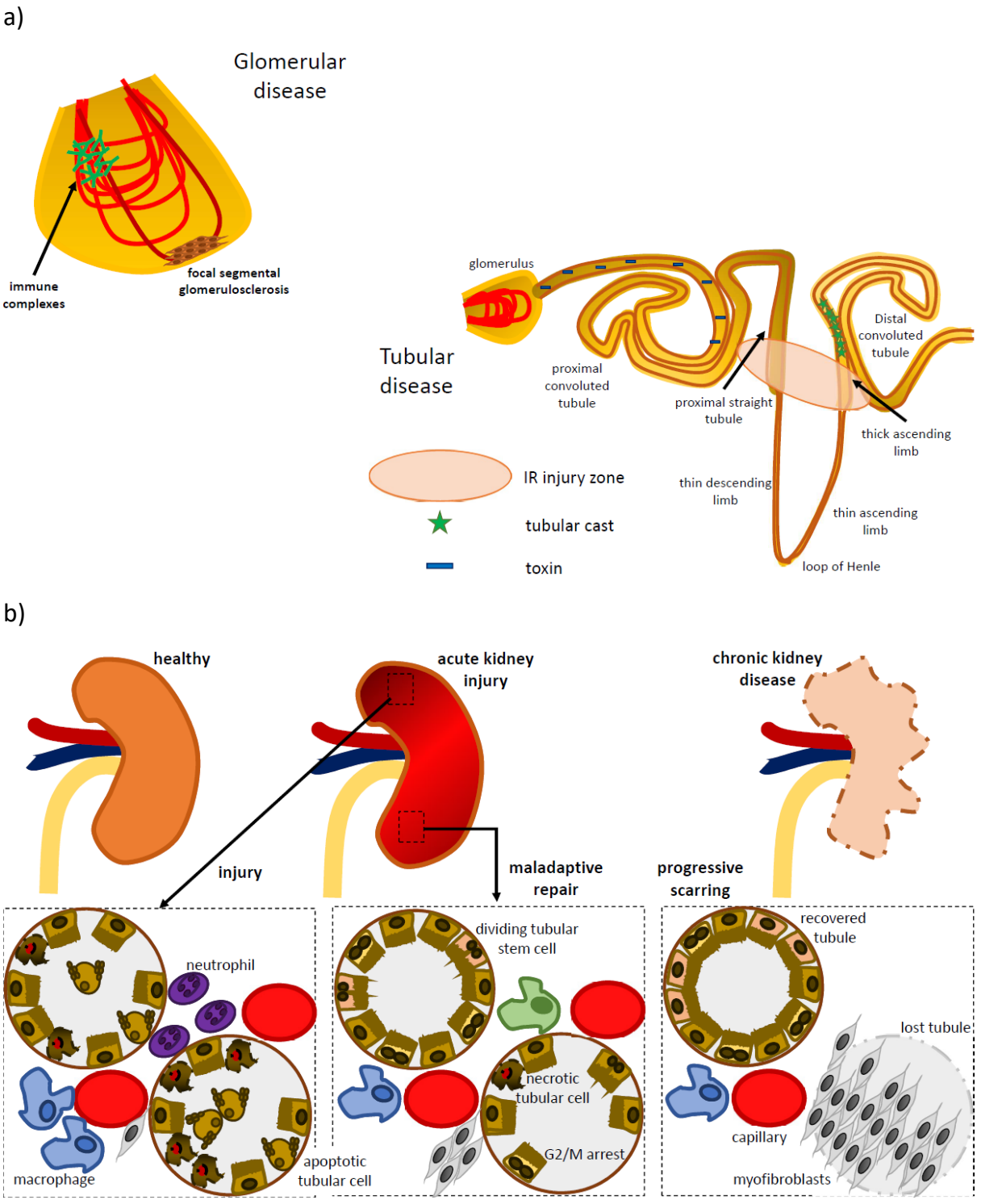

Figure 1-1 Schematic of mechanisms in kidney disease (modified from [10] and [11]).

a) mechanisms of glomerular vs. tubular injury. Immune complexes containing immunoglobulins (green,) or parietal epithelial cell proliferation (brown) cause glomerular injury (left side of the panel), while casts, toxins or ischemia-reperfusion (IR) cause tubular injury (right side of the panel). b) mechanisms of acute vs. chronic injury. Upon acute injury, inflammation and cell death occur. This injury phase is followed by a repair phase which sometimes recovers injured parts of the kidney, but often maladaptive repair processes lead to tubular atrophy, interstitial fibrosis and progressive scarring.

1.1.2 Acute kidney injury (AKI)

According to AKIN [12], AKI is defined by either an increase of the serum creatinine concentration by 0.3mg/dl or more within 48 hours or an urine excretion of less than 0.5ml/kg body weight/hr for more than six hours. The AKIN classification also grades the severity according to the absolute changes in the parameters stated above (also see Tab. 1-2). Creatinine is a muscle degradation product, which is supposed to be stably excreted by the muscles, freely filtered by the kidney and neither tubularly secreted nor absorbed, hence making it an "ideal" solute to estimate the glomerular filtration rate, GFR, i.e. the amount of fluid filtered by the kidney per time [13]. This filtrate, called primary urine, passes through the tubule apparatus (see Fig. 1a), where secretion as well as absorption of water and certain solutes occurs to meet the current needs of the body. The net product of these processes along the tubule leads to a given composition (concentrated vs. dilute) and amount of secondary urine.

Table 1-2 AKIN classification of acute kidney injury (aus [12])

Stage	Serum creatinine criteria	Urine output criteria
1	Increase in serum creatinine of more than or equal to 0.3 mg/dl (≥ 26.4 µmol/l) or increase to more than or equal to 150% to 200% (1.5- to 2-fold) from baseline	<0.5ml/kg/hr for > 6 hours
2	Increase in serum creatinine to more than 200% to 300% (> 2- to 3-fold) from baseline	<0.5ml/kg/hr for >12 hours
3	Increase in serum creatinine to more than 300% (> 3-fold) from baseline (or serum creatinine of more than or equal to 4.0 mg/dl [≥ 354 µmol/l] with an acute increase of at	<0.3 ml/kg/hr for > 24 hours or anuria for 12 hours

least 0.5 mg/dl [44 µmol/l])

The AKIN definition therefore focusses on an acute decrease in GFR, which is a functional parameter. Apart from the limitations of GFR estimation based on serum concentrations of solutes such as creatinine (or others such as cystatin-c [14]) rather than actually measuring GFR, AKI in many cases involves many pathogenic events before an actual GFR drop, which is a rather late event in AKI development [1]. A new development in the field of AKI therefore is the advent of biomarkers of actual kidney injury (as opposed to markers of kidney function) [15]. Especially two markers, namely IGFBP-7 and TIMP-2, deserve special attention, as their measurement (marketed as NEPHROCHEK®) has been approved by the FDA for diagnosing AKI in the intensive care setting [16]. Despite these advances in diagnosing AKI earlier in the course of disease, therapeutic options continue to be limited. The current guideline [17] emphasizes sufficient volume administration to AKI patients and the avoidance of additional nephrotoxic substances (such as aminoglycoside antibiotics), but does not list a single targeted intervention for treating AKI. Given the insight into the common pathogenetic factors in AKI (see Fig. 1b) research into possible pharmacological AKI interventions focusses mainly on three fields: a) immunomodulation, as AKI is associated with a substantial immune activation [18], b) cell death, as recently the pharmacological inhibition of programmed, non-apoptotic cell death routines have been shown to result in the amelioration of various mouse models of AKI [19], c) kidney regeneration, as it has become apparent that there is a renal stem cell niche [20] and these cells have an, albeit limited, capacity to regenerate glomerular and tubular structures upon damage [21]. Interestingly, these three fields seem to be heavily interconnected, as, for example, immune cells have the capacity to both induce cell death [22] (also see below) as well as regeneration [23].

1.1.3 Chronic kidney disease (CKD)

Chronic kidney disease, i.e. the irreversible loss of kidney function, is currently defined by the international non-profit foundation “Kidney Disease: Improving Global Outcomes” (KDIGO) in their guideline on CKD, initially published 2004 [24] and last updated 2013 :as follows. “CKD is defined as abnormalities of kidney structure or function, present for 3 months, with implications for health”. This very broad definition, which specifically emphasizes on the temporal aspect (3 months, hence separating CKD from AKI), is specified by either markers of kidney damage (see Tab. 2) or a decreased GFR below 60ml/min/1,73m² body surface. Once CKD is diagnosed, it can be classified according to the “CGA” system: cause, GFR category, and albumin category (see Tab. 2 for details). The importance of a detailed classification of CKD is outlined by the great difference in risks of major complications of CKD dependent on CKD stage; e.g. the relative risk of all-cause mortality per year for a patient with CKD-G5A3 is 6.6 (!), 1.3 for CKD-G3aA1 and 1.0 (hence unchanged compared to healthy individuals) for CKD-G2A1. As outlined above in the AKI section, also the CKD classification relies on the filtration function of the kidney, albeit with two important differences: 1. In addition to GFR, albuminuria and hence a marker of glomerular basement membrane (GBM) tightness/functionality is included, therefore allowing an early diagnosis of GBM malfunction before an actual GFR decline (which occurs later during disease, as outlined above); 2. CKD can be diagnosed in the absence of both GFR decline and albuminuria, e.g. after kidney transplantation. This definition takes into account that even a healthy kidney of a living donor undergoes ischemia-reperfusion injury during transplantation, so the majority of transplant biopsies show histopathological abnormalities even with a GFR > 60ml/min/1.73m² [24].

Table 1-3 Definition and classification of chronic kidney disease ([24])

Criteria for CKD (either of the following present for > 3 months)

Markers of kidney damage (one or more)	Albuminuria (AER > 30 mg/24 hours; ACR >30 mg/g [>3 mg/mmol]) Urine sediment abnormalities Electrolyte and other abnormalities due to tubular disorders Abnormalities detected by histology Structural abnormalities detected by imaging History of kidney transplantation
Decreased GFR	GFR < 60 ml/min/1.73 m²

C: Cause of CKD:

Assign cause of CKD based on presence or absence of systemic disease and the location within the kidney of observed or presumed pathologic-anatomic findings.

G: GFR categories in CKD

GFR category	GFR (ml/min/1.73 m²)	Terms
G1	=> 90	Normal or high
G2	60-89	Mildly decreased*
G3a	45-59	Mildly to moderately decreased
G3b	30-44	Moderately to severely decreased
G4	15-29	Severely decreased
G5	<15	Kidney failure

A: Albuminuria categories in CKD

Category	ACR (mg Albumin / g Creatinine)	Terms
A1	< 30	Normal to mildly increased
A2	30-300	Moderately increased
A3	> 300	Severely increased

In addition to the filtration function the kidney plays an important role in a variety of other physiologically relevant processes in the body, so the presence of CKD has an impact on a

variety of other organs[1]: endothelial damage in all vessel through reno-parenchymatous hypertension, osteoporosis and increased vascular calcification (i.e. arteriosclerosis) through defective 1α-hydroxylation of 25-hydroxyvitamin D3 and consecutive secondary hyperparathyroidism, anemia through an insufficiency of renal erythropoietin production, and acidosis through insufficient renal bicarbonate production. While the management of CKD and even its most severe form, end-stage renal disease (ESRD), is far advanced through the possibility of renal replacement therapy (RRT) such as hemodialysis, peritoneal dialysis and renal transplantation, as well as through management of the aforementioned multi-system complications (e.g. blood pressure control, administration of recombinant erythropoietin and active 1alpha,25-dihydroxyvitamin D3)[25], once a GFR decline has occurred during CKD development, “downstaging” of the GFR category is currently impossible. This effect is at least partly due to the fact that after nephron loss (either during AKI episodes or due to a progressive underlying kidney disease) the space of lost tubules is taken by mesenchymal cells and extracellular matrix, leading to the common histopathological finding of both tubular atrophy and interstitial fibrosis (IF/TA) in biopsies of CKD patients; interestingly, despite the plethora of underlying causes for CKD (e.g. genetic, autoimmune, metabolic, paraneoplastic diseases), the finding of IF/TA in all CKD patients is in line with at least a common pathway towards the end of CKD development, opening an avenue for possible common therapeutic interventions in later stage all-cause CKD (beyond earlier AKI damage control and consequent treatment of the underlying cause of CKD). Driven by the prominent finding of IF/TA in CKD, research in the CKD therapy area has so far focus mainly on two principles: fostering epithelial repair/regeneration on the one hand, inhibiting/reversing interstitial fibrosis on the other [26]. Despite major efforts to develop anti-fibrotic treatments for clinical use, no such agent has been approved until

today [27]. Conversely, there have been recent advances in the field of kidney regeneration, again showing an important role of immune cells, namely macrophages [28-30]

1.1.4 Mouse models of AKI and CKD

1.1.4.1 Ischemia-reperfusion injury (IRI)

IRI is the prototypic injury occurring on solid organ transplantation [31]. As there is an organ shortage for kidney transplantation, characterizing the pathophysiology of IRI during renal transplantation is paramount [32] .The IRI model of AKI induces damage specifically to the S3 segment of the proximal tubule. The mechanism involves intrinsic tubule cell damage [33] as well as a marked immunopathology [34]. The intrinsic damage in tubule cells is mediated by a succinate accumulation during ischemia, which leads to exaggerated ROS production upon reperfusion through respiratory-chain electron transfer reversal [35] and subsequent cell injury and death, e.g. by ferroptosis [19]. This tubular cell death acts as a "danger signal", hence activating the immune system, a phenomenon dubbed "necroinflammation" [36]. As the immune activation leads to more immune-mediated cell death, a deleterious amplification loops ensues [37], with the maximum of neutrophil influx between 6 and 12 hours of reperfusion [38] and the maximal injury around 24 hrs [31], followed by a regeneration phase that lasts up to 3 weeks [29]. In contrast to the deleterious roles, immune cells also play an important role in the resolution of inflammation and the induction of epithelial regeneration (as outlined above)[23].

1.1.4.2 Acute oxalate crystallopathy (AOC)

Based on the clinical finding that acute events, such as ethylene glycol poisoning, can lead to acute oxalate crystal mediated kidney injury [39], a mouse model of AKI by acute calcium-oxalate supersaturation was developed [40]. Upon administration of a single high dose of sodium oxalate, calcium oxalate crystals are formed in vivo and lead to cast formation along

the entire tubule system, therefore causing obstruction of the tubule and inflammation [40]. The injury peaks 24hrs after oxalate injection [40], followed by a regeneration phase of several days. As with other crystallopathies [22], the inflammatory response to calcium oxalate is driven mainly by NLRP3-mediated IL-1β secretion [40], but calcium oxalate crystals also directly induce tubular cell death in the form of necroptosis [41].

1.1.4.3 Chronic oxalate crystallopathy (COC)

Primary hyperoxaluria is human disease characterized by urolithiasis and nephrocalcinosis, as well as ocular and vascular calcifications [42]. As affected patients develop ESRD in their young adulthood [43], a mouse model of chronic oxalate overload was to developed [44] to mimic the human disease. Indeed, mice on an oxalate-rich, calcium-free diet develop CKD after around 2 weeks of feeding and reach ESRD by 3 weeks of diet [45]. While the NLRP3-inflammasome is also crucially involved in the pathogenesis of the model [44], the disease development is independent of IL-1β [30], suggesting a non-canonical role of NLRP3 in this context. Indeed, blockage of TGF-β, a known mediator of non-canonical NLRP3 signaling [46], ameliorated the nephrocalcinosis-related CKD phenotype in mice [47]. As in AKI, macrophages play an important role also in COC [30].

1.1.4.4 Unilateral ureteral obstruction (UUO)

In contrast to the aforementioned, intra-renal models of injury, the UUO model induces renal injury by a post-renal problem, namely the total obstruction of a ureter. The ensuing congestion of urine before the obstruction eventually jams up through the proximal ureter, renal pelvis, renal collecting ducts and tubules into the glomerulum, causing a total shutdown of glomerular filtration in the affected kidney [48]. Additionally, the increased intratubular hydrostatic pressure leads to decreased peritubular capillary perfusion and

subsequent hypoxia, producing the IF/TA phenotype of CKD [49]. This CKD phenotype is reached rather soon after 10d [50], with early pathological changes of immune cell influx and activation as well as changes in collage synthesis being detectable 2d upon obstruction. Interestingly, when obstruction is reversed after IF/TA induction, progression of the CKD phenotype is stopped [51], but tubular repair does not occur before 6 weeks of regeneration[50].

1.1.4.5 Diabetic nephropathy (DN)

Kidney disease in diabetes in mouse and man is a direct consequence of hyperglycemia. The elevated blood glucose concentrations injure the kidney at least by two distinct mechanisms: a) a non-enzymatic glycation of glomerular basement membrane (GBM) proteins, creating so called “advanced glycation end-products” (AGEs), which in turn activate podocytes, mesangial cells and infiltrating immune cells through ligation of the receptor for AGE (RAGE), leading to pro-inflammatory gene expression [52], [53]. During the course of DN, virtually all glomerular cells begin to express RAGE 8559486, amplifying the inflammatory response and ultimately causing the histopathological correlate of DN, nodular glomerulosclerosis [54]. b) As glucose is freely filtered in the glomerulum, increased blood glucose concentrations are translated 1:1 to increased glucose concentrations in the primary urine. As an important nutrient, filtered glucose is then reabsorbed along the proximal tubule, a process that involves sodium-glucose-cotransporters (e.g. SGLT2) [55]. With increased glucose concentration and reabsorption, this mechanisms causes an inadequate sodium retention (causing hypertension), [56] as well as glomerular hyperfiltration through altered sodium concentrations at the macula densa [57]. Given the latter mechanism, DN development in the mouse model is greatly increased by early

uninephrectomy [58], rendering the remaining nephrons especially sensitive to hyperfiltration and establishing DN at 24wks of age. This is further corroborated by the finding that SGLT2 inhibition slows progression of DN both in mice [59] and humans [60].

1.1.4.6 Lupus nephritis (LN)

While human systemic lupus erythematosus (SLE) and its renal manifestation, LN, is a genetically heterogeneous and in most cases polygenic disease [61], one of the most commonly used mouse models of LN, the MRL-Fas^{lpr} model, exploits a spontaneous mutation ("lymphoproliferation", thus lpr) that first occurred in the Jackson Laboratories [62]: the mutation was later mapped to the death receptor Fas/CD95 [63], linking cell death regulation to lupus pathogenesis. In MRL-Fas^{lpr} mice, the defect in apoptosis induction conferred by the lpr mutation [64] leads to dramatic polyclonal lymphoproliferation with diffuse lymphadenopathy, [62] secondary necrosis in lymphoid organs, autoimmunization with autoantibody production [65] and SLE development including LN starting at 12wks of age. While the later stage pathogenic events specifically involve adaptive immune cells [66], the early events in lupus pathogenesis also involve the innate immune system [67].

1.1.4.7 Anti-GBM disease (aGBM)

The human anti-GBM disease (also called "Goodpasture syndrome") is recapitulated in the mouse by the injection of polyclonal antibodies directed against GBM antigens [68]. Importantly, the model can be induced both acutely by a single large dose of anti-GBM antibodies leading to crescentic glomerulonephritis (referred to as the heterologous model) and subacutely by repetitive small dose aGBM antibodies, which induce secondary antibodies and therefore leading to immune complex glomerulonephritis (referred to as the autologous model). [69] In the heterologous model injury peaks at 24 hrs after antibody

injection with following regeneration for 7 days [70], while in the autologous model immunization can be performed over a time course of 4 weeks with increasing disease activity over the following three months [71] or in a shortened protocol of immunization 3 d prior to aGBM antibody injection and readout after 14 d [72]. The pathogenesis in the aGBM involves NLRP3, extracellular histones as well as neutrophil extracellular traps [70].

1.1.4.8 Adriamycin-induced focal segmental glomerulosclerosis (FSGS)

Human focal segmental glomerulosclerosis (FSGS) is a etiopathologically heterogeneous group of diseases sharing a histological (terminal) phenotype [73]. Some forms of FSGS are steroid-responsive and tend to recur after kidney transplantation, hence are considered to have a strong autoimmune component [74]. Conversely, it is now known that many cases of (steroid-resistant) FSGS are caused by genetic lesions, specifically by gene mutations in podocyte-expressed structural proteins [75]. The heterogeneity in human FSGS can be mirrored by the use of several different mouse models, each of them differentially involving either the autoimmune or the genetic components of FSGS [76]. In this regard, the model of adriamycin nephropathy in rodents [77] has minimal immune-mediated pathology and therefore is operational also in heavily immunocompromised animals [78]. Interestingly, SCID mice are even more susceptible to Adriamycin nephropathy and this finding is pheno-copied by the depletion of CD4+ T cells [79], suggesting a protective role of the adaptive immune system in adriamycin nephropathy. In Balb/c mice, 1-2 weeks after a single injection of adriamycin (also referred to as doxorubicin), a FSGS phenotype of proteinuria, glomerular endothelial thinning and podocyte loss is induced [80].

1.2 Interleukin-22 biology

The biology of IL-22 with special regard has been extensively reviewed [81] [82], [83], [84] and will be briefly outlined below.

1.2.1 IL-22

IL-22 is a member of the IL-10 cytokine family sharing a basic intron/exon structure of usually five coding exons as well as common structural features [85]. These common structures share about 13- 25% of amino acids and contain six to seven anti-parallel arranged α-helices [86]. The human, rat and mouse IL-22 genes are located on chromosomes 12, 7 and 10, respectively, spanning around 5 kilobases, the mouse gene containing an additional 6^{th} exon. [87]. Despite differences in gene size, both mouse and human secreted IL-22 has a length of 146 amino acids and a 79% sequence homology [88]. After cleavage of a 33 amino acid signal peptide, the apparent size of mature, monomeric IL-22 is about 17 kDa. A special feature of IL-22 is the distribution of secreting and receptor expressing cells: while except for paraneoplastic expression IL-22 is only secreted by immune cells [89], the IL22-receptor (IL22R) is expressed by epithelial cells in different tissues throughout the body [90]. These expression patterns create a unidirectional, immune-epithelial signaling interface. By means of this interface, IL-22 producing cells, such as group 3 innate like lymphocytes (ILC3s) [91], monocytes (Mo), dendritic cells (DCs) and macrophages (MΦ) [92, 93] and T-helper cells with a Th17- or Th22 polarization [94] can activate epithelial cells upon sensing of specific microenvironmental factors. These factors include both endogenous (e.g. kynurenins) [95] or exogenous (e.g. dioxine) [96] ligands (both mediated by the transcription factors aryl hydrocarbon receptor (Ahr) [97]), other cytokines (e.g. IL-23 [98]) or “danger-associated molecular patterns” (DAMPs) (e.g. through

the activation of Toll-like receptors (e.g. TLR4) [99]). Interestingly, Ahr-dependent IL-22 induction by endogenous ligands has been shown to occur in a Notch-dependent manner [100] and mediated by Notch target genes [101], establishing a Notch/Ahr/IL22 signaling axis *in vivo* [102].

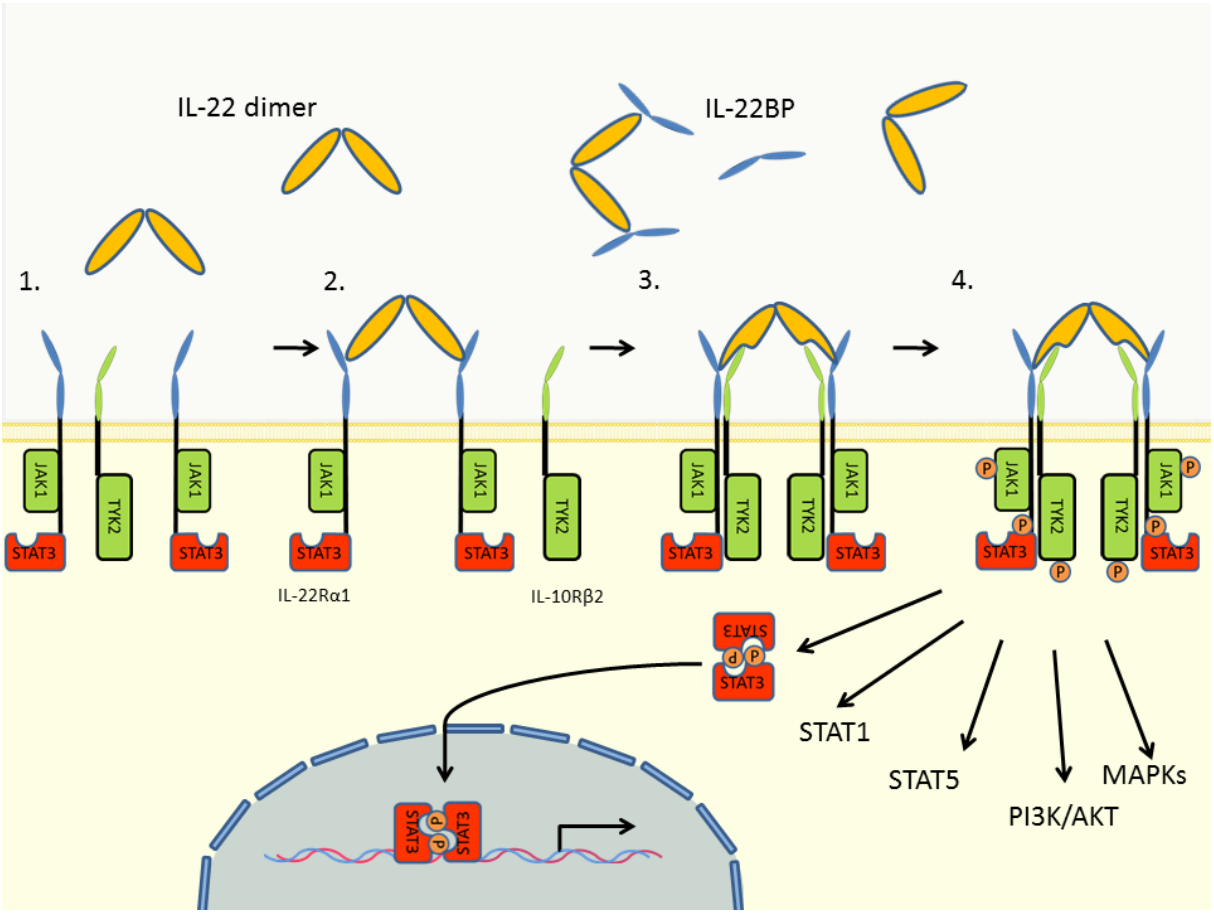

Figure 1-4 Schematic of IL-22 biology (from [81]).

IL-22 activates cellular responses via its heterodimeric receptor consisting of the IL-22RA1 chain mostly expressed in epithelial cells and the ubiquitously expressed IL-10R2 chain. In the steady state, IL-22RA1 and IL-10Rbeta2 are associated with their corresponding tyrosine kinases JAK1 and TYK2, respectively (1). Native IL-22 binds to IL-22RA1 with high affinity (KD ranging from 1 to <20 nM) (2.). The conformational change in IL-22 after binding to the IL-22RA1 chain leads to a significantly higher affinity towards IL-10Rbeta2 (3.). Upon ternary complex formation, JAK1 and tyrosine kinase 2 (TYK2) phosphorylate STAT3 as well as STAT1 and STAT5. Additionally, MAPKs and the phosphoinositide 3-kinase (PI3K)/Akt pathway are activated as well (4.). Dimerized phosphoSTAT3 can then translocate to the nucleus to activate IL-22-induced STAT3-dependent gene expression. Under steady-state conditions, IL-22 bonding protein (BP), the soluble receptor of IL-22, inhibits effects of IL-22.

1.2.2 IL-22 receptor

The functional IL22R is a heterodimer, made of one IL-10Rβ2 and one IL22Rα1 chain, respectively [103]. Common to other heterodimeric type II cytokine receptors, the IL22R undergoes ternary complex formation upon IL-22 binding [81]. The tissue- specificity of IL22R expression in conferred by limited IL22Rα1 expression [89], while IL-10Rβ2 is expressed by a wide array of cells and tissues [104]**.** Upon cytokine binding, the IL22R recruits the tyrosine kinases Jak1 and Tyk2 via its intracellular signaling domains [105], leading to the phosphorylation of STAT proteins (Figure 2). This is followed by nuclear translocation of STAT and a gene expression response in the target cell [106]. Alternative downstream signaling mediators have been identified, including Akt, MAPK [107] , mTOR and PI3K [108]. Upon STAT activation, two signaling feedback loops have been proposed: a positive loop involving STAT3-dependent IL-20 expression [109], which can, albeit with a reduced affinity, directly bind and ligate the IL22R [104]; and a negative loop involving STAT3-driven miRNA-197 expression, which in turn downregulated IL22R [110]. In addition to these feedback loops, IL22 signaling is further refined by the modulation through a soluble IL22-decoy receptor, also referred to as the IL-22 binding protein (IL-22BP) [111]. IL-22BP is coded for by an own gene, IL22RA2 in humans [112] and mice [113]. IL-22BP is normally secreted by DCs [114], but this process is inhibited by NLRP3 activation [115]. While this regulatory loop enables maximal IL-22 effects during tissue injury-mediated inflammasome activation, insufficient IL-22BP concentrations are also shown to cause chronic inflammation-mediated colon cancer in mice [115].

1.2.3 Functions of IL-22

IL-22 signaling leads to several events in the target cell (also recently rev. in [116] [81]): a) barrier function reinforcement through upregulation of S100 proteins [117], mucins [118], and defensins [119]; b) cell-death blockade by upregulation of reg genes [120] and anti-apoptotic Bcl-2 and Bcl-X_L, [121] combined with downregulation of proapoptotic Bax and Bad [122]; c) cell proliferation via RBL2, cyclin D1 and CDKN4 [123], and the PI3K/Akt/mTOR pathway [108] ; d) elicitation of an acute phase reaction in the liver [124]; e) attraction of immune cells via chemokines[125] [126] [127]. These response patterns are fine-tuned through the balance of downstream effector activation (e.g. MAPK vs. PI3K/Akt/mTor/ vs. STAT pathway activation) 25740595 and additional regulators such as and SirT1- [128] and SOCS1/3- [129, 130] mediated STAT3 inhibition or proteasomal receptor degradation controlled by GSK-3β-phosphorylation of IL22Rα1 [131].

1.2.4 Interleukin-22 in kidney disease

As the IL22R is expressed in the kidney [90], [103] and given the aforementioned effects of IL-22, a role of IL-22 in kidney disease seems plausible. Available evidence indeed suggests that IL-22 plays an important protective role in acute kidney injury: Xu et al. [122] could show that IL-22 specifically protects proximal tubular epithelial cells upon renal ischemia reperfusion injury and that this mechanism is mediated by STAT3 and Akt phosphorylation, increased anti-apoptotic Bcl-2 expression, downregulation of pro-apoptotic factors such as Bad, and ultimately increased tubular cell survival. These effects, which were achieved through a viral-driven transgenic IL-22 overexpression, proved to be significant not only in respect to reduced histopathologic lesions in the affected kidney, but also significantly reduced serum retention parameters as well as increase overall survival of mice post-IRI.

[122] These findings were confirmed independently by another group [92], that showed similar results by the use of recombinant IL-22 injections, accompanied by data on a disease aggravation through antibody blockade of IL-22 as well as genetic deficiency. In addition to those finding, Kulkarni et al. pinpointed DCs and macrophages as the source of endogenous IL-22 secretion during renal IRI and showed that TLR4 ligation in those cells, presumably through HMGB1 or other DAMPs occurring post-IRI. While the effects of IL-22 in the setting of renal IRI hence are described, there is little evidence on the role of IL-22 in other models of acute kidney injury or chronic kidney disease.

1.3 Aims and hypotheses

1.3.1 Aims of the thesis project

As it had been shown that IL-22 plays an important protective role in acute ischemic injury, we were interested in defining the role of IL-22 in other acute models of kidney injury as well as models of chronic kidney disease. To this end we characterized the gene expression of the Notch/AhR/IL-22 axis in the AOC, COC, UUO, DN, LN, aGBM and FSGS model, respectively.

Next, we compared the gene expression patterns observed in the mouse models with the Notch/AhR/IL-22 axis gene expression in corresponding human kidney diseases to determine the relevance of findings in mouse model for actual human disease settings.

To further explore an active role of IL-22 in these models beyond a mere association with AKI and ensuing CKD, we finally used IL22 knock-out mice in the AOC and UUO model and

characterized their phenotype along with cell culture experiments to identify the underlying mechanisms of IL-22 effects on disease development.

1.3.2 Hypotheses

We hypothesized that

1. IL-22, as well as its upstream regulators from the Notch and AhR signaling pathways, were differentially expressed during the induction of ischemia-reperfusion injury, acute and chronic oxalate crystallopathy, unilateral ureteral obstruction as well as diabetic nephropathy, lupus nephritis, anti-GBM disease, and adriamycin-induced focal segmental glomerulosclerosis.

2. the observed patterns of Notch/AhR/IL-22 axis gene expression correlate with the respective gene expression found in corresponding human kidney disease.

3. IL-22 exerts an active protective role during acute kidney injury as well as chronic kidney disease development rather than only being a biomarker for disease activity.

    a) IL-22 functions as a survival factor for renal tubular epithelial cells, ameliorating acute tubular cell death and subsequent tubular atrophy

b) IL-22 functions as a regeneration-promoting factor on tubular cells or renal progenitor cells, reinstituting tubular cell function after injury and avoiding secondary healing responses, i.e. fibrosis

2 Material and methods

2.1 Material

2.1.1 Animal experiments

2.1.1.1 Animals

IL22-/- BALB/cJ	Genentech, Inc., South San Francisco, CA, USA
BALB/cByJ	Charles River, Sulzfeld, Germany
C57/BL6/N	Charles River, Sulzfeld, Germany
C57BLKS/J	Jackson Laboratories, Bar Harbor, ME, USA
C57BLKS/J-Leprdb	Jackson Laboratories, Bar Harbor, ME, USA
MRL-Faslpr	Harlan Winkelmann, Borchen, Germany

2.1.1.2 Housing

Makrolone cages type 2	Techniplast, Hamburg, Germany
Standard chow	Sniff Spezialdiäten, Soest, Germany
rCOC diet (50 µmol/g sodium oxalate, calcium free)	Sniff Spezialdiäten, Soest, Germany
Bedding	Zoonlab, Castrop-Rauxel, Germany
Nestlets	Zoonlab, Castrop-Rauxel, Germany
Polycarbonate retreats	Zoonlab, Castrop-Rauxel, Germany

2.1.1.3 Genotyping

Proteinase K (20mg/ml)	Merck, Darmstadt, Germany
Gelatine	Sigma-Aldrich, München, Germany
Potassium chloride	Merck, Darmstadt, Germany
Magnesium chloride	Merck, Darmstadt, Germany
NP40	Fluka/Sigma, München, Germany
Tris-HCl	Roth, Karlsruhe, Germany
Tween-20	Fluka/Sigma, München, Germany
10x-PE-buffer (Thermopol buffer)	New England BioLabs, Frankfurt, Germany
Taq-DNA-Polymerase	New England BioLabs, Frankfurt, Germany

1,25mM dNTP	Fermentas, St. Leon-Rot, Germany
Agarose powder	Invitrogen, Karlsruhe, Germany
Ethidium bromide (10 mg/ml)	Fluka/Sigma, München, Germany
Xylene cyanol	Roth, Karlsruhe, Germany
Bromophenol blue	Roth, Karlsruhe, Germany
Glycerine	Roth, Karlsruhe, Germany
Boric acid	Fluka/Sigma, München, Germany
Tris	Roth, Karlsruhe, Germany
DNA-ladder (small fragments)	Fermentas, St. Leon-Rot, Germany
IL22 genotyping primer	Metabion, München, Germany

2.1.1.4 Narcosis, surgical procedures, injectables

100 Series Vaporizer for Forene	Smiths Medical PM, Inc.,Norwell, USA
Isofluran Forene®	Abbott, Wiesbaden, Germany
Midazolam	Ratiopharm GmbH, Ulm, Germany
Fentanyl	Janssen Janssen-Cilag, Neuss, Germany
Dorbene vet.	Pfizer GmbH, Berlin, Germany
Flumazenil	Hameln pharma plus GmbH, Hameln, Germany
Naloxon	Inresa Arzneimittel GmbH, Freiburg, Germany
Revertor	CP-Pharma GmbH, Burgdorf, Germany
Buprenorphin	Bayer, Wuppertal, Germany
Acutenaculum	Medicon, Tuttlingen, Germany
Anatomical forceps	Medicon, Tuttlingen, Germany
Aneurysm Clip	Medicon, Tuttlingen, Germany
Clip Applying Forceps	Medicon, Tuttlingen, Germany
Scissors	Medicon, Tuttlingen, Germany
Surgical forceps	Medicon, Tuttlingen, Germany
Scalpel	pfm medical ag, Köln, Germany
Temperature control unit HB 101/2	Panlab Bioresearch, Barcelona, Spain
Coated Vicryl, PS-2 19 mm, Mersilene 4-0, Ethibond 5-0	Ethicon, Johnson & Johnson Medical GmbH, Norderstedt, Germany
Doxorubicin hydrochloride	Pharmacia&Upjohn, Erlangen, Germany

PTX-001 sheep anti-rat GBM serum	Probetex Inc., San Antonio, TX, USA
Sodium oxalate	Merck, Darmstadt, Germany

2.1.1.5 Blood drawing

Blaubrand® micropipettes 20µl	Brand, Wertheim, Germany
Eppendorf tubes 1,5 ml	TPP, Trasadingen, Switzerland
EDTA	Biochrom KG, Berlin, Germany

2.1.1.6 Organ removal

RNAlater®	life Technologies, Darmstadt, Germany
Histo casettes	NeoLab, Heidelberg, Germany
Shandon® Formal-Fixx	Thermo Fisher Scientific, Waltham, MA, USA

2.1.2 Serum chemistry tests

Creatinine FS kit	DiaSys Diagnostic Systems, Holzheim, Germany
BUN FS kit	DiaSys Diagnostic Systems, Holzheim, Germany
Murine albumin-ELISA-Set	Bethyl Laboratories, Montgomery, TX, USA

2.1.3 Histological analyses

Paraffin	Merck, Darmstadt, Germany
Ammonium persulfate (APS)	Bio-Rad, München, Germany
Xylol	Merck, Darmstadt, Germany
Ethanol	Merck, Darmstadt, Germany
Periodic acid-Schiff (PAS) reagent	Bio-Optica, Mailand, Italy
Hematoxylin	Merck, Darmstadt, Germany
Methanol	Merck, Darmstadt, Germany
Masson Goldner Trichrom Staining kit	Morphisto, Frankfurt, Germany
WEIGERT iron hematoxylin	Morphisto, Frankfurt, Germany
H2O2	BD Biosciences, San Diego, CA, USA
Periodic acid	Sigma-Aldrich, St. Louis, MO, USA
Thiosemicarbazide	Sigma-Aldrich, St. Louis, MO, USA
Formaldehyde	ThermoFisher, Waltham, MA, USA
Hydrogennitrate	Sigma-Aldrich, St. Louis, MO, USA

Silvernitrate	Sigma-Aldrich, St. Louis, MO, USA
Methenamin	Sigma-Aldrich, St. Louis, MO, USA
Disodiumtetraborate	Carl Roth, Karlsruhe, DE
Eosin (1mg/ml)	Sigma-Aldrich, St. Louis, MO, USA
Gold-Chloride	Sigma-Aldrich, St. Louis, MO, USA
Antigen unmasking solution	Vector, Burlingame, CA, USA
Avidin	Vector, Burlingame, CA, USA
Biotin	Vector, Burlingame, CA, USA
ABC substrate solution	Vector, Burlingame, CA, USA
Methyl green staining solution	Fluka/Sigma, München, Germany
Vecta Mount® mounting media	Vector, Burlingame, CA, USA
SuperFrost+® slides	Menzel-Gläser, Braunschweig, Germany
L. tetragonolobus lectin	Vector Labs, Burlingame, CA, USA
Anti-CD31-Ab	Dianova, Hamburg, Germany
Anti-aquaporin 1-Ab	Millipore, Burlington, MA, USA
Anti-aquaporin 2-Ab	Abcam, Cambridge, United Kindom
Anti-neutrophil/Ly6B.2-Ab	BioRad, München, Germany
Anti-THP-Ab	Cedarlane, Burlington, Canada
Anti-F4/80 -Ab	Bio-Rad Laboratories, Hercules, CA, USA
Anti-IL-22 -Ab	SantaCruz Biotechnology, Dallas, TX, USA
Cell death detection (TUNEL) kit	Roche, Mannheim, Germany

2.1.4 Cell culture

6-well plate	Costar Corning, Schiphol-Rijk, Netherlands
24-well plate	Nunc, Wiesbaden, Germany
96-well plate	TPP, Trasadingen, Switzerland
ECIS 8-well arrays	Ibidi, Martinsried, Germany
DMEM media	Invitrogen, Karlsruhe, Germany
EGM-MV media	Lonza, Basel, Switzerland

REBM basal media	Lonza, Basel, Switzerland
REBM media bullet kit	Lonza, Basel, Switzerland
human hepatocyte growth factor	Peprotech, Rocky Hill, NJ
Fetal calf serum (FCS)	Biochrom KG, Berlin, Germany
Ultra-pure FCS	Hyclone, Logan, UT, USA
Penicillin / Streptomycin (100x)	PAA Laboratories, Pasching, Austria
Dulbecco's PBS (1x)	PAN Biotech GmbH, Aidenbach, Germany
rhIL-22 & rmIL-22	Immunotools, Friesoythe, Germany
MTT assay kit	Promega, Madison, WI, USA
Cytotoxicity Detection Kit (LDH)	Sigma-Aldrich, St. Louis, MO, USA

2.1.5 Reverse transkriptase-quantitative polymerase chain reaction

2.1.5.1 RNA-Isolation

PureLink® RNA Mini Kit	ambion, Darmstadt, Germany
RNAse-free DNAse Set	Qiagen GmbH, Hilden, Germany
β-Mercaptoethanol	Roth, Karlsruhe, Germany
100 % Ethanol	Merck, Darmstadt, Germany

2.1.5.2 cDNA-Synthesis

5x FS buffer	Invitrogen, Karlsruhe, Germany
25 mM dNTPs	GE Healthcare, München, Germany
0,1 M Dithiothreitol	Invitrogen, Karlsruhe, Germany
linear acrylamide	ambion, Darmstadt, Germany
Hexanucleotide-Mix	Roche, Mannheim, Germany
Diethylpyrocarbonate (DEPC)	Fluka/Sigma, München, Germany
RNAsin	Promega, Mannheim, Germany
Reverse Transkriptase „SS-II“	Invitrogen, Karlsruhe, Germany

2.1.5.3 quantitative polymerase chain reaction

LightCycler® 96-well plate	Roche, Mannheim, Germany
10x-Taq-buffer	Fermentas, St. Leon-Rot, Germany
25 mM dNTPs	Fermentas, St. Leon-Rot, Germany
PCR-optimizer	Bitop AG, Witten, Germany
Bovine serum albumin	Fermentas, St. Leon-Rot, Germany

SYBRgreen I	Fluka/Sigma, München, Germany
25 mM MgCl2	Fermentas, St. Leon-Rot, Germany
300 nM PCR-Primer	metabion, Martinsried, Germany

2.1.6 Chemicals

Potassium chloride	Merck, Darmstadt, Germany
Potassium dihydrogenphosphate	Merck, Darmstadt, Germany
Potassium hydroxide	Merck, Darmstadt, Germany
Sodium acetate	Merck, Darmstadt, Germany
Sodium chloride	Merck, Darmstadt, Germany
Sodium citrate	Merck, Darmstadt, Germany
Sodium dihydrogenphosphate	Merck, Darmstadt, Germany
Disodium hydrogenphosphate	Merck, Darmstadt, Germany

2.1.7 Western blotting

RIPA buffer	Sigma-Aldrich, St. Louis, MO, USA
cOmplete™ Protease-Inhibitor	Roche Life Science, Basel, Switzerland
Protein standard	BioRad, München, Germany
Bradford reagent	BioRad, München, Germany
Bromphenolic blue	Merck, Darmstadt, Germany
SDS	BioRad, München, Germany
beta-mercaptoethanol	Carl Roth, Karlsruhe, Germany
Protein-Marker IV	PeqLab, Erlangen, Germany
Immobilon®-PVDF membrane	Millipore, Schwalbach, Germany
Filter Whitman papers	Millipore, Schwalbach, Germany
Milk powder	Sigma-Aldrich, St. Louis, MO, USA
TAE	Sigma-Aldrich, St. Louis, MO, USA
Agarose	MP Biomedicals, Eschwege, Germany
Acrylamide	Carl Roth, Karlsruhe, Germany
Ammoniumperoxodisulfate	BioRad, München, Germany
TEMED	BioRad, München, Germany
Amersham ECL WB Detection Kit	GE Healthcare, Amersham, UK
Stripping-Buffer Restore™	ThermoFisher, Waltham, MA, USA

Rabbit anti-mouse Bad antibody	Cell Signaling Technology, Danvers, MA, USA
Rabbit anti-mouse p-Akt antibody	Cell Signaling Technology, Danvers, MA, USA
Rabbit anti-mouse Stat3 antibody	Cell Signaling Technology, Danvers, MA, USA
Rabbit anti-mouse p-stat3 antibody	Cell Signaling Technology, Danvers, MA, USA
Rabbit anti-mouse b-actin antibody	Cell Signaling Technology, Danvers, MA, USA
Goat anti-rabbit IgG, HRP-linked	Cell Signaling Technology, Danvers, MA, USA

2.1.8 Primer sequences

Murine Primers

Murine	Forward (5'-3')	Reverse (5'-3')
18s	GCAATTATTCCCCATGAACG	AGGGCCTCACTAAACCATCC
DLL1	GCTGGAAGTAGATGAGTGTGCTC	CACAGACCTTGCCATAGAAGCC
DLL3	CCAGCACTGGATGCCTTTTACC	ACCTCACATCGAAGCCCGTAGA
DLL4	GGGTCCAGTTATGCCTGCGAAT	TTCGGCTTGGACCTCTGTTCAG
DLK1	TACCCTAGCCCAAGACTCCA	TACCCTAGCCCAAGACTCCA
DLK2	GGAGGCCACTGTGTGTATGA	CGTCCACATTGACCTCACAG
JAG1	TGCGTGGTCAATGGAGACTCCT	TCGCACCGATACCAGTTGTCTC
JAG2	CGCTGCTATGACCTGGTCAATG	TGTAGGCGTCACACTGGAACTC
NOTCH1	GCTGCCTCTTTGATGGCTTCGA	CACATTCGGCACTGTTACAGCC
NOTCH2	CCACCTGCAATGACTTCATCGG	TCGATGCAGGTGCCTCCATTCT
NOTCH3	GGTAGTCACTGTGAACACGAGG	CAACTGTCACCAGCATAGCCAG
NOTCH4	GGAGATGTGGATGAGTGTCTGG	TGGCTCTGACAGAGGTCCATCT
ADAM17	TGTGAGCGGTGACCACGAGAAT	TTCATCCACCCTGGAGTTGCCA
PSEN1	GAGACTGGAACACAACCATAGCC	AGAACACGAGCCCGAAGGTGAT
BSG	ACATAGTGGACGCAGATGACC	GCGTGGATACCACCACATACT
RBP-J	TGGCTACATCCATTACGGGCAG	GTGGAGTTGTGATACAGGGTCG
HES1	GGAAATGACTGTGAAGCACCTCC	GAAGCGGGTCACCTCGTTCATG
HES5	GTGACTTCTGCGAAGTTCCTG	GGCCCTGAAGAAAGTCCTCTA
HEY1	CCAACGACATCGTCCCAGGTTT	CTGCTTCTCAAAGGCACTGGGT
HEYL	CTGGAGAAAGCTGAGGTCTTGC	ACCTCAGTGAGGCATTCCCGAA
AHR	CTGGTTGTCACAGCAGATGCCT	CGGTCTTCTGTATGGATGAGCTC
ARNT	CTCACGAAGGTCGTTCATCTGC	CCACAAAGTGAGGTTCTCCTTCC

ARNT2	GAAGACGCTGATGTCGGACAAG	CAGAGTTGTGCCGTGACAGGAA
CYP1A1	GACCCTTACAAGTATTTGGTCGT	GGTATCCAGAGCCAGTAACCT
CYP24A1	CTGCCCCATTGACAAAAGGC	CTCACCGTCGGTCATCAGC
IL22	TGGGATTTGTGTGCAAAAGCA	TAATTTCCAGTCCTGTCTTCTG
IL22RA1	CTACGTGTGCCGAGTGAAGA	AAGCGTAGGGGTTGAAAGGT
IL22RA2	CCAAACCAGTCTGAGAGCACCT	CAGGACAATGCCTGAGCCTTTC
IL10R2	TGCTTCTCCGTCCTCCAGAGTT	GCTCTCTGAGTTCCTTCATAGGC
STAT3	AGGAGTCTAACAACGGCAGCCT	GTGGTACACCTCAGTCTCGAAG
CASP1	TCAGCTCCATCAGCTGAAAC	TGGAAATGTGCCATCTTCTTT
CASP8	ATGGCTACGGTGAAGAACTGC	TAGTTCACGCCAGTCAGG
COL1A1	ATGTTCAGCTTTGTGGACCTC	TCATAGCCATAGGACATCTGG
FADD	CACACAATGTCAAATGCCACCTG	TGCGCCGACACGATCTACTGC
KIM1	TGGTTGCCTTCCGTGTCTCT	TCAGCTCGGGAATGCACAA
NGAL	ATGTCACCTCCATCCTGG	GCCACTTGCACATTGTAG
SSeCKs	TGAAGCAATCCACAGAGAAGC	CTCATCAAACACTTCCGTTGC
TIMP2	GCAACAGGCGTTTTGCAATG	AGGTCCTTTGAACATCTTTATCTGC
Transgelin	AGCGGACACTAATGAACCTGGG	ACTGGTTGTCCGAGAAGTTCCG

Human Primers

Human	Forward (5'-3')	Reverse (5'-3')
18s	GCAATTATTCCCCATGAACG	AGGGCCTCACTAAACCATCC
DLL1	TGCCTGGATGTGATGAGCAGCA	ACAGCCTGGATAGCGGATACAC
DLL3	CACTCAACAACCTAAGGACGCAG	GAGCGTAGATGGAAGGAGCAGA
DLL4	CTGCGAGAAGAAAGTGGACAGG	ACAGTCGCTGACGTGGAGTTCA
DLK1	AAG GAC TGC CAG AAA AAG GAC	GCA GAA ATT GCC TGA GAA GC
DLK2	GGCAGGCAAGTTCTGTGACAAAG	CATGGAAGCCTGGTAAGCACAC
JAG1	TGCTACAACCGTGCCAGTGACT	TCAGGTGTGTCGTTGGAAGCCA
JAG2	GCTGCTACGACCTGGTCAATGA	AGGTGTAGGCATCGCACTGGAA
NOTCH1	GGTGAACTGCTCTGAGGAGATC	GGATTGCAGTCGTCCACGTTGA
NOTCH2	GTGCCTATGTCCATCTGGATGG	AGACACCTGAGTGCTGGCACAA
NOTCH3	TACTGGTAGCCACTGTGAGCAG	CAGTTATCACCATTGTAGCCAGG
NOTCH4	TTCCACTGTCCTCCTGCCAGAA	TGGCACAGGCTGCCTTGGAATC

ADAM17	AACAGCGACTGCACGTTGAAGG	CTGTGCAGTAGGACACGCCTTT
PSEN1	GCAGTATCCTCGCTGGTGAAGA	CAGGCTATGGTTGTGTTCCAGTC
BSG	GGCTGTGAAGTCGTCAGAACAC	ACCTGCTCTCGGAGCCGTTCA
RBP-J	TCATGCCAGTTCACAGCAGTGG	TGGATGTAGCCATCTCGGACTG
HES1	GGAAATGACAGTGAAGCACCTCC	GAAGCGGGTCACCTCGTTCATG
HES5	TTGTTCTGTGTTTGCATTTAAG	AGAAAGTCCTCTACAGGCTG
HEY1	TGTCTGAGCTGAGAAGGCTGGT	TTCAGGTGATCCACGGTCATCTG
HEYL	TGGAGAAAGCCGAGGTCTTGCA	ACCTGATGACCTCAGTGAGGCA
AHR	GTCGTCTAAGGTGTCTGCTGGA	CGCAAACAAAGCCAACTGAGGTG
ARNT	CTGTCATCCTGAAGACCAGCAG	CTGGTTCTCATCCAGAGCCATTC
ARNT2	GGAATGCCTACTCCAGTCTTGC	CTTTGCCACTGCGACCAGACTT
CYP1A1	GATTGAGCACTGTCAGGAGAAGC	ATGAGGCTCCAGGAGATAGCAG
CYP24A1	CATCATGGCCATCAAAACAAT	GCAGCTCGACTGGAGTGAC
IL22	TCACCCTTGAAGAAGTGCTGT	ACATGTGCTTAGCCTGTTGCT
IL22RA1	GGTCAACCGCACCTACCAAATG	TGATGGTGCCAAGGAACTCTGTG
IL22RA2	GCCGAAAGAAGCTACCCAGTGT	GGTCCAAGTTCTTCAGCTCTGG
IL10R2	GGCTTCCTCATCAGTTTCTTCC	TTCCACACATCTCTCTTCACTTCTC
STAT3	CTTTGAGACCGAGGTGTATCACC	GGTCAGCATGTTGTACCACAGG

2.1.9 Machines

2.1.9.1 Microplate reader

ELISA-reader Tecan, GENios Plus	Tecan, Crailsheim

2.1.9.2 Cell culture

Laminar flow hood Class II, Typ A/B3	Baker Company, Sanford, ME, USA
Neubauer-counting chamber	Roth, Karlsruhe, Deutschland
Incubator Type B5060 EC-CO2	Heraeus Sepatech, Osterode
ECIS Model Z Theta	Ibidi, Martinsried, Germany

2.1.9.3 Microtome and microscopy system

Microtome Jung CM 3000	Leica, Solms
Light microscope Leica DMRBE	Leica Microsystems, Wetzlar
Light microscope Leica Wild MPS52	Leica Microsystems, Wetzlar

Digital camera DC 300F	Leica Microsysteme, Cambridge, UK

2.1.9.4 Nucleic acid analysis

Thermo cycler UNO-II	Biometra, Göttingen
Thermomixer 5436	Eppendorf, Hamburg
Photometer DU 530	Beckman Coulter, Fullerton, CA, USA
Photometer Ultrospec 1000	Amersham, Freiburg
PCR-Gel- chamber	PeqLab Biotechnologie, Erlangen
LightCycler 480 PCR machine	Roche Diagnostics, Mannheim
Rotilabo®-Mikropistill	Carl Roth GmbH, Karlsruhe

2.1.9.5 Centrifuges

Centrifuge Megafuge 1.0R	Heraeus Sepatech, Osterode
Centrifuge 5415 C	Eppendorf, Hamburg
Centrifuge 5418	Eppendorf, Hamburg

2.1.9.6 Balances

Benchtop BP 110S	Sartorius, Göttingen
Benchtop Mettler PJ 3000	Mettler Toledo, Gießen

2.1.9.7 Other devices

Vortex Genie 2™	Scientific Industries, Bohemia, NY, USA
Pippet Pipetman® P	Gilson, Middleton, WI, USA
Pipet tips Typ Gilson®	Peske, Aindling-Arnhofen
pH meter WTW	WTW GmbH, Weilheim
Water bath HI1210	Leica Microsysteme, Solms

2.1.9.8 Software

Acrobat Writer	Adobe Systems, Dublin, Ireland
CellQuest	BD Biosciences, Heidelberg
Endnote x4	Thomson-Reuters, New York, NY, USA
Office 2007	Microsoft, Redmond, WA, USA
QWin	Leica Microsystems, Wetzlar
Windows XP Professional	Microsoft, Redmond, WA, USA

2.2 Methods

2.2.1 Animal experiments

2.2.1.1 Housing

Cages, bedding, nestlets, mouse retreats, food, and water were sterilized by autoclaving before use. Mice were kept under a 12-hour light/dark cycle in groups of 5 mice/cage and allowed access to food and water *ad libitum*. Housing, breeding and all experimental procedures detailed below were performed in strict accordance with the European protection laws of animal welfare, and with specific approval by the local government authority (Regierung von Oberbayern).

2.2.1.2 Sacrifice

Unless otherwise stated below, at the respective end point of each experiment, mice were anaesthetized using an Isofluran chamber (~150 cm^3, oxygen flow of 1l/min, targeted minimum alveolar concentration [$MAC_{Isofluran}$] between 2-3%), bled into EDTA-containing eppendorf tubes and sacrificed by cervical dislocation. After a midline incision from the pubic bone to the xiphoid process of the sternum, the peritoneal cavity was opened and kidneys harvested and peeled from its fascia. Renal artery, vein and ureter were cut at the hilus. Next, the kidney was cut into three parts, the middle part encompassing the pyelon being fixed by immersion in 4% formalin, and one pole being immersed in RNAlater solution for subsequent RNA isolation, the other poled being snap frozen in liquid nitrogen for subsequent protein analysis.

2.2.1.3 Renal ischemia-reperfusion injury

Ischemia reperfusion injury was induced as previously described ([132]). Briefly, 8-10-week-old mice were anesthetized by fully antagonizable anesthesia (medetomidine 0.5 µg/g

mouse body weight i.p., midazolam 5 µg/g mouse body weight i.p., fentanyl 0.05 µg/g mouse body weight i.p.) and surgical tolerance assessed by clipping the tail with the anatomical forceps. Mice were placed on a heating plate and a rectal probe was inserted for online temperature monitoring. After a ~0.5cm cranio-caudal flank incision, the kidney was carefully luxated out of the body and the renal pedicle was clamped with microaneurysm clamp. Successful clamping was assessed by paling of the clamped kidney. During ischemia, clamped kidneys were kept inside the body, with only the clamp handle protruding over the skin level and mice were put inside an incubator (ambient temperature was adjusted so that the mouse core temperature stayed between 36.0 an 38.0°C). Ischemic times varied and are given the respective figures in the results section. After ischemic times were completed, the clamps were removed and reperfusion visually assessed (change from pale to hyperemic color). Estimated fluid losses were adjusted by 0,2 ml NaCl 0,9% i.p. and the flank incision was closed by sequentially suturing the peritoneum and the skin. The anaesthesia was antagonized (atipamezole 0.5 µg/g mouse body weight s.c., flumazenil 0.5 µg/g mouse body weight s.c. naloxone 1.2 µg/g mouse body weight s.c.) and post-operative pain medication was administered (Buprenorphin 0.05 µg/g mouse body weight s.c.). Also, reperfusion times varied and are given the respective figures in the results section. Control mice for gene-expression experiments were sham-operated (anaesthesia, skin incision, skin suture, anatgonization, pain medication was all performed, but no actual renal clamping).

2.2.1.4 Renal acute oxalate crystallopathy (rAOC)

The rAOC model was induced as described [40]): For the induction of the rAOC model, 6- to 8-week-old mice received a single dose of sodium oxalate 100µg/g mouse body weigt intraperitoneally. For the next 24 hours, drinking water was prepared to also contain 3%

sodium oxalate and thereafter was replaced by oxalate-free water again. Mice were sacrificed as described above at the indicated time points in the results section.

2.2.1.5 Chronic oxalate nephropathy

The rCOC model was induced as described [44]: 8- to 12-wk-old gender-matched C57BL/6 mice were housed as indicated above, their rCOC diet containing 50 µmol/g sodium oxalate and being calcium-free. Before the induction of the model mice were fed a calcium-free, oxalate-free diet to deplete any remaining intestinal calcium. rCOC diet was administered for 7d or 14d, to produce a progressive CKD.

2.2.1.6 Unilateral ureteral obstruction

UUO surgery was performed as described [133]: 8–12 weeks old, sex- and age- matched C57BL/6 mice (gene expression profiling experiments) and Balb/c wild-type and Il22-deficient mice (knock out mouse experiments; generated by Genentech, kindly provided by PD Dr. Sebastian Kobold, LMU) were anesthetized by fully antagonizable anesthesia (medetomidine 0.5 µg/g mouse body weight i.p., midazolam 5 µg/g mouse body weight i.p., fentanyl 0.05 µg/g mouse body weight i.p.) and surgical tolerance assessed by clipping the tail with the anatomical forceps. Mice were placed on a heating plate and a ~0.5cm suprapubic transverse incision was made. The bladder was freed from adhesions and gently luxated out of the body; then the left ureter was identified and peri-ureteral fat was removed with caution not to induce bleeding. After sufficient preparation of the ureter, the ureter was ligated using 4-0 Mersilene sutures, carefully tying at least two knots to avoid later insufficiency of the suture. Afterwards, the bladder was repositioned and antagonists (atipamezole 0.5 µg/g mouse body weight s.c., flumazenil 0.5 µg/g mouse body weight s.c. naloxone 1.2 µg/g mouse body weight s.c.) as well as post-operative pain medication were administered (Buprenorphin 0.05 µg/g mouse body weight s.c.). After the indicated time

point in the results section, mice were sacrificed and kidneys harvested as described above, with the contralateral kidney serving as an intra-individual control. Control mice for gene-expression experiments were sham-operated (anaesthesia, skin incision, skin suture, anatgonization, pain medication was all performed, but no actual ureteral ligation).

2.2.1.7 Lupus nephritis

Experiments for lupus nephritis were performed as described ([134]): Female MRL wild-type or $Fas^{lpr/lpr}$ mice were kept as described above and sacrificed at the time points indicated in the results section.

2.2.1.8 Diabetic nephropathy

Experiments were performed as described ([135]): 6 weeks old male C57BLKS/J wild-type or C57BLKS/J-$Lepr^{db/dp}$ mice underwent uninephrectomy after anaesthesie by fully antagonizable anesthesia (medetomidine 0.5 µg/g mouse body weight i.p., midazolam 5 µg/g mouse body weight i.p., fentanyl 0.05 µg/g mouse body weight i.p.). After surgical tolerance was assessed by clipping the tail with the anatomical forceps, mice were placed on a heating plate and a ~1cm cranio-caudal flank incision was made. The left kidney was carefully luxated out of the body and the renal pedicle was sutured with Ethibond 5-0, carefully tying the suture to avoid fatal bleeding after kidney resection. After the resection of the kidney, estimated fluid losses were adjusted by 0,2 ml NaCl 0,9% i.p. and the flank incision was closed by sequentially suturing the peritoneum and the skin. The anaesthesia was antagonized (atipamezole 0.5 µg/g mouse body weight s.c., flumazenil 0.5 µg/g mouse body weight s.c. naloxone 1.2 µg/g mouse body weight s.c.) and post-operative pain medication was administered (Buprenorphin 0.05 µg/g mouse body weight s.c.). Mouse were then kept individually to avoid fighting, given the particularly bad wound healing in C57BLKS/J-$Lepr^{db/dp}$ mice. At 16 weeks of age, all uninephrectomized 57BLKS/J wild-type and

Lepr$^{db/dp}$ mice with blood glucose concentrations >11 mmol/L and creatinine/albumin ratios >3 g were sacrificed and the remaining kidney was harvested.

2.2.1.9 Anti-GBM disease

The induction of the heterologous model of aGBM disease was performed as described ([70]): 6-8-week-old mice received a single injection of 100 µl aGBM serum i.v., were sacrificed 24 hours later and kidneys were harvested.

2.2.1.10 Adriamycin-induced focal segmental glomerulosclerosis

The induction of the adriamycin nephropathy model was performed as described ([136]): 6-week-old Balb/c mice received an injection of adriamycin/doxorubicin (13 µg/g mouse body weight) i.v. were sacrificed 24 hours later and kidneys were harvested.

2.2.2 Colorimetric serum parameter measurement

Kits for serum creatinine as well as blood urea nitrogen (BUN) measurements were used according to the manufactures instructions.

2.2.3 Histological evaluation

2.2.3.1 Paraffinization of tissues

After overnight fixation in 4% formalin, the tissues which were already in histocassettes were subjected to an increasing ethanol series (2x 70%, 80%, 95%, and 3 x 100% ethanol), being immersed in each solution for one hour. After ethanol, histocassettes were immersed sequentially for three times in xylene for 1.5 hours each, followed by two paraffin immersions for 2 hours each at 60°C. After this, tissues were repositioned in the histocassette for optimal sectioning position and embedded in a paraffin block.

2.2.3.2 Preparing tissue sections

Paraffin blocks were cooled down close to 0°C for optimal sections and cut into a water bath using the microtome to produce sections of 2 µm thickness. Swimming sections were then carefully mounted on ammonium per sulfate coated cover slides and dried for 12 hours at 37°C.

2.2.3.3 Staining

2.2.3.3.1 Periodic Acid Schiff Staining (PAS)

After deparaffinization in xylene and rehydration in a decreasing ethanol series, 2 µm tissue sections were stained for 10 min in 0.5% periodic acid by full immersion and subsequently rinsed with distilled water. This was followed by a 20 min immersion- incubation in Schiff reagent, after which again slides were rinsed with distilled water. Next, slides were covered for two minutes with 0.55% potassium metabisulfite, counterstained with Mayer's hemalaun reagent for 3 min and washed under running water for 10 min. Finally, slides were dehydrated in an increasing ethanol series, quickly immersed in xylene and covered with a drop of VectaMount media and a coverslip.

2.2.3.3.2 Sliver stain

After deparaffinization in xylene and rehydration in a decreasing ethanol series, 2 µm tissue sections were stained 15 min in 1% periodic acid, immersed for 5 min in distilled water, covered with 0,5% thiosemicarbazide and immersed again 5 min in distilled water. After this, sections were immersed for approximately 5- 10 min in the silver staining solution (stocked from 55ml methenamine, 2,8ml silver solution and 6,6ml sodium borate solution) at 63° C (final duration based on coloring of the slide), quickly rinsed with distilled water, incubated for 15 min in gold-chloride solution and rinsed again with distilled water. Staining was completed by covering the section with hydrogen nitrate formaldehyde for 1 min,

rinsing twice and fixing for 10 min by immersion in sodium borate solution. The fixing solution was then washed of for 2 min under running water followed by a 2 min counterstaining with hematoxylin, 5 min rinse under running water and 10 quick immersions into eosin. Finally, slides were dehydrated in an increasing ethanol series, quickly immersed in xylene and covered with a drop of VectaMount media and a coverslip.

2.2.3.3.3 Masson-Goldner-Trichrom-Färbung

After deparaffinization in xylene and rehydration in a decreasing ethanol series, 2 µm tissue sections were stained for 3 min in Weigert's iron hematoxylin, rinsed for 10 min under running water, stained with Goldner solution I (Ponceau Acid Fuchsin) for 10 min, rinsed with 1% acetic acid for 30 sec., differentiated approximately 1-2 min. until full collagen bleaching in Goldner solution II (Phosphomolybdic Acid-Orange G), rinsed with 1% acetic acid for 30 sec. again, and finally stained with Goldner solution III (Light Green Stock Solution) for 5 min. After a last rinse with 1% acetic acid for 5 min, slides were dehydrated in an increasing ethanol series, quickly immersed in xylene and covered with a drop of VectaMount media and a coverslip.

2.2.3.3.4 Immunohistochemistry

After deparaffinization in xylene and rehydration in a decreasing ethanol series, 2 µm tissue sections were washed 7 min with PBS and blocked for 20 min in methanol containing 3% H_2O_2. Next, sections were immersed in water containing 1% antigen-unmasking solution and boiled in a microwave for 4x2,5 min. After a second PBS wash for 7 min, sections were blocked for 15 min with avidin and 15 min with biotin, respectively. Primary antibody stainings were either performed for 1 hour at room temperature or overnight at 4° C. After washing off the primary antibody with PBS, sections were incubated for 30 min with

secondary antibodies with the given species specificity to bind primary antibodies. After washing off the secondary antibody again with PBS for 7 min, sections were incubated in 0,1% ABC substrate solution in PBS for 30 min and washed sequentially with PBS followed by TRIS hydrochloride. Staining was visualized by incubation with DAB substrate (staining intensity and hence incubation time were set by adjudication from light microscopy) and counterstaining was done by methyl green. Finally, slides were dehydrated in an increasing ethanol series, quickly immersed in xylene and covered with a drop of VectaMount media and a coverslip.

2.2.3.3.5 Immunofluorescence

After deparaffinization in xylene and rehydration in a decreasing ethanol series, 2 µm tissue sections were washed 7 min with PBS and immersed in water containing 1% antigen-unmasking solution and boiled in a microwave for 4x2,5 min. After a second PBS wash for 7 min, sections were blocked for 15 min with avidin and 15 min with biotin, respectively. Primary antibody stainings were performed for 1 hour at room temperature, followed by a 7 min wash in PBS and the secondary antibody incubation lasting 30 min. For IF costainings using terminal deoxynucleotidyl transferase dUTP nick end labeling (TUNEL), the antibody staining was followed by an incubation with the TUNEL enzyme according to the manufactures instructions. After the staining, slides were dehydrated in an increasing ethanol series, quickly immersed in xylene and covered with a drop of VectaMount media and a coverslip.

2.2.3.3.6 Image analysis

Tubular injury and interstitial fibrosis on PAS stained sections was assessed by digital morphometry in ImageJ. A grid containing 120 (12x 10) sampling points was superimposed on representative photography of kidney sections. Tubular dilation, atrophic or necrotic

tubular cells and interstitial matrix under each grid point were counted, respectively, and frequencies expressed as a percentage of all sampling points. For CD31, Lectin and TUNEL staining, ImageJ was used to quantify the percentage of positive area per side after threshold quantitation. For IL-22 stainings, IL22+ cells were counted in 9 high-power fields from each kidney selected at random. All assessments were performed with the observer blinded to the experimental condition.

2.2.4 Protein isolation and western blotting

Total protein was extracted from tissues by homogenization and repeated pulses of sonication in RIPA buffer containing protease and phosphatase inhibitor on ice. After in additional incubation for 2 hours at 4°C, samples were spun for 20 min with 10,000 g at 4 °C and supernatants used for further processing. Protein concentrations were estimated using the Bradform method, adjusted by addition of H2O (if necessary) and mixed 1:1 with 2x loading buffer. Proteins were then heat denatured, separated by SDS-PAGE and transferred to a polyvinylidene difluoride membrane. To avoid nonspecific binding, membranes were blocked for 2 h at room temperature with 5% milk or BSA (for phosphoproteins) in Tris-buffered saline buffer. Membranes were then incubated overnight at 4°C with primary rabbit antibodies against mouse Bad, p-Akt, Stat3, p-stat3 and b-actin. After washing, membranes were incubated with peroxidase-conjugated anti-rabbit IgG secondary antibodies in Tris-buffered saline buffer for 1 hour at room temperature. After thoroughly washing the membrane at least three times, staining was visualized using an enhanced chemiluminescence system according to the manufacturer's instructions. Staining intensity was quantified using ImageJ.

2.2.5 Nucleic acid analysis-based experiments

2.2.5.1 Polymerase-chain-reaction based genotyping

Mice were marked by the earhole punch technique (side and position of the earhole indicating the number of the respective mouse) and hence the generated ear punch biopsies were used for DNA isolation. For this, tissue was lysed in 200µl PBND-buffer (2,5ml 2M KCl, 1ml 1M Tris-HCl (pH8,3), 0,25ml 1M MgCl2, 10ml, 0,1% Gelatine, 0,45ml 100% NP-40, 0,45ml 100% Tween-20; H2O ad 100 ml) containing 1µl protein kinase K (20 mg/ml) for 4 hours at 56° C on a shaker. After a quick spindown for 2 min at 12,000 g the supernatant containing the DNA was used. PCR was performed using 1µl of the supernatant, a PCR mastermix (2,5µl 10x-PE buffer, 2,0µl 1,25mM dNTP, 0,5µl Taq polymerase, 17,0µl H2O) and 2 µl of either IL22 wild-type or IL22 KO primer pairs (1 µl of forward and reverse primer, respectively) for a total of two reactions per animal with a reaction volume of 25 µl each. PCR samples of known KO and wild-type animals were used as controls as well as H2O instead of DNA containing supernatant as a non-template control. PCR settings used were: preincubation at 94° C for 15 min, 30 cycles of 30 sec./94° C -> 60 sec/61°C -> 90 sec./72°C, and a final 72° C step for 10 min. After this, 4µl of the PCR reaction were mixed with 6x loading buffer (3ml glycerol; 0,5ml 5% bromphenol blue; 0,5ml 5% xylenecyanol; H20 ad 6ml) and gently pipetted into the pockets of an agarose gel containing ethidium bromide immersed in in TBE-Puffer (108 g Tris; 55 g boric acid; 5,84 g EDTA; H2O ad 10 l). Gels were run for 30 min at 200 V using a DNA ladder for estimation of sufficient fragment separation.

2.2.5.2 RNA isolation

For RNA isolation, PureLink® RNA Mini Kit were used according to the manufacturer's instructions. Tissues were lysed in lysis buffer containing 1% beta-mercaptoethanol by

means of homogenization and vortexing and lysated mixed 1:1 with 70% ethanol. The resulting viscous fluid was pipetted on silica columns and spun for 15 sec. at 12,000 g. After washing the membrane once with washing buffer I and washing buffer II from the RNA isolation kit, a DNAse digestion step using RNAse-free DNAse was performed on the membrane for 15 min, and membranes were washed again with washing buffer II. After this membranes were dried and incubated with RNAse-free water to elute purified RNA. Purity, quanity and quality of RNA isolated was assessed by optical densitometry, and sufficient quality was assumed at a 260nm/280nm OD ratio between 1.95 and 2.05.

2.2.5.3 cDNA preparation from murine solid organs

cDNA was obtained by RNA reverse transcription of 1µg RNA in 10µl RNAse-free H2O (incubated for 5 min at 65°C and then cooled on ice) in a master mix (8µl 5x- superscript II buffer, 0.8µl 25mM dNTPs, 2µl 0,1M DTT, 0.5µl linear acylamide [15µg/ml], 0.43µl hexanucleotides, 1µl RNAsin [40U/µl], 0.87 µl SuperScript II enzyme, and 16.4µl RNase-free H2O) for 90 min at 42°C. After transcription, the RT enzyme was inactivated by a a 5 min incubation at 85° C.

2.2.5.4 Quantitative real-time RT-PCR (qPCR)

For qPCR, each PCR reaction (20 µl) was prepared using 1.2 µl of gene-specific primers, 10 µl of a qPCR master mix (2ml 10x-Taq buffer; 150µl 25 mM dNTPs; 4ml PCR optimizer; 200µl BSA (20 mg/ml); 40µl SYBRgreen I; 2,4ml 25mM MgCl2; H_2O ad 10ml) and 2 µl of the aforementioned cDNA preparation in 6,8 µl H_2O. Amplification and detection of cDNA was performed on a LC480 Roche using the following protocol: initiation phase at 95◦C, annealing phase at 60◦C, and amplification phase at 72◦C was performed for a total of 40

amplification steps. Gene-specific primers were temperature-optimized and designed to generate amplicons between 80 and 200 bp. 18s rRNA expression was used as the housekeeper. Primer efficiencies were tested prior to experiments and ensured to be between 1.6 and 2. Unspecific binding and dimer formation was minimized by *in silico* analysis prior to experiments and excluded by inspection melting curves of NTCs as well as RT- controls. The efficiency-corrected quantitation was performed automatically by the LightCycler 480 based on extern standard curves describing the PCR efficiencies of the target and the reference genes (ratio=EtargetΔCPtarget (control − sample)/ErefΔCPref (control − sample)). The high confidence algorithm was applied in order to minimize the risk of false-positive crossing point (Cp). If samples did not rise above the background fluorescence (Cp or quantitation cycle Cq) of 35 cycles during the amplification reaction they were regarded as not detectable, whereas samples with Cp between 5 and 35 cycles were regarded as detectable.

2.2.6 Cell culture

The HK2 cell line, and theK4 cell line as well as the murine MTC cells were cultured under sterile conditions at 37°C and 5% CO2 in medium consisting of DMEM, 10% fetal bovine serum (FBS), and 1% penicillin/streptomycin. The human renal progenitor cells (RPC) were a gift of Prof. Paola Romagnani (University of Florence) 16885410. These cells were cultured in EBM-MV media containing 20% FCS. All cells were tested routinely every six months for mycoplasm contamination, grown to not more than 80-90% confluency before splitting and frozen aliquots of earlier passages were routinely thawed to perform experiments with cells of approximately the same passage.

2.2.6.1 iTEX differentiation

iTEX tubulogenic differentiation was performed as described by Sagrinati et al. (16885410). RPCs were cultured in REBM basal media with the addition of the "REBM bullet kit" (containing hydrocortisone, hEGF, FBS, epinephrine, insulin, triiodothyronine, transferrin, and gentamicin/amphotericin-B) as well as 50 ng/ml hepatocyte growth factor. Full differentiation was seen after 21 d of culture, indicated by marker gene expression of SLC9A3, SLC12A3, AQP1, and AQP.

2.2.6.2 3-(4,5-dimethylthiazol-2-yl)-2,5-diphenyltetrazolium bromide (MTT) assay

For the 3-(4,5-dimethylthiazol-2-yl)-2,5-diphenyltetrazolium bromide (MTT) assay was, 5000 cells/well were seeded in a 96-well microculture plate in 100 µl serum-free media. After cell adhesion for 4 h, either CaOx or IL-22 were added to the cells in the concentration indicated in the figure legends and incubated for 48 h. Cells treated with serum-free medium only or 10% FBS supplemented media served as negative and positive controls, respectively. Then, 15 µL MTT reagent (5 mg/mL) was added to each well and the plate was incubated at 37°C for 3 h, after which 100 µL 10% HCl-SDS was added to each well and plates were kept at room temperature overnight. Optical density (OD) was quantified via a 96-well plate reader to record the absorbance at 570 nm.

LDH release assay

LDH assays were performed according to the manufacturer's instructions. 100 µl of cell culture supernatants were mixed 1:1 with the LDH working solution from the kit and incubated for 20 min in the dark. Optical density (OD) was quantified via a 96-well plate reader to record the absorbance at 492 nm. Supernatants from cells treated media only or Triton-X were used as negative and positive controls, respectively, and cytotoxity was calculated in percent (%) as

$(OD_{sample}-OD_{negative\ control})/(OD_{positive\ control}-OD_{negative\ control})*100$

2.2.6.3 Scratch-induced wound healing assay

HK2 cells and K4 cells were cultured in 6-well plates to confluency. Artificial "scratch wounds" were created with a 20 µl pipette tip and wells were quickly rinsed with PBS to remove semi-attached cells and hence create clean margins of the scratch. rhIL-22 was then added to the cells as indicated in the figures. Cells treated with medium only served as negative and cells treated with 10% FBS served as positive controls, respectively. After the time points indicated in the figures, two photographs per wound were taken on a phase contrast microscope. Image analysis (i.e. scratch diameter) was performed in Image J.

2.2.6.4 Epithelial barrier testing via electric cell–substrate impedance sensing (ECIS)

10,000 HK2 cells/well were seeded into ECIS 8-well arrays in serum free DMEM overnight in the incubator at 37°C, while primary murine cells were seeded at 40,000 cells/well in ECIS arrays with DMEM medium including 10% FBS. For the growth inhibition experiment, the electric fence was executed every 5 min, while for wound healing assays, electric damage was caused by the application of 3 mA at 60 kHz for 60 sec to HK2 cells at confluency (indicated by stable capacitance at 64,000 Hz). Isolated murine primary tubular cells were stimulated with PBS or 20 µg/mL histones at confluency. Six hours later, histones were washed off by exchanging medium, then 1 ng/mL of rmIL-22 or PBS was added to each well. The value of capacitance just before adding histone and immediately after medium exchange was set as 0 or 1, respectively. The three different set-ups are shown in Fig. 2-1.

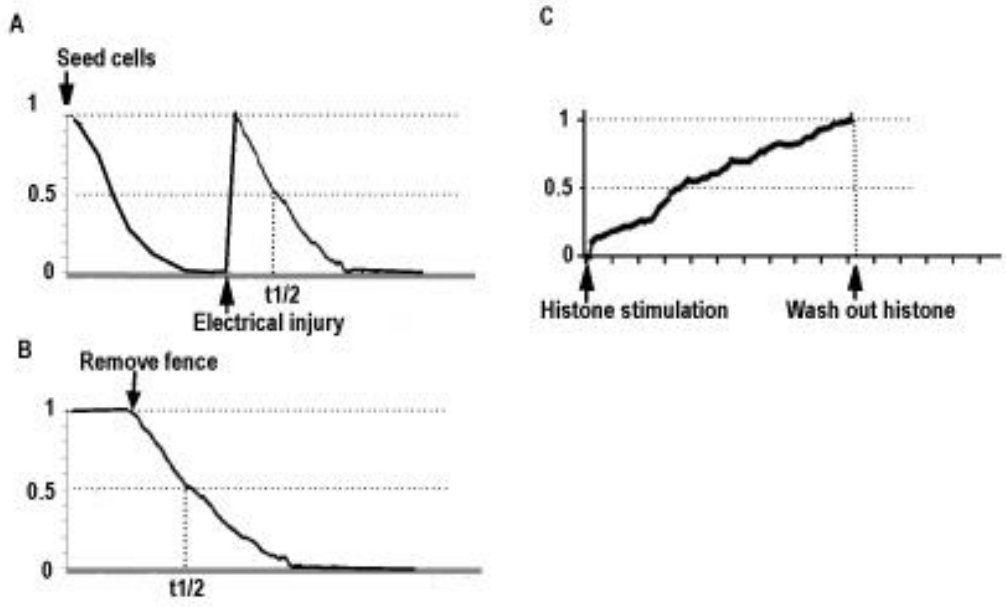

Figure 2-1 ECIS experiments.

A) Electrical injury experiment set-up. B) Electrical fence growth inhibition experimental set-up. C) Histone stimulation experimental set-up from primary murine tubular epithelial cells.

2.2.7 Microarray-based human gene expression analyses

Data on human microarray-based gene expression from kidney biopsies were generously provided by Prof. Dr. Clemens Cohen and PD Dr. rer. nat. Maja Lindenmeyer from the multi-institutional European Renal cDNA Bank (ERCB) consortium. [137] The ERCB consortium preserves kidney biopsies in RNA later directly after biopsy [138] and later isolates RNA for cDNA transcription and microarray analysis using the affymetrix HG-U133Plus2.0 and the Array HG-U133A Array. Expression data from different hybridizations were RMA normalized and gene expression data on the gene level are based on the most recent probe-sets (including remapping of some probes initially assigned to different genes by the manufacturer). All procedures involving patients were performed in strict compliance with the Declaration of Helsinki in its current version and are approved by all institutional review

boards of participating institutions. Details of statistical analysis of microarray data are outlined below.

2.2.8 Statistical analyses

Unless indicated otherwise, data are shown as mean+−S.E.M. GraphPad Prism software was used to perform univariate ANOVA (statistical significance was assumed at $p<0.05$) to assess comparison between groups and post hoc Bonferroni's correction was applied in order to correct for multiple comparisons. For microarray studies on human biopsies, significance analysis of microarrays (SAM) was performed calculating q-values for each analysed gene according to the Benjamini Hochberg method [139] (targeting a false-discovery rate $q<0.05$). For correlation between murine and human tissue samples, Spearman's r was calculated in GraphPad Prism.

3 Results

The following 2 sections were published in "Weidenbusch M, Rodler S, Song S, Romoli S, Marschner JA, Kraft F, Holderied A, Kumar S, Mulay SR, Honarpisheh M, Kumar Devarapu S, Lech M, Anders HJ. Gene expression profiling of the Notch-AhR-IL22 axis at homeostasis and in response to tissue injury. Biosci Rep. 2017 Dec 22;37(6). pii: BSR20170099."

3.1 Notch-AhR-IL22 Pathway Expression in Acute Renal Inflammation and Regeneration

In order to analyze dynamic changes of the Notch/AhR/IL-22 axis under pathological conditions., we first chose two murine models of acute renal inflammation to study Notch-AhR-IL22 pathway expression. The absolute and relative gene expressions for renal ischemia/reperfusion injury (rIRI) and acute renal oxalate-crystallopathy (rAOC) are shown in Figure 3a+b. Interestingly, a dose-dependent induction of the Notch-AhR-IL22 pathway was found in rIRI with increasing ischemic time. Most profound upregulation was seen 24 hours after 35 min of rIRI for JAG1, JAG2, NOTCH1-3 and HEYL as well as for IL22RA2, IL10R2 and STAT3 (Figure 3-1). A very similar pattern of gene expression was also seen in rAOC after 24 hours (Figure 3-4). Importantly, while in rIRI IL-22 was downregulated, in rAOC IL-22 gene expression peaked after 24 hours of injury. This increase was only temporally, as IL-22 levels decreased again in the regeneration phase. Of note, the IL-22 expression in rAOC correlated with the Notch target genes Hes1 and Hes5, which also showed transient upregulation followed by prolonged downregulation during the 24 and 48 hours of regeneration after injury. Interestingly, this pattern was not observed in the regeneration phase after rIRI, where Hes1, Hes5, Hey1 and HeyL all were significantly induced, with HeyL still being upregulated ten days after initial injury (Figure 3-3). With increasing ischemic time, Periodic acid-Schiff's Staining (PAS) at the cortico-medullary junction (i.e. the maximum damage zone) showed more general injury (e.g. more hyaline material within renal tubules) as well as more intrarenal inflammation indicated by a higher neutrophil influx. Concomitantly, there were decreased intact distal tubular cells, indicated by less Tamm-Horsfall protein (THP) positive cells. Consistent with increasing inflammation, the number of IL-22 producing cells increased with ischemic time. (Figure 3-2). In rAOC, hyaline material within tubules in the entire kidney peaked after 24 hours of oxalate injury, and then decreased after 48 hours post-

injury. was Again, there was similar pattern for intrarenal IL-22 expression in thesesamples with IL-22 positive cells peaking at 24 hours of oxalate injury and decreasing thereafter (Figure 3-5). In conclusion, several members of the Notch-AhR-IL22 pathway are differentially regulated during specific phases of acute kidney injury and regeneration.

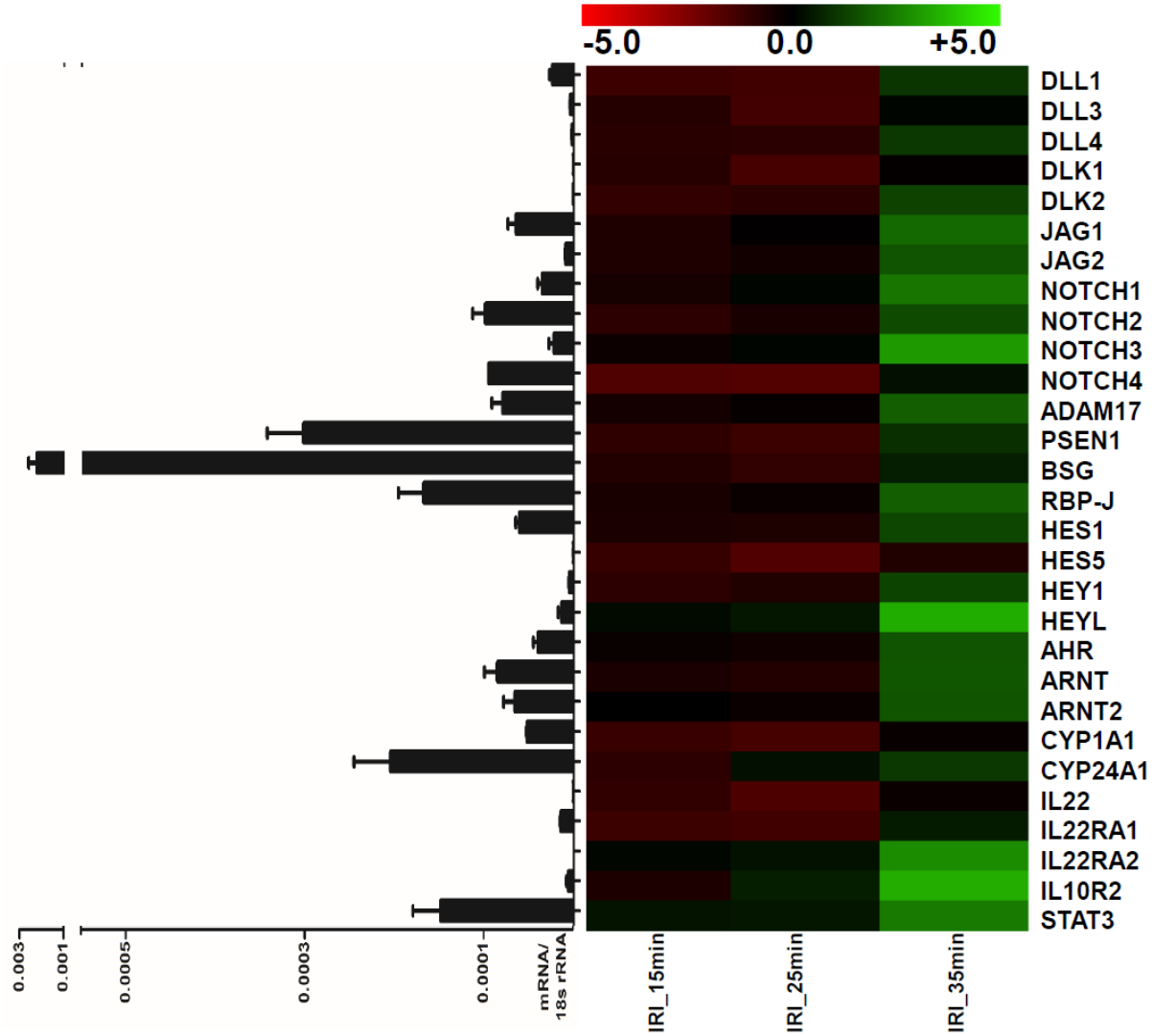

Figure 3-1 Notch-AhR-IL22 Pathway Expression in Acute Renal Inflammation and Regeneration.

Gene expression for IRI. A dose-dependent induction of Notch-AhR-IL22 pathway was found in IRI with increasing ischemic time. Heat maps showing log(2) fold-changes of the respective sample compared to healthy controls; the table displays red to green shades for higher and lower relative mRNA expression levels, respectively. Bar graphs next to the heat map show absolute levels of respective mRNA expression, normalized to 18s rRNA expression, of healthy murine kidney samples.

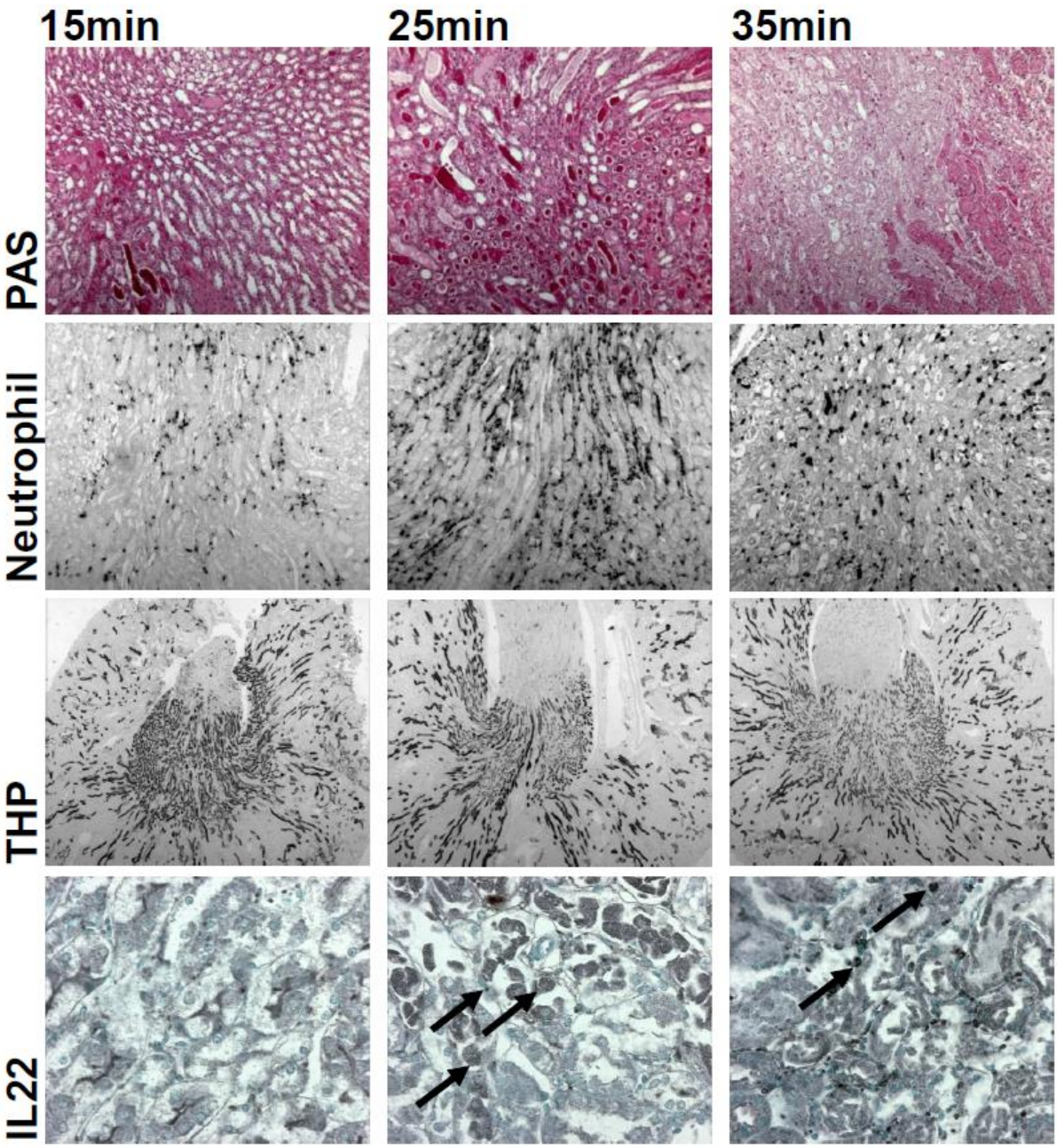

Figure 3-2 Histological staining of the murine kidneys in acute renal inflammation and regeneration.

Renal ischemia-reperfusion injury with increasing ischemia time; PAS staining (first row) for evaluation of general injury (e.g. hyaline casts), IHC for evaluation of neutrophil influx (indicating intrarenal inflammation) (second row), anti-THP for intact distal tubular cells (third row), and anti-IL22 for IL-22 positive cell enumeration. In rIRI models, with the ischemic time increasing, hyaline material, neutrophil- and IL-22 positive cell numbers increased while THP staining decreased. Magifications are 100x for THP, 200x for PAS and Neutrophil staining, and 400x for IL-22 staining

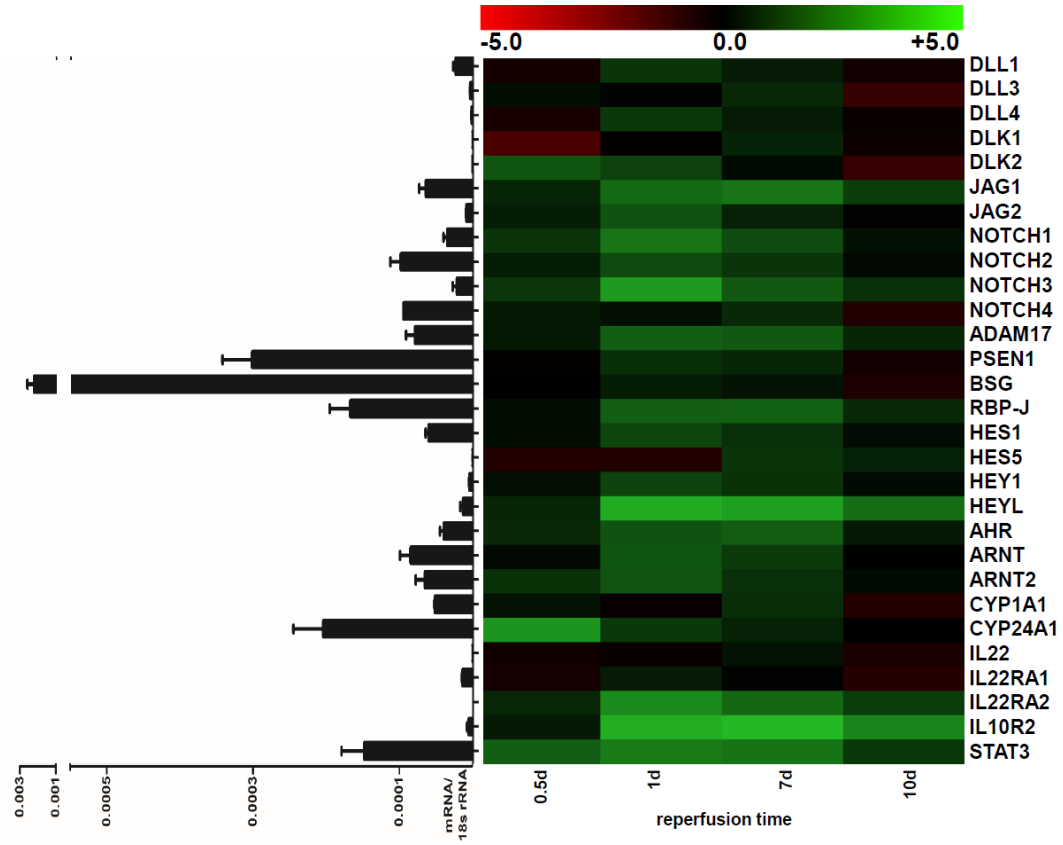

Figure 3-3 Notch-AhR-IL22 Pathway Expression in Acute Renal Inflammation and Regeneration.

Gene expression for IRI regeneration phase. Hes1, Hes5, Hey1 and HeyL all were significantly induced, with HeyL still being upregulated ten days after initial injury. Heat maps showing log(2) fold-changes of the respective sample compared to healthy controls; the table displays red to green shades for higher and lower relative mRNA expression levels, respectively. Bar graphs next to the heat map show absolute levels of respective mRNA expression, normalized to 18s rRNA expression, of healthy murine kidney samples.

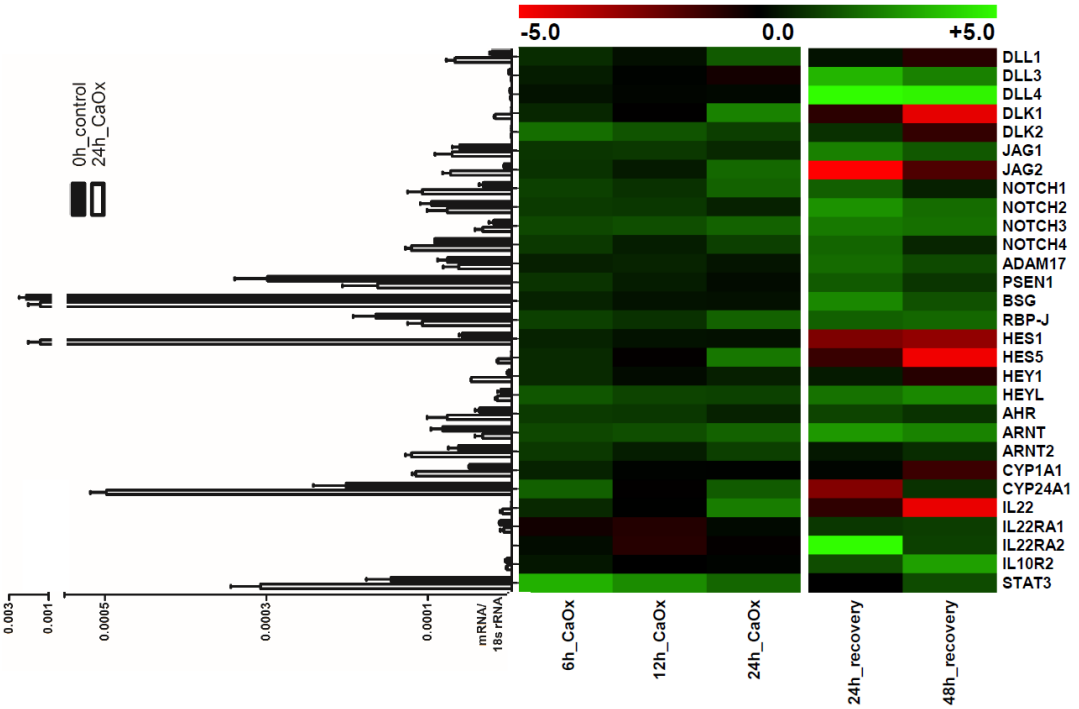

Figure 3-4 Notch-AhR-IL22 Pathway Expression in Acute Renal Inflammation and Regeneration.
Gene expression for AOC after 24 hours. The IL-22 expression increased temporally after 24 hours of injury and correlated with Hes 1 and Hes 5.

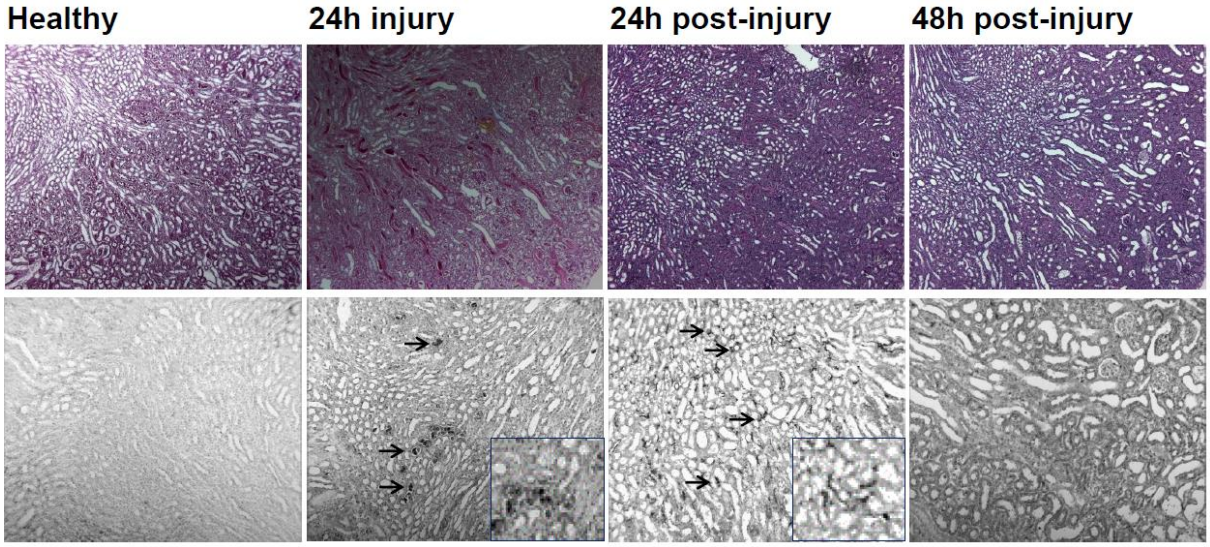

Figure 3-5 Histological staining of the murine kidneys in acute renal inflammation and regeneration.
PAS staining in rAOC showing the hyaline material (i.e. injury) peak after 24 hours of oxalate injury and a steady decrease post-injury thereafter, along with a similar course for IL-22 positive cells. Magifications are 200x for PAS and IL-22 staining; inserts are 400x. Arrows are indicating IL-22 positive cells in the renal interstitium.

3.2 Notch-AhR-IL22 Pathway Expression in Chronic Tubular Atrophy

Acute inflammation is followed by regeneration to restore tissue homeostasis, but if the injurious trigger persists, irreversible damage of tissues occurs. In the kidney, this leads to epithelial atrophy, which is accompanied by interstitial fibrosis caused by maladaptive repair mechanisms. We therefore next analyzed two mouse models of chronic tubular injury and atrophy. While short exposure to oxalate crystals induces reversible rAOC, long term oxalate overload induces renal chronic oxalate crystallopathy (rCOC) like in primary hyperoxaluria type 1. Another well characterized model of chronic kidney disease (CKD) is unilateral ureteral obstruction (UUO), in which intraluminal hydrostatic pressure induces the tubular atrophy. Gene expression patterns of the Notch-AhR-IL22 pathway in both models are shown in Figures 3-6 and 3-8. While Notch4 was upregulated already after seven days of rCOC and stayed upregulated thereafter, Notch1 and Notch2 were upregulated only after 14 days of rCOC, while Notch3 was not significantly regulated. Among the most highly induced both after 7 and 14 d of rCOC was Hey1, with six- and eight-fold upregulation, respectively.

Interestingly, while both Ahr and Arnt2 were induced in rCOC, Arnt was not regulated. The gene expression pattern in UUO was somewhat distinct from the one seen in rCOC. In UUO, a strong upregulation of Hes5, concomitant with an upregulation of IL-22, was seen at all time points. In conclusion, also in chronic tubular atrophy specific regulation of the Notch-AhR-IL22 pathway was regulated, albeit less pronounced than in the acute injury models. Histological staining in chronic tubular atrophy showed diffuse increasing renal fibrosis (extensive green-bluish areas in Masson Trichrom staining) after 14 days of rCOC, and a moderate increase of IL-22 positive cells after 14 days of rCOC (Fig. 3-7). Silver and F4/80 stainings in the UUO model show increasing fibrosis (indicating worsening kidney function) and peritubular macrophage influx (indicating persisting inflammation) along with increasing numbers of IL-22 expressing cells (Figure 3-9) after ureteral ligation over time.

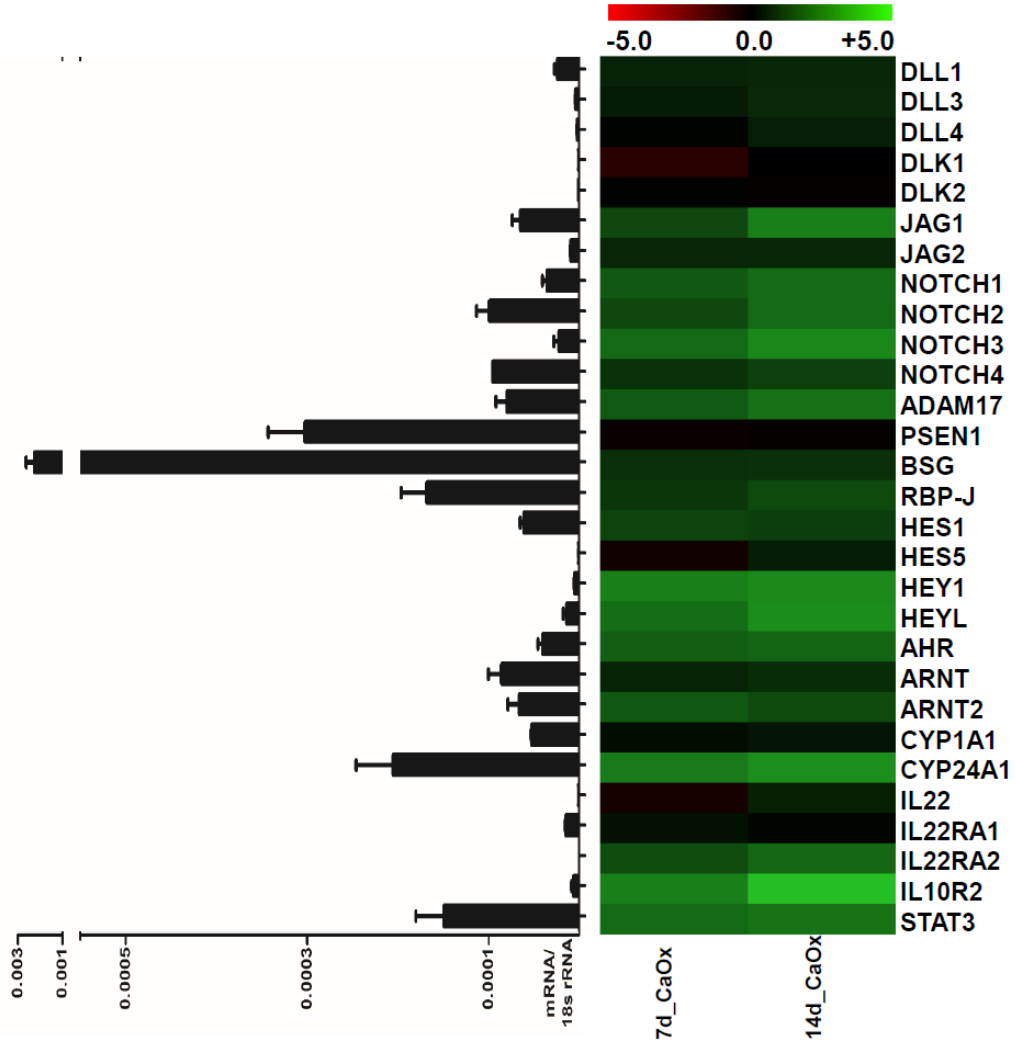

Figure 3-6 Notch-AhR-IL22 Pathway Expression in Chronic Tubular Atrophy.

Gene expression pattern in rCOC models. Notch4 was upregulated after seven days of rCOC and stayed upregulated, Notch1 and Notch2 were upregulated only after 14 days, while Notch3 was not significantly regulated. Hey1 was the most highly induced gene after 7 and 14 days. Both Ahr and Arnt2 were induced, while

Arnt was not regulated. Heat maps showing log(2) fold-changes of the respective sample compared to healthy controls; the table displays red to green shades for higher and lower relative mRNA expression levels, respectively. Bar graphs next to the heat map show absolute levels of respective mRNA expression, normalized to 18s rRNA expression, of healthy murine kidney samples.

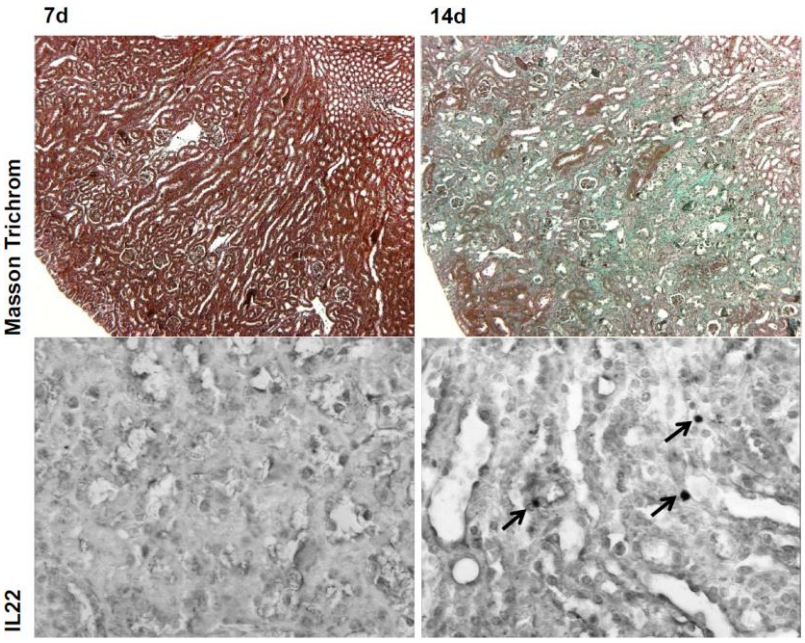

Figure 3-7 Histological staining in chronic tubular atrophy.
In rCOC models, Masson Trichrom staining showed more fibrosis (green) in kidney after 14 days of rCOC, meanwhile, IL-22 staining was also increased after 14 days of rCOC. Magifications are 200x for Masson Trichrom and 400x for IL-22 staining.

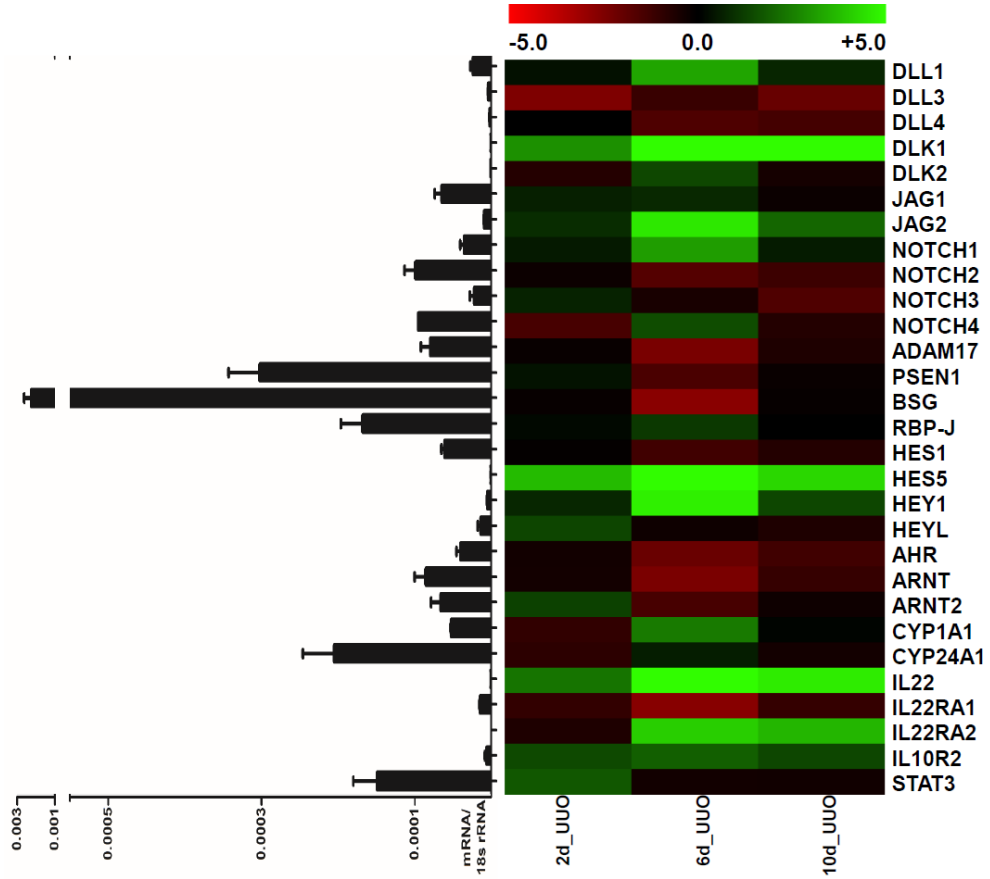

Figure 3-8 Notch-AhR-IL22 Pathway Expression in Chronic Tubular Atrophy.
Gene expression pattern in UUO models. A strong upregulation of Hes5, and IL-22, was seen at all time points.

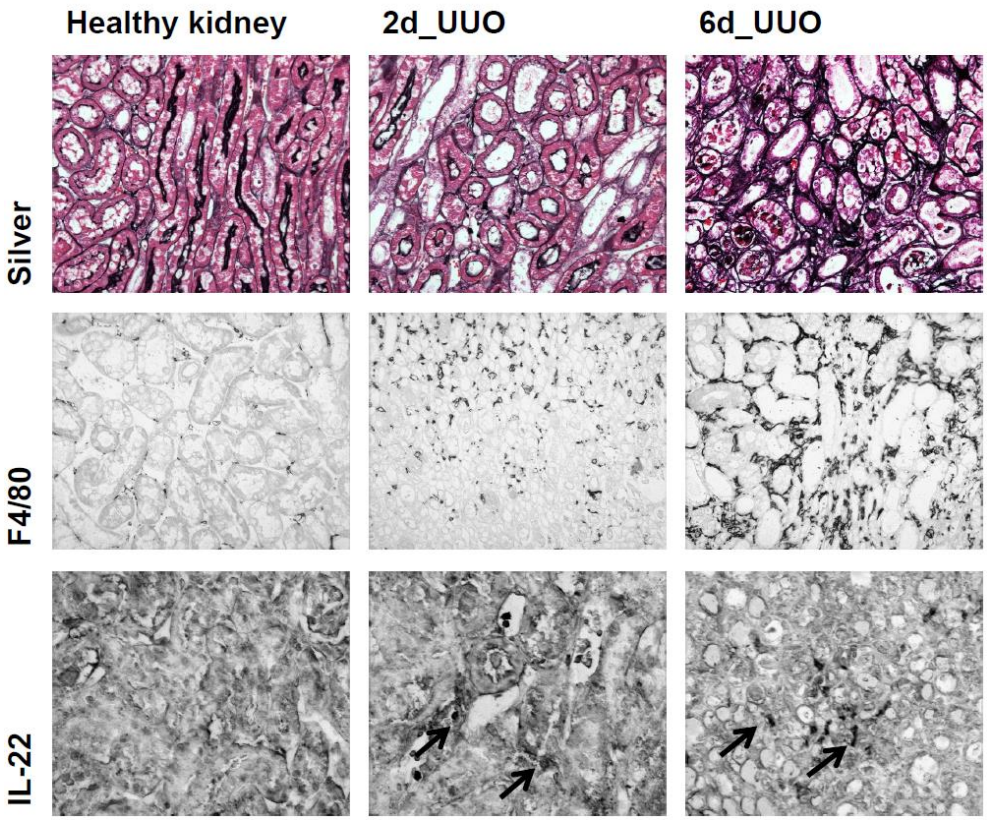

Figure 3-9 Histological staining in chronic tubular atrophy.

Silver and F4/80 stainings in the UUO model show increasing fibrosis (indicating worsening kidney function) and macrophage influx (indicating persisting inflammation) along with increasing numbers of IL-22 expressing cells Magifications are 200x for Silver, F4/80 and IL-22 staining Arrows are indicating IL-22 positive cells in the renal interstitium.

3.3 Notch/AhR/IL-22 axis gene expression in mouse models of glomerular injury

After we had explored Notch/AhR/IL-22 axis gene expression patterns in models of acute and chronic tubular injury, we analyzed Notch/AhR/IL-22 axis gene expression in models of glomerular injury, namely lupus nephritis, anti-GBM disease (Fig. 3-10), adriamycin-induced nephropathy, and diabetic nephropathy (Fig. 3-11). Compared to the gene expression patterns seen in models of tubular injury, we observed significantly more heterogeneity in the glomerular models.

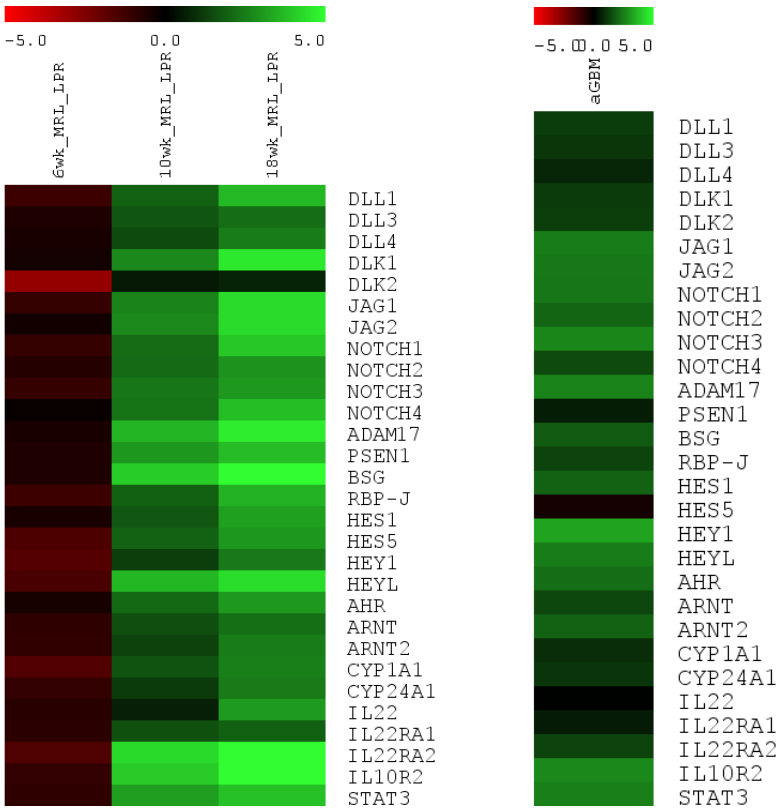

Figure 3-10 Gene expression of the Notch/AhR/IL-22 axis in murine lupus nephritis and aGBM disease. Data from groups of 5-6 mice per group of each time point and expression normalized to age matched MRL-Fas wild-type mice for lupus nephritis and saline-injected C57/BL6/N mice for anti-GBM disease, respectively.

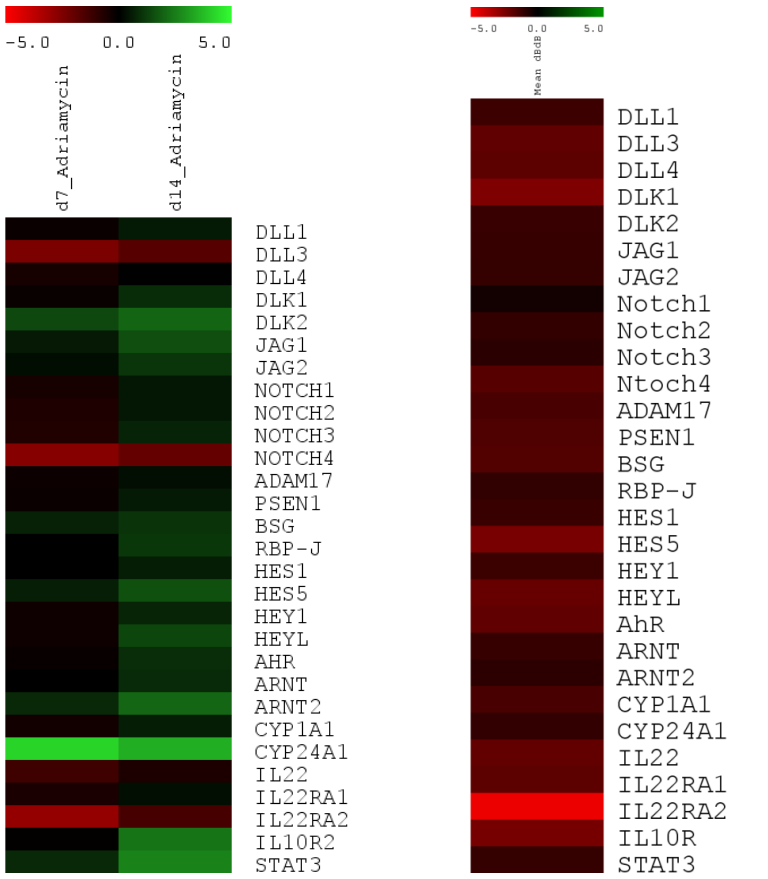

Figure 3-11 Gene expression of the Notch/AhR/IL-22 axis in adriamycin-induced nephropathy and diabetic nephropathy. Data from groups of 5-6 mice per group of each time point and expression normalized to age matched saline-injected BALB/cByJ mice for adriamycin-induced nephropathy and C57BLKS/J-Lepr wild-type mice for diabetic nephropathy, respectively.

3.4 Notch/AhR/IL-22 axis gene expression in human glomerular kidney disease

As we had explored Notch/AhR/IL-22 axis gene expression patterns in models of glomerular injury in mice, we sought to utilize microarray data from the ERCB consortium for Notch/AhR/IL-22 axis gene expression in human disease. For this, we selected patients with lupus nephritis (n=32; Fig. 3-12 left hand side), rapidly progressive glomerulonephritis (n=22; Fig. 3-12 right hand side), focal segmental glomerulonephritis (n=24; Fig. 3-13 left hand side), and diabetic nephropathy (n=12; Fig. 3-13 right hand side). Gene expression was normalized to biopsies of living donors (n=21). Unfortunately, while there are human homologues of all genes of our murine Notch/AhR/IL-22 gene panel, not all of the human homologues are covered by probes on the microarray platforms used by the ERCB consortium. Hence, those genes are marked grey in the heatmaps, as no expression values are available for those genes. Also, in contrast to the gene expression data from our mice experiments, where total kidney RNA isolated were used, the ERCB consortium micro-dissects the human biopsies to subsequently analyze glomerular and tubulointerstitial transcriptomes separately from each other.

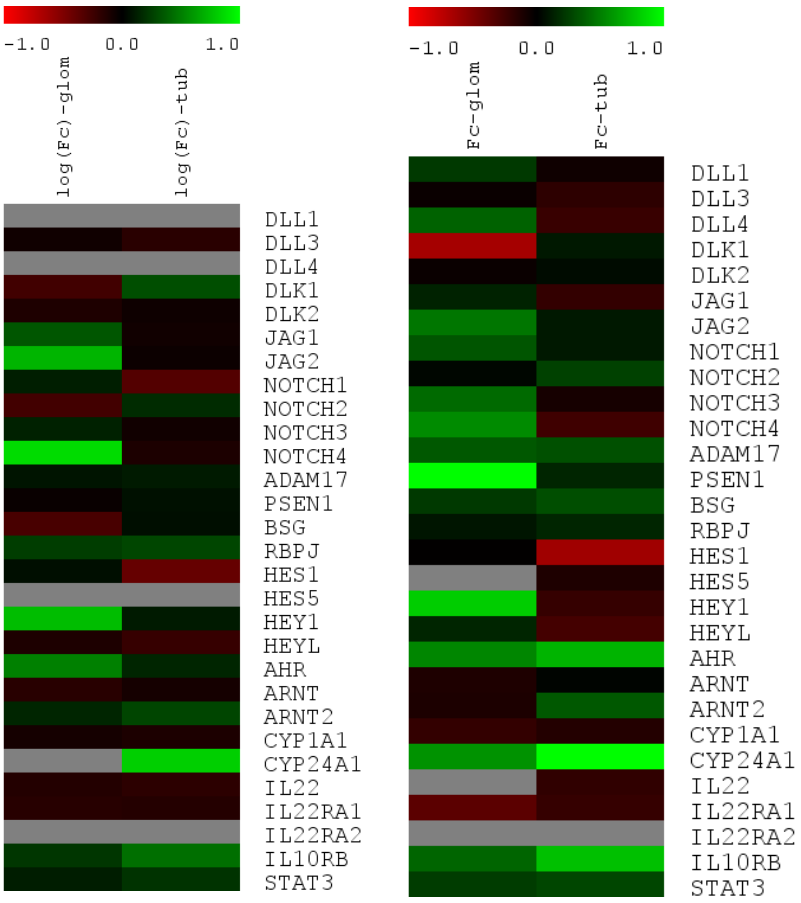

Figure 3-12 Gene expression of the Notch/AhR/IL-22 axis in human LN and RPGN. Grey bars indicate genes were no gene expression data were available. For details and sample number per disease see text. glom *glomerular*, tub *tubular*, log *decadic logarithm*, Fc *fold-change*.

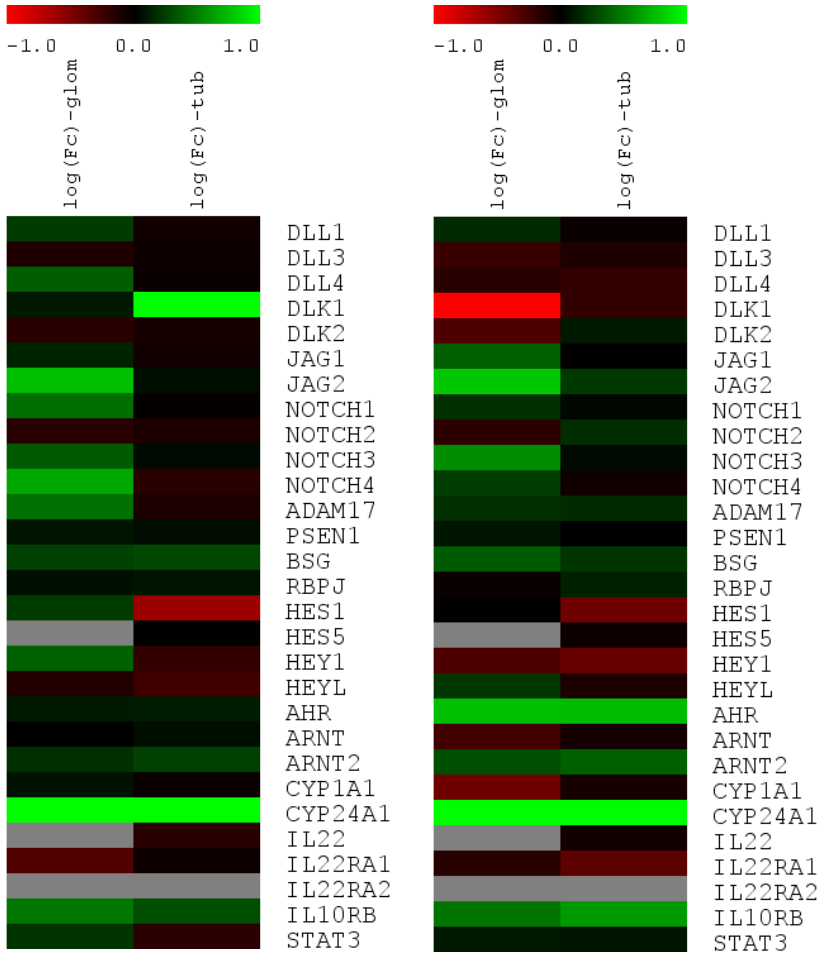

Figure 3-13 Gene expression of the Notch/AhR/IL-22 axis in human FSGS and DN. Grey bars indicate genes were no gene expression data were available. For details and sample number per disease see text. glom *glomerular*, tub *tubular*, log *decadic logarithm*, Fc *fold-change*.

3.5 Correlation between mouse models and human disease

We next sought to correlate the changes in gene expression of the Notch/AhR/IL-22 axis seen in humans and mice. For this purpose, we identified pairs of mouse models and corresponding human disease settings: the anti-GBM mouse model and rapidly progressive glomerulonephritis (RPGN), lupus nephritis (LN) in mice and men, adriamycin-induced nephropathy and focal-segmental glomerusclerosis, and diabetic nephropathy in mice and men. We then performed correlation analyses calculating Spearman correlation coefficients of gene expression for the entire Notch/AhR/IL-22 axis (Fig. 3-14). Significant correlations of gene expression were found for the anti-GBM mouse model and rapidly progressive glomerulonephritis (RPGN) ($r=0.51$, $p<0.01$) and for diabetic nephropathy ($r=0.37$, $p<0.05$).

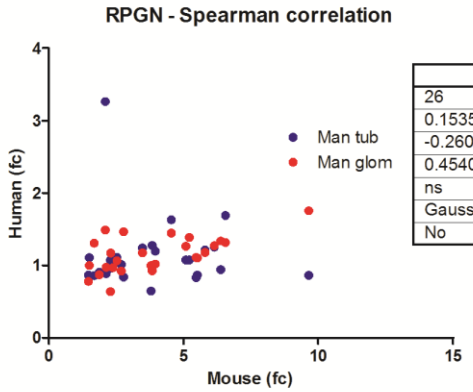

Man tub	Man glom
26	26
0.1535	0.5111
-0.2600 to 0.5195	0.1424 to 0.7553
0.4540	0.0076
ns	**
Gaussian Approximation	Gaussian Approximation
No	Yes

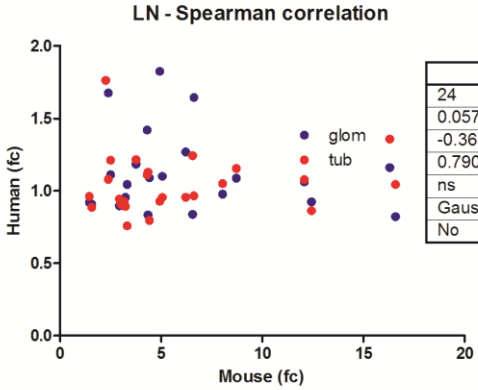

glom	tub
24	25
0.05739	0.1369
-0.3653 to 0.4605	-0.2845 to 0.5140
0.7900	0.5140
ns	ns
Gaussian Approximation	Gaussian Approximation
No	No

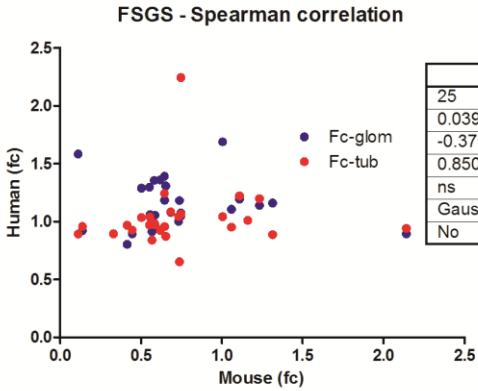

Fc-glom	Fc-tub
25	27
0.03962	0.2686
-0.3719 to 0.4382	-0.1358 to 0.5963
0.8508	0.1755
ns	ns
Gaussian Approximation	Gaussian Approximation
No	No

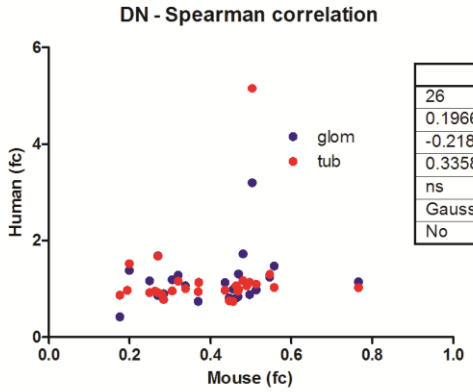

glom	tub
26	28
0.1966	0.3744
-0.2181 to 0.5512	-0.01017 to 0.6625
0.3358	0.0497
ns	*
Gaussian Approximation	Gaussian Approximation
No	Yes

Figure 3-14 Mouse/man correlation of gene expression of the Notch/AhR/IL-22 axis. glom *glomerular*, tub *tubular*, ns *non-significant*, * p<0.05

3.6 IL-22 protects tubular cells from calcium oxalate toxicity *in vitro*

As we saw an induction of IL22 gene expression in the acute oxalate nephropathy model, we stimulated a murine tubular epithelial cell line (MTC) with oxalate crystals *in vitro* and observed the effect of IL-22 administration on cell death as measured by LDH release into the supernatant as well as metabolic activity as indicated by the MTT assay (Fig. 3-15). While 1 mg of calcium oxalate (CaOx) crystals was able to kill 100% of MTC cells, this toxicity was reduced by IL-22 administration to around 20%. At the same time, IL-22 increased the metabolic activity of MTCs to around 140% compared to 5% FCS (positive control) despite the presence of CaOx crystals, while with CaOx crystals alone the metabolic activity of MTCs was decreased to around 60%.

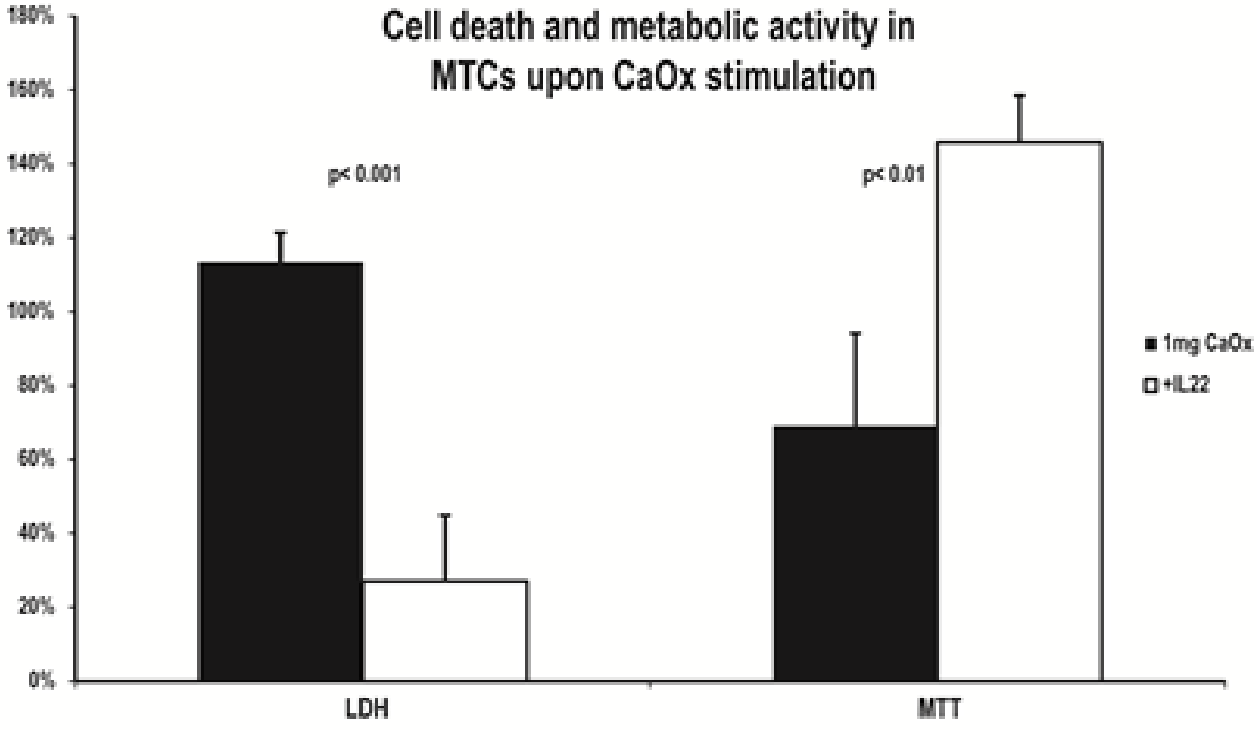

Figure 3-15 Effect of IL-22 on calcium oxalate toxicity in murine tubular cells. Data are representative of three independent experiments. CaOx *calcium oxalate*, MTC *murine tubular cells,* LDH *lactate dehydrogenase*, MTT *3-(4,5-dimethylthiazol-2-yl)-2,5-diphenyltetrazolium bromide.*

3.7 *IL22*-deficiency does not change the acute phase of rAOC *in vivo*

Given the effect of IL-22 on MTCs *in vitro*, we speculated that IL-22 might play a role also in rAOC in vivo. Interestingly, we did not find any difference in both the histopathological appearance or in gene expression of kidney injury markers between $IL22^{+/+}$ and $IL22^{-/-}$ 24 hours after rAOC (Fig. 3-16). Consistent with this, the expression TNFa, iNOS, CXCL2 and IL-6 were not changed at the time of maximal injury during rAOC

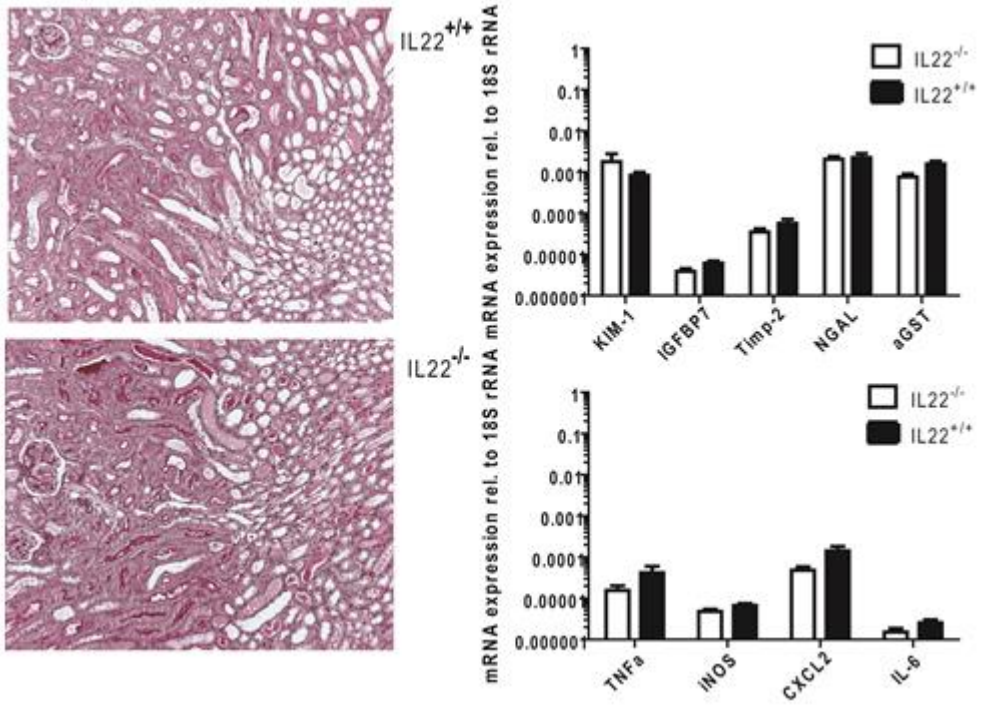

Figure 3-16 Histology and renal RTqPCR-based gene expression of injury markers and pro-inflammatory mediators in the injury phase of renal acute oxalate crystallopathy. n=5-6 mice per group.

3.8 *IL22*-deficiency does impair the regeneration after rAOC *in vivo*

When we followed mice after the induction of rAOC beyond the injury phase (i.e. 24 hours after oxalate injection), we noticed a delayed recovery of *IL22*-deficient animals. 48 hours after oxalate injection, serum creatinine and serum BUN of *IL22*-deficient mice was still highly elevated, while those parameters already started to decrease in *IL22*-competent mice (Fig. 3-17a). Conversely, the administration of rec. IL-22 24 hours after the oxalate injection into wild-type mice led to a significantly lower serum BUN 48 hours after the oxalate injection. Note that also the vehicle (PBS) has a positive effect on the

recovery compared to the values of untreated *IL22*-competent mice. Finally, when we followed mice even beyond 48 hours after oxalate injection, we observed a progressive mortality of *IL22*-deficient animals, which was not seen in wild-type animals (Fig. 3-17b). Taken together, while IL-22 does not play a role in the injury phase of rAOC, it has an important, non-redundant role during recovery from rAOC in mice.

a)

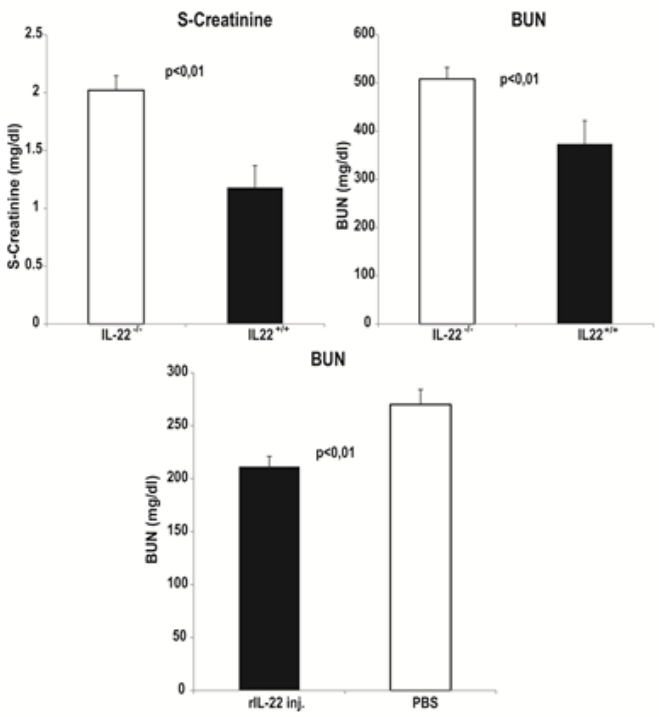

b)

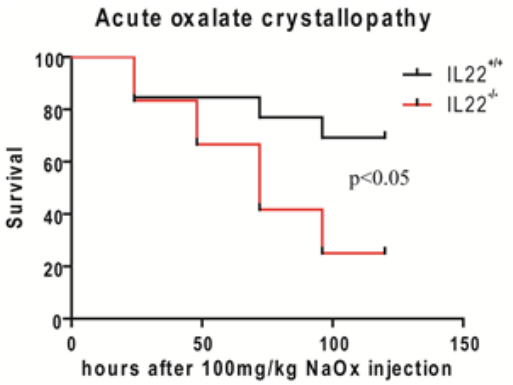

Figure 3-17 a) Serum creatinine and blood urea nitrogen during regeneration phase of renal acute oxalate crystallopathy.

b) Kaplan-Meier plots of $IL22^{+/+}$ and $IL22^{-/-}$ mice after CaOx injection. Group size: $IL22^{+/+}$ n=10 and $IL22^{-/-}$ n=12. BUN *blood urea nitrogen*, NaOx *sodium oxalate*, PBS *phosphate buffered-saline*.

3.9 IL-22 protects human tubular epithelial cells, but not renal progenitors from calcium oxalate toxicity *in vitro*

Given the positive effects of IL-22 on murine tubular epithelial cells during CaOx toxicity *in vitro* and the role of IL-22 in murine rAOC *in vivo*, we next stimulated both human renal progenitor cells (RPCs) and induced tubular epithelial cells (iTEX) made from RPCs with CaOx crystals in the presence or absence of IL-22. As shown in Fig. 3-18, while IL-22 does not protect RPCs from CaOx-induced cell death, such a protection is seen in iTEX cells, both early and late after CaOx stimulation and also mostly irrespective of CaOx dose. This effect is nicely paralleled by an increase of IL22-receptor expression during iTEX differentiation (data not shown). Taken together, IL-22 protects differentiated human tubular epithelial cells from CaOx toxicity *in vitro*, while it has no effect on human RPCs.

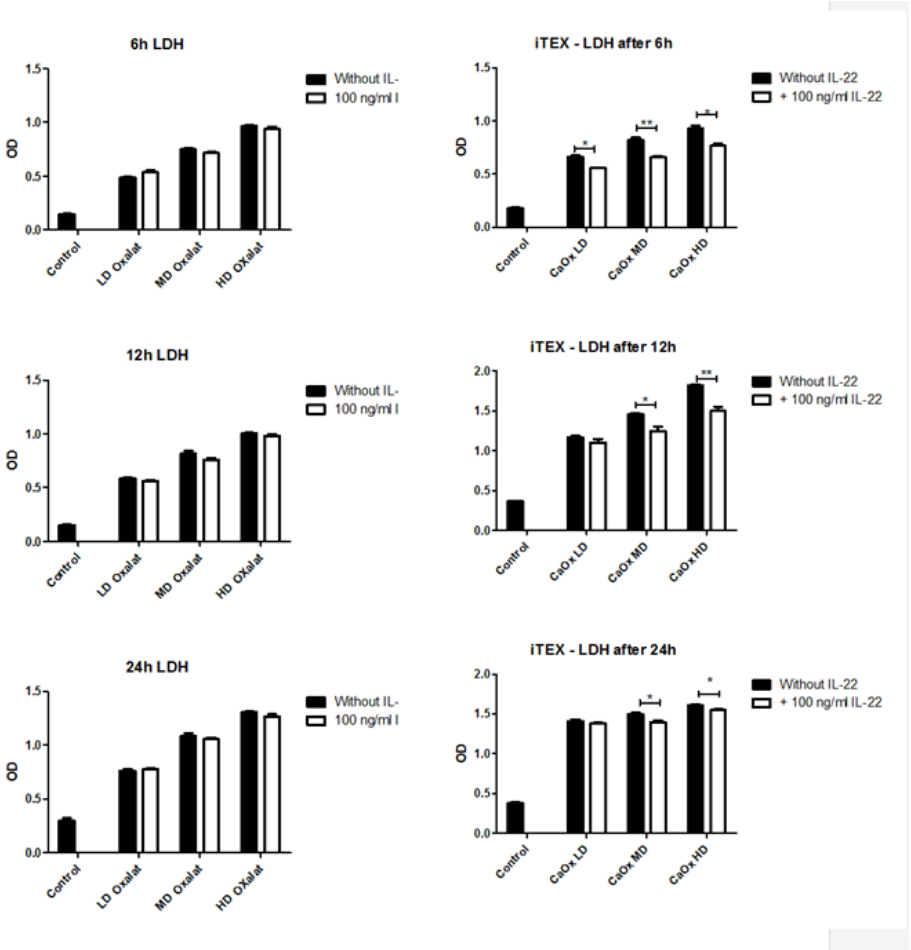

Figure 3-18 Effect of IL-22 on calcium oxalate toxicity in human renal progenitor cells (RPCs) and induced tubular epithelial cells (iTEX). Data are representative of three independent experiments. LDH *lactate dehydrogenase*, OD *optical density*, * $p<0.05$, ** $p<0.01$

3.10 IL-22 in unilateral ureteral obstruction

This section was published in "Marc Weidenbusch, Shangqing Song, Takamasa Iwakura, Chongxu Shi, Severin Rodler, Sebastian Kobold , Shrikant R. Mulay, Mohsen M. Honarpisheh & Hans-Joachim Anders. IL-22 sustains epithelial integrity in progressive kidney remodeling and fibrosis. Physiological Reports 2018 (6):15,e 13817".

3.10.1 IL22 expression increases after unilateral ureteral obstruction

We characterized the time course of IL-22 expression after UUO, performing renal IL-22 immunohistochemical stainings on day 1, day 5, and day 10 upon UUO in BALB/c mice (Fig 3-19). Mice genetically deficient in IL-22 were used as a negative control and indeed did not show any signal compared to secondary antibody incubation alone. Conversely, wild-type BALB/c mice showed scattered IL22+ cells in the interstitial space at baseline. This signal dramatically increased, as IL22+ cells accumulated after UUO progressively from day 1 to day 10. To rule out a strain specific effect, we used cDNA of UUO kidneys of C57Bl/6 mice from the gene expression project to perform RT-qPCR for IL-22 mRNA expression. Also in C57Bl/6 mice subjected to UUO, we found a significant increase of IL22 mRNA on day 10 after UUO. In conclusion, IL22 expression in the kidney increases during chronic injury.

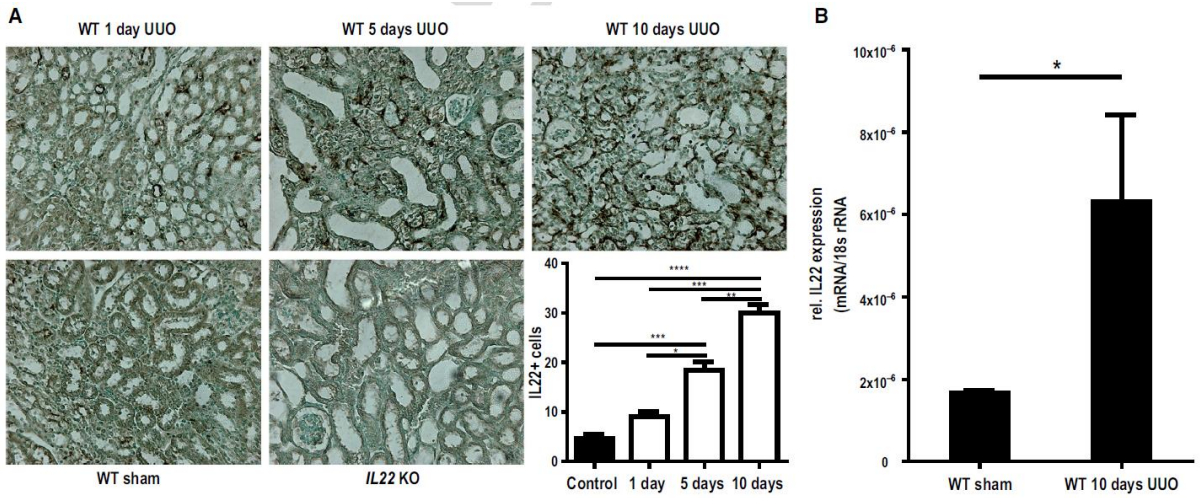

Figure 3-19 IL-22 expression after unilateral ureteral obstruction (UUO).

(A) Immunohistochemical IL-22 staining shows a progressive enrichment of interstitial IL22+ cells after UUO in Balb/C mice ($IL22^{-/-}$ UUO mice from day 5 are shown as negative staining control). (B) IL-22 gene expression is also significantly upregulated after 10d of UUO in C57/Bl6 mice. WT wild-type, KO knock-out *P < 0.05, **P < 0.01, ***P < 0.001.

3.10.2 *Il22*-deficient mice suffer from more UUO-induced tubular injury, but not tubular dilation and interstitial fibrosis

After left-sided UUO, all mice macroscopically developed hydronephrosis with progressive renal pelvis dilation and thinning of renal parenchyma (not shown). Upon histopathological evaluation by silver staining, we found tubular injury (as indicated by tubular flattening or karyorrhexis) to be significantly increased in *Il22*-deficient mice at both 5 days and 10 days after UUO surgery compared to wild-type mice (Fig. 3-20a+b). Of note, no differences in tubular dilation or interstitial fibrosis were detected between knock out and wild-type mice (Fig. 3-20 a+b). We concluded that IL-22 specifically protects tubular epithelial cells from UUO-induced chronic injury. To further corroborate this hypothesis, we next sought to quantify gene expression changes in UUO kidneys of both $Il22^{-/-}$ and $Il22^{+/+}$ mice by means of RTqPCR. Consistent with the histopathological findings, markers of tubular injury, such as kidney-injury molecule-1 (Kim1), neutrophil gelatinase-associated lipocalin (NGAL), insulin-like growth factor binding protein 7 (IGFBP7) and tissue inhibitor of metalloproteinase 2 (TIMP2) were increased in $Il22^{-/-}$ compared to $Il22^{+/+}$ mice both on day 5 and day 10 after UUO (Fig. 3-21 a), while we could not detect any significant differences in the expression of fibrotic markers such as COL1A1, transgelin or SSeCKs between $Il22^{-/-}$ and $Il22^{+/+}$ mice (Fig. 3-21b). Taken together, these data show that *Il22* deficiency increases tubular injury upon UUO but does not affect tubular dilation and interstitial fibrosis.

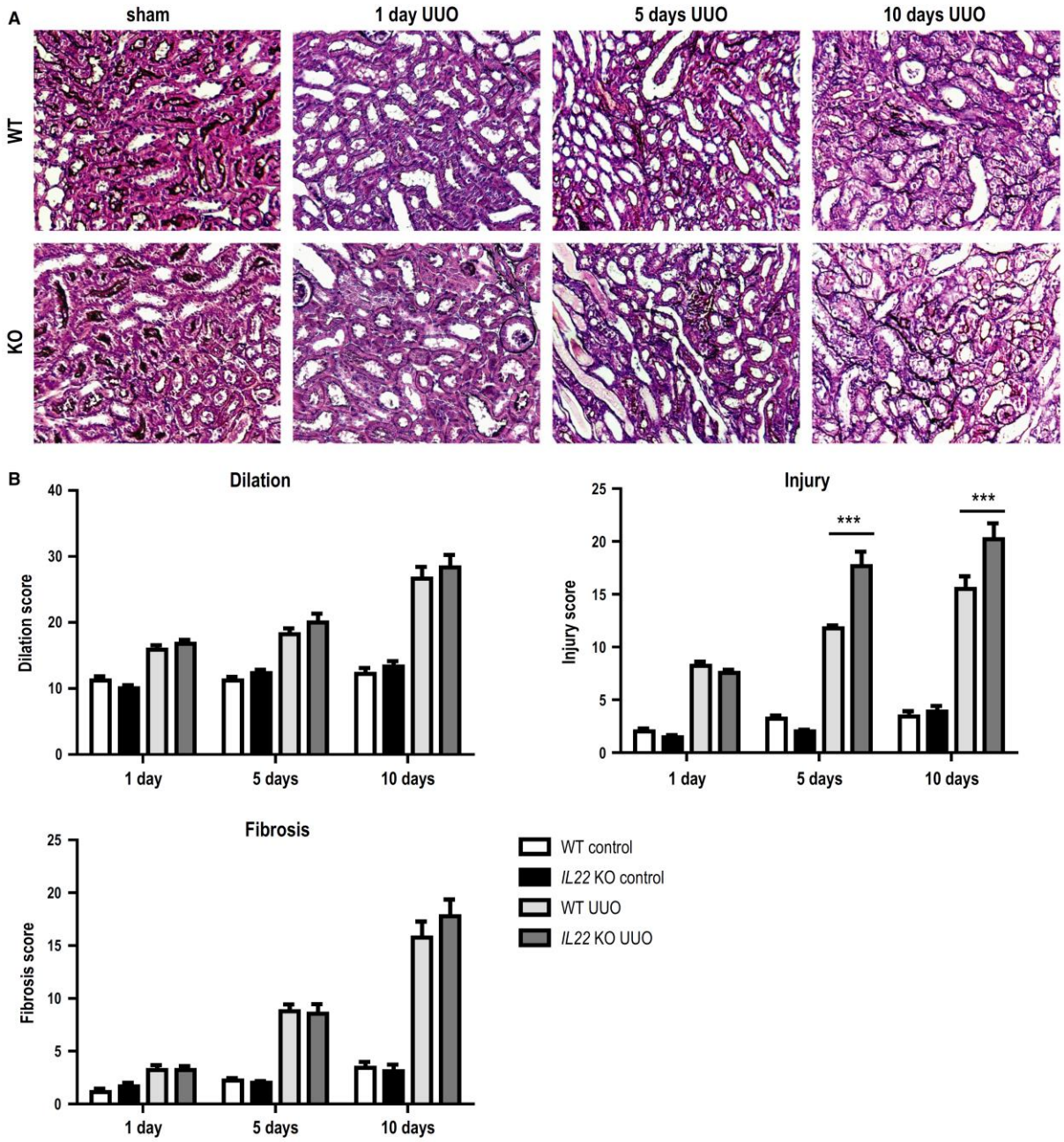

Figure 3-20 Histopathological changes after UUO in IL22+/+ and IL22-/- mice.

(A) Representative sections and (B) morphometric scores on tubular dilatation, tubular injury and interstitial fibrosis in IL22+/+ and IL22−/− mice after UUO. *** P < 0.001.

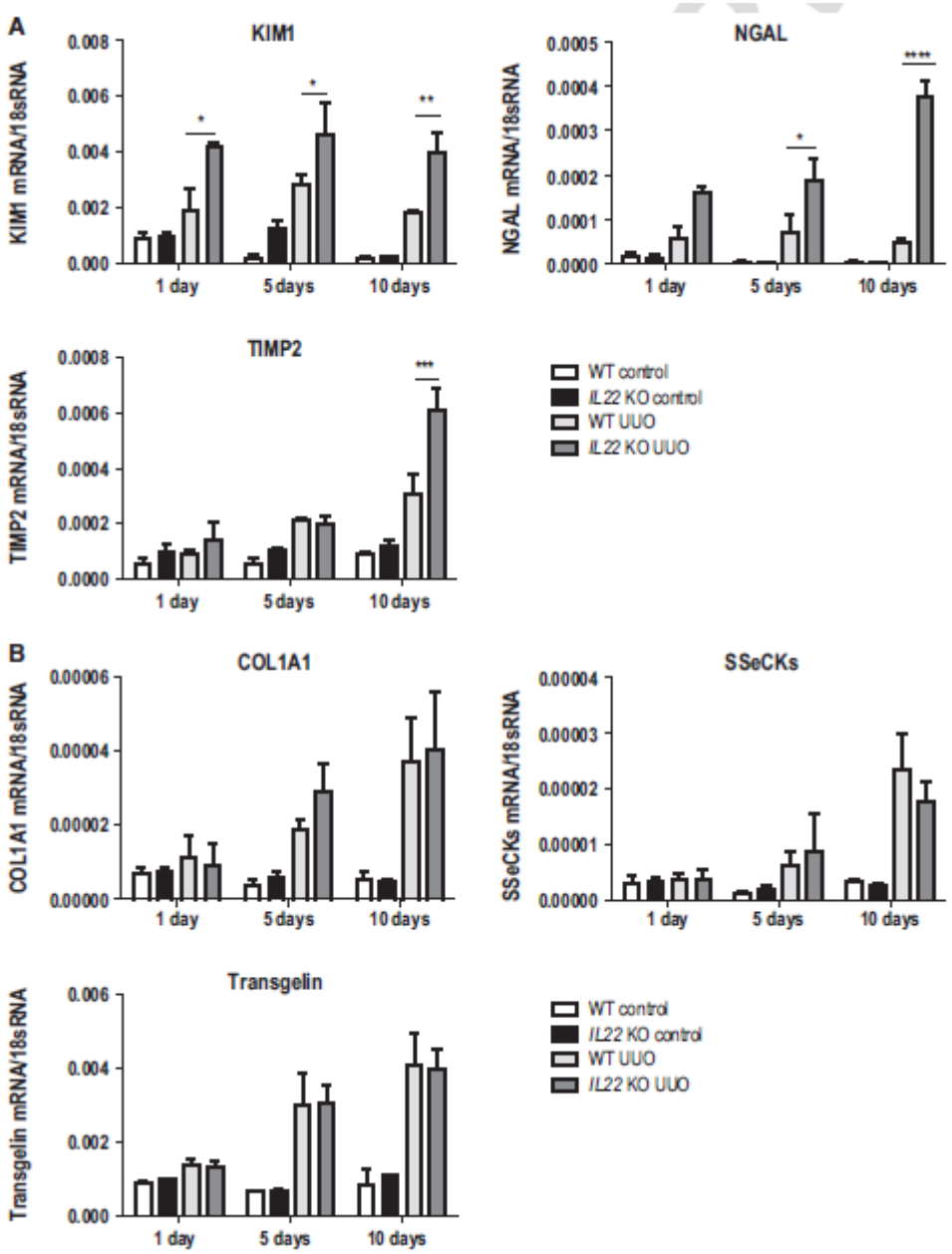

Figure 3-21 Gene expression of injury and fibrosis markers after UUO.

Markers of (A) kidney injury and (B) kidney fibrosis determined by reverse transcriptase quantitative PCR (RTqPCR). TIMP2 tissue inhibitor of metalloproteinases 2, NGAL neutrophil gelatinase-associated lipocalin, KIM1 kidney injury molecule 1, SSeCKs src-suppressed C-kinase substrate, COL1A1 collagen type 1 alpha 1. *P < 0.05, **P < 0.01, ***P < 0.001, ****P < 0.0001.

3.10.3 *Il22* deficiency leads to loss of proximal tubule cell mass through increased cell death upon UUO

To further classify the tubular cell phenotype of *IL22*-deficient animals, we performed *Lotus tetragonolobus* lectin staining to quantify proximal tubule cell mass. As shown in figure 3-22a, Lectin positive staining was markedly decreased in $Il22^{-/-}$ mice compared to $Il22^{+/+}$ mice 10 days post UUO (80% vs. 54%, respectively; $p<0.01$). Consistent with increased tubular cell death, there was an increase in TUNEL+ cells observed in $Il22^{-/-}$ mice compared to $Il22^{+/+}$ mice (Fig. 3-22b). Next, we performed TUNEL co-stainings with AQP1 and AQP2 to localize proximal and distal tubules, respectively. Interestingly, TUNEL positivity colocalized with AQP1+ proximal tubules exclusively, indicating that indeed increased cell death after UUO was the cause of the marked loss of proximal tubule cell mass in $Il22^{-/-}$ animals (Fig 3-22c). As TUNEL positivity is not truly specific for apoptosis (as previously thought), we performed additional gene expression analysis for FADD, CASP8 and CASP1 (Fig. 3-22d). All markers showed marked increases in $Il22^{-/-}$ mice compared to $Il22^{+/+}$ mice, corroborating the finding of increased tubular cell demise and subsequent tubular atrophy upon UUO in the absence of IL-22.

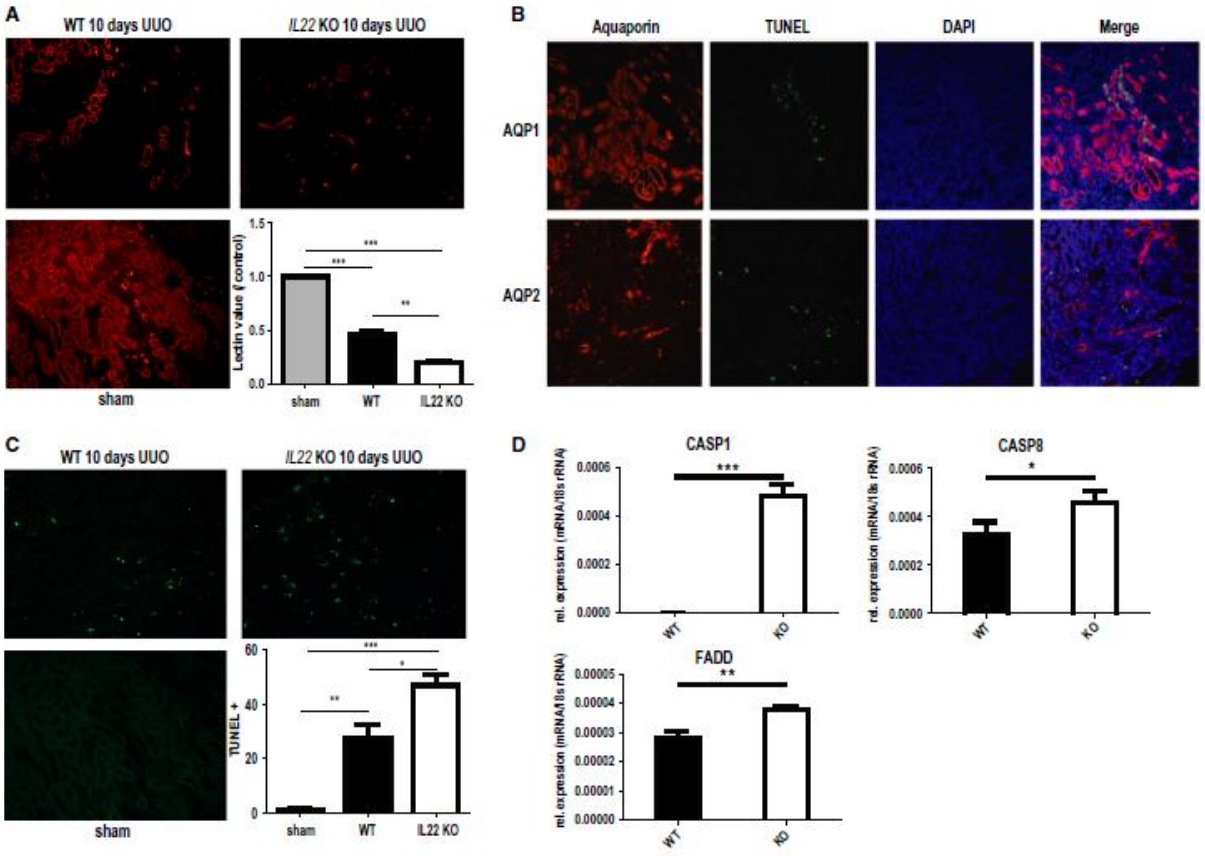

Figure 3-22 Tubular atrophy and tubular cell death after UUO.

(A) Immunofluorescence staining and quantitation of intact proximal tubular cell mass with Lotus tetragonolobus lectin in IL22+/+ and IL22−/−mice after 10d UUO. (B) TUNEL (TdT-mediated dUTP-biotin nick end labeling) staining and quantitation of cell death in IL22+/+ and IL22-/-mice after 10d UUO. (C) TUNEL (shown in green) co-immunostaining with aquaporin 1 (shown in orange, upper panel) and aquaporin 2 (shown in orange, lower panel) for localization of dying cells after UUO. (D) RTqPCR-based gene expression of apoptotic markers in IL22+/+ and IL22-/-mice after 10d UUO. CASP caspase, DAPI 40,6-Diamidin-2-phenylindol, FADD Fas-associated protein with death domain. *P < 0.05, **P < 0.01, ***P < 0.001.

3.10.4 *Il22* activates STAT3 and AKT signaling pathways upon UUO

IL-22 signaling has been shown to involve the downstream activation of both STAT3 and AKT pathways. Indeed we found decreased phosphorylation of both STAT3 and AKT in UUO kidneys of *Il22*$^{-/-}$ mice vs. *Il22*$^{+/+}$ mice at day 5 (Fig. 3-23a,c+d). Consistent with the abovementioned finding of increased cell death in *Il22*$^{-/-}$ mice, we also found increased protein levels of BAD, a pro-apoptotic mediator and known target of pAKT (Fig. 3-23b). Taken together, these finding indicate that IL-22 signaling activates STAT3 and AKT signaling pathways upon UUO.

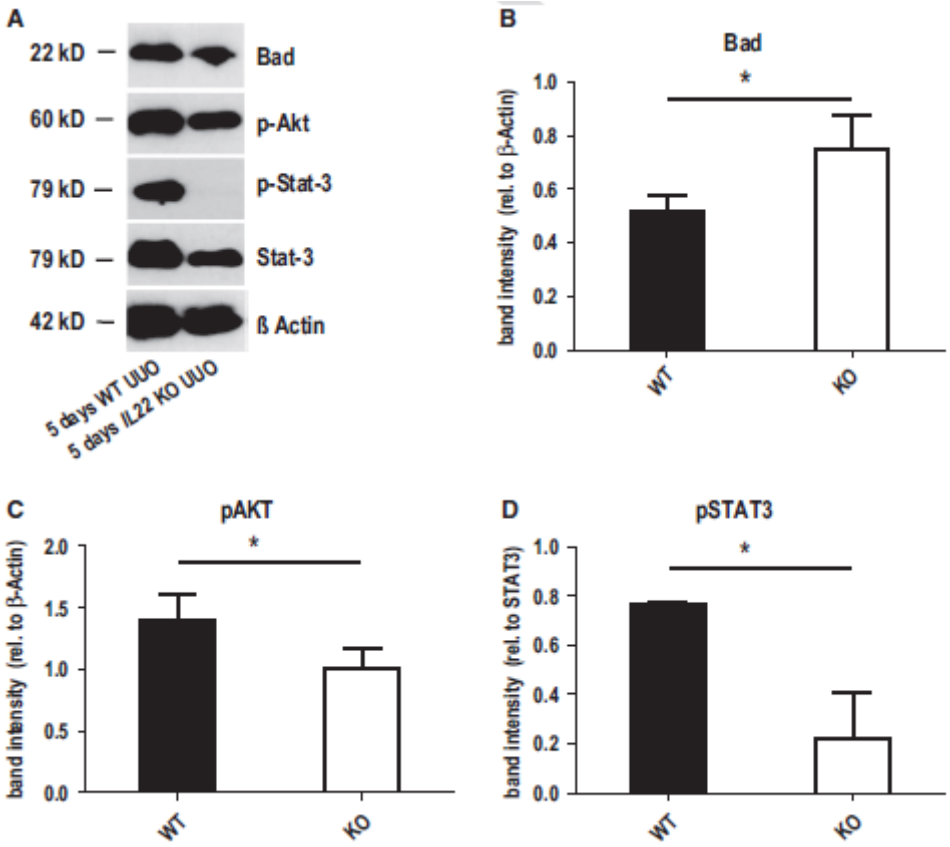

Figure 3-23 Tissue western blots after UUO in IL22+/+ and IL22−/−mice.

(A) Gel staining and (B)–(D) staining quantitation of western blots forthe apoptotic inducer Bad (B) and IL-22 receptor downstream signaling mediators STAT3 and Akt (C and D) in IL22+/+ and IL22-/-mice after 5d UUO. *P < 0.05.

3.10.5 *Il22* deficiency does not affect the rarefaction of peritubular microvasculature upon UUO

To investigate whether IL-22 plays an additional role on renal endothelium, CD31 staining was performed to analyze vascular rarefaction, which typically accompanies interstitial fibrosis in UUO. Compared with contralateral control kidneys, obstruction of the ureter induced a significant reduction in CD31 expression both at 5 days and 10 days post surgery (Fig. 3-24), as expected. Nevertheless, there was no difference of CD31 expression in kidneys dependent on *Il22* genotype, indicating that IL-22 has no effect on renal endothelial cells.

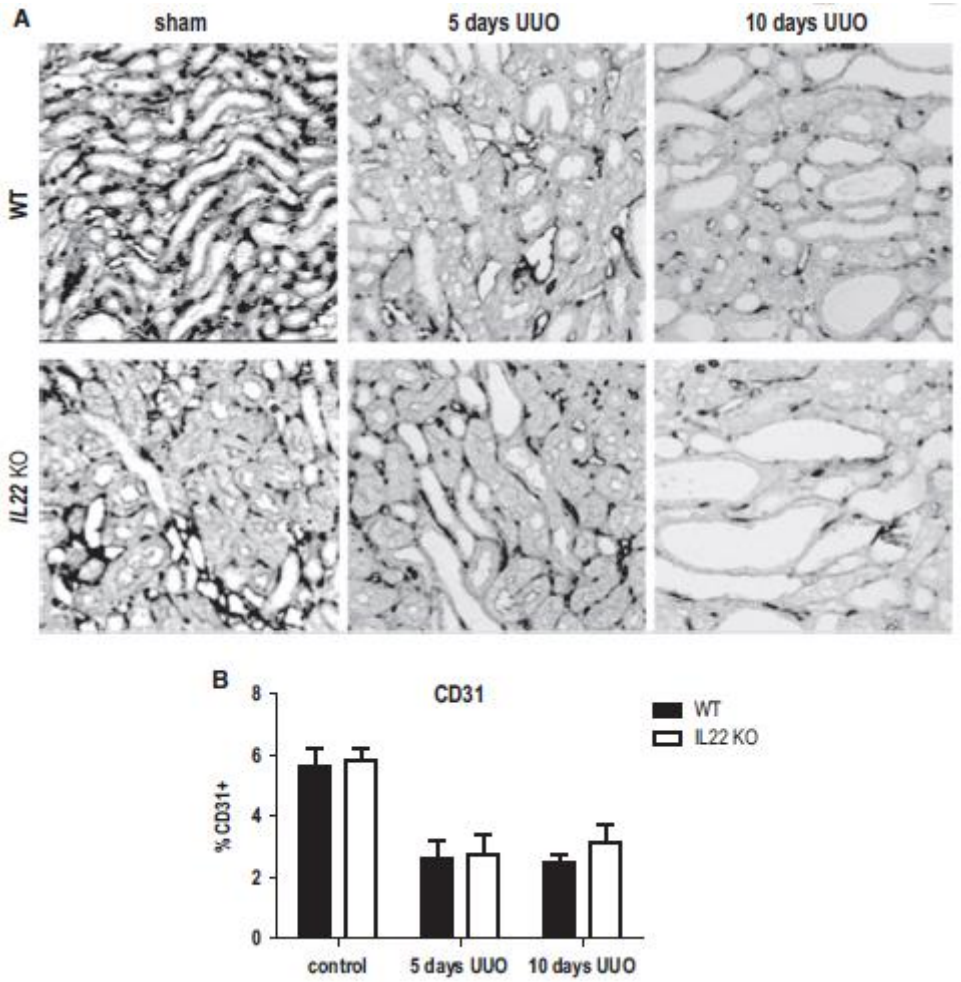

Figure 3-24 Capillary rarefaction after UUO in IL22+/+ and IL22−/− mice.

(A) Immunohistochemical CD31 staining and (B) CD31 staining quantitation in IL22+/+ and IL22-/-mice after 10d UUO.

3.10.6 IL-22 enhances proliferation of human tubular cells, but not fibroblasts *in vitro*

To evaluate if the effects of IL-22 seen after UUO in mice were transferable to human CKD, we performed experiments with human cells *in vitro*. First, we performed MTT assays in HK2 cells and K4 cells (human proximal tubular cell line and human fibroblast cell line, respectively) to evaluate the effect of IL-22 on human cell proliferation. After culturing for 24 hours, HK2 cells treated with each concentration of rhIL-22 proliferated remarkably compared with the medium group. Nonetheless, this phenomenon was not observed in K4IM cells, revealing that IL-22 increased proliferation in a epithelial cell type-specific manner (Fig. 3-25).

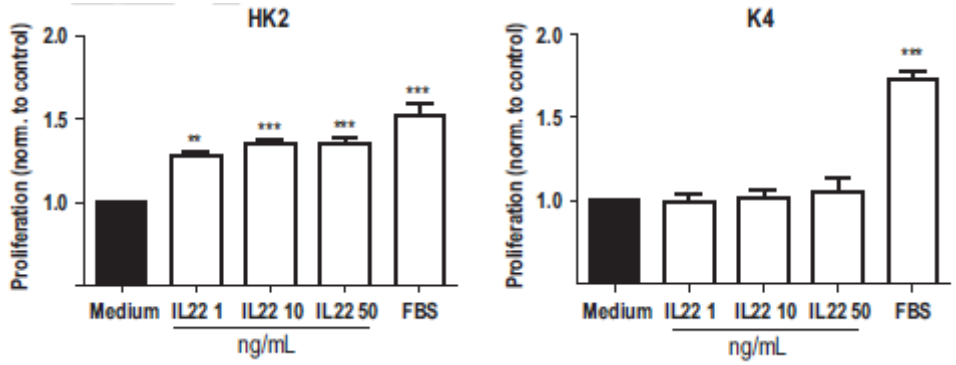

Figure 3-25 Effects of IL-22 on human tubular epithelial cells and fibroblasts.

Tetrazolium Reduction (MTT) assays with human tubular epithelial cells (HK2) and human dermal fibroblasts (K4) and increasing doses of recombinant human IL-22. Significance is indicated for comparison with control. **P < 0.01, ***P < 0.001.

3.10.7 IL-22 enhances migration, re-epithelialization and barrier function of both murine and human tubular epithelial cells

To mimic epithelial monolayer injury and re-epithelialization, we performed mechanical scratch assays of HK2 cells and K4 cells in the presence or absence of IL-22. In HK2 cells, IL-22 enhanced wound closure after 24 hours in a dose dependent manner (Fig. 3-26A), while no such effect was seen in scratch assays with K4 cells (Fig. 3-26B). To further characterize the effect of IL-22 on tubular epithelial cell barrier function, ECIS assays were performed allowing online monitoring of renal epithelial monolayers. As described in methods, $t_{1/2}$ was used to measure the effect of IL-22 on migration and proliferation capacities. Consistent with the results of scratch assays, $t_{1/2}$ in fence experiments, which mimic wound closure, was significantly shorter after rhIL-22 treatment (Figure 3-26C, E-H), confirming an IL-22-induced increase of cell migration and proliferation. To analyze the role of IL-22 on recovery after injury, electrical damage was executed to confluent HK2 cell monolayers. Again, IL-22 treatment shortened $t_{1/2}$ compared to vehicle (Figure 3-26D), indicating that IL-22 facilitates recovery after injury in human tubular cells. To further examine the role of IL-22 on recovery after kidney injury, murine primary tubular cells were stimulated with histones, which is released from dying tubular cells after kidney injury, then directly damages tubular cells, and promotes inflammation [28]. The

results showed that cells treated with IL-22 became confluent within 4h after removal of histones, while cells treated only with PBS did not show any regrowth during that time (Figure 3-26I-K), suggesting that IL-22 enables recovery after kidney injury.

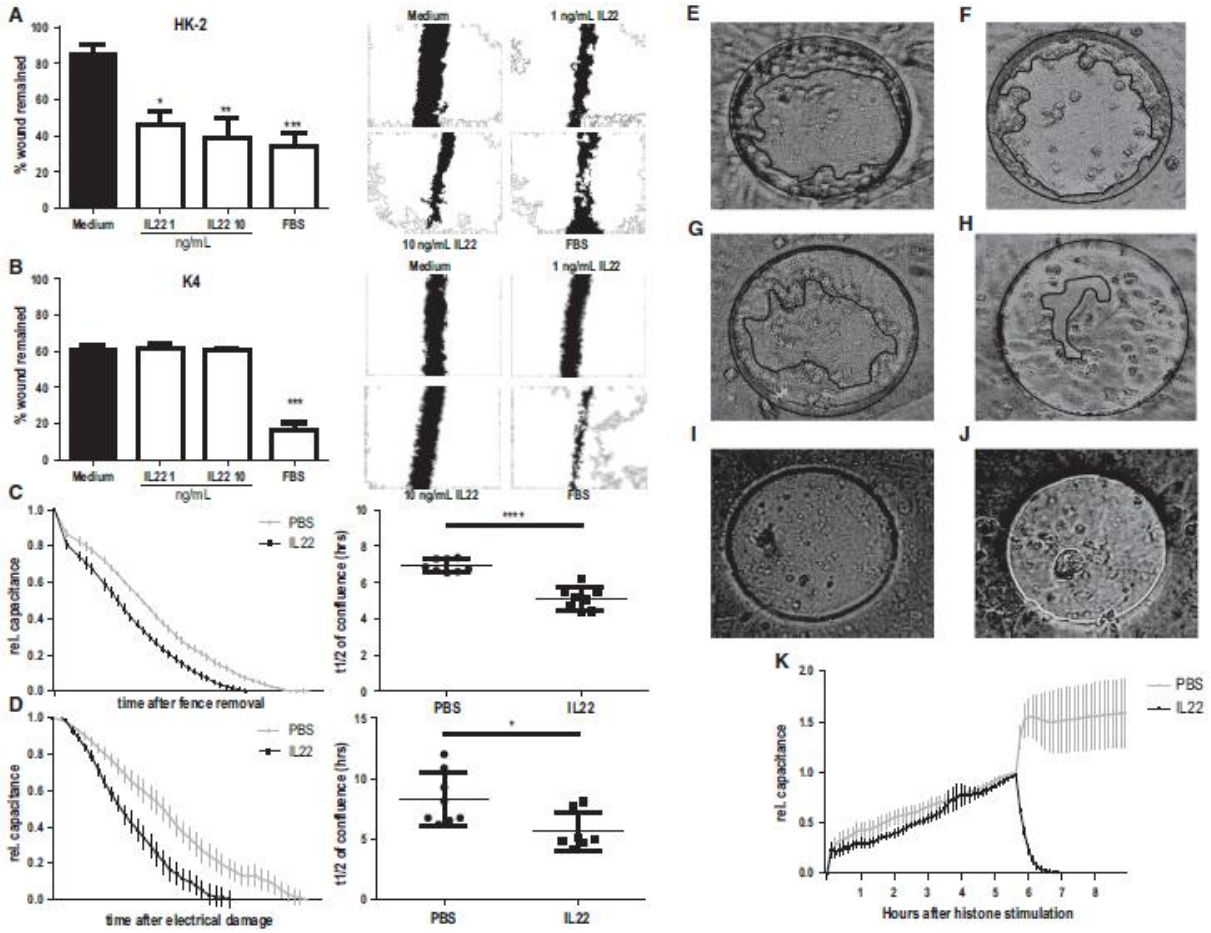

Figure 3-26 Effects of IL-22 in a human cell culture model of wound healing.

Scratch assays of (A) human tubular epithelial cells (HK2) and (B) human dermal fibroblasts (K4) increasing doses of recombinant human (rh)IL-22. Left side: Bar graphs for quantitation; right side: representative images for each condition. Significance is indicated for comparison with control. (C–K) Electric Cell-substrate Impedance Sensing (ECIS) experiments. Capacitance curves (left panel) and capacitance t1/2 comparison for vehicle (PBS) and rhIL-22 treatments of HK2 cells in C) fence removal and D) electrical damage experiments. (E–H) Photographs of ECIS device just after removing fence (E and F) or 5 h after removing fence (G and H). HK2 cells were treated with PBS (E and G) or rhIL-22 (F and H). Five hours later, wound is smaller in rhIL-22 treated well (H) than PBS treated well (G). (I and J) Photographs of ECIS device 4 h after exchanging medium with cells treated with vehicle (I) or rmIL-22 (J). (K) Capacitance curves for histone stimulation and subsequent vehicle (PBS) and rhIL-22 treatment of primary murine tubular epithelial cells. Note that no t1/2 can be calculated for vehicle treatment. *P < 0.05, **P < 0.01, ***P < 0.001.

4 Discussion

We had hypothesized, that IL-22, as well as its upstream regulators from the Notch and AhR signaling pathways, were differentially expressed during the induction and progression of several models of acute and chronic kidney disease. Indeed, we found differential expression of many genes of the Notch-AhR-IL22 pathway after kidney injury, with somewhat distinct patterns depending on the timing of injury (i.e. acute vs. chronic) and the intrarenal compartment of injury (i.e. tubular vs. glomerular injury). The most pronounced finding when comparing gene expression between different models was the expression pattern observed in diabetic nephropathy. In sharp contrast to the upregulation of the Notch-AhR-IL22 pathway gene expression, albeit in varying extents, in all other models, in diabetic nephropathy we found a significant downregulation of Notch-AhR-IL22 pathway gene expression. Interestingly, a recent publication on the role of IL-22 in diabetic nephropathy [140] also found IL-22 to be downregulated in diabetic mice. We cannot explain this apparent very divergent regulation of the Notch-AhR-IL22 pathway in diabetic nephropathy, hence the characterization of Notch-AhR-IL22 pathway gene expression in other models of diabetic nephropathy, e.g. the streptozotocin – induced model [141] or the Akita model [142], might be helpful to clarify if our findings can be recapitulated independent of the leptin receptor deficiency in our model of diabetic nephropathy.

In both acute and chronic models of tubular and glomerular injury, we found Notch ligands upregulated early after injury. While this upregulation was seen for both JAG genes and DLL genes in the acute models and in the tubular injury models, where the regeneration phase was studied, was transient in its nature, in chronic tubular and glomerular injury JAG, but not DLL genes were upregulated persistently with a non-significant trend towards the

additional upregulation of the endogenous Notch inhibitors DLK1 and DLK2 in the tubular models. Of note, this trend reached significance in the models of chronic glomerular injury. These findings could be explained by a pro-regenerative effect of the Notch pathway, which is turned on upon renal injury. As soon as the injury subsides, the pathway activation ceases, so in transient models of tubular injury, we observe only a transient upregulation of Notch ligands. If the injury persists, such as during continued renal obstruction or continued inflammation during lupus nephritis, Notch ligands stay upregulated. In order to inhibit overshooting regeneration, harbouring the risk of carcinogenesis [143], the Notch inhibitors are co-upregulated. Consistent with such a theory, both gain-of-function mutations/upregulation of Notch receptors and ligands [144], [145]) as well as loss-of-function mutations/downregulation of DLK1 [146], [147] and DLK2 [148] have been implicated in carcinogenesis. Nevertheless, these hypotheses on the effects of the expression patterns observed remain speculative. Taken together, on Notch ligands are differentially expressed during experimental kidney injury and regeneration.

As the induction of IL-22 gene expression in many cells is Ahr-dependent, it is noteworthy that we found an upregulation of Ahr upon renal in all models except for unilateral ureteral obstruction and diabetic nephropathy. Of note, in UUO we concomitantly observed the highest induction of IL-22 of all models studied. This finding raises the question if intrarenal IL-22 production is Ahr-dependent. Previous studies convincingly showed that myeloid cells produce IL-22 in the kidney upon injury and that IL-22 production in these cells can be induced by FICZ, a known Ahr ligand [92], but other IL-22 producing cells might exist. Additionally, we analysed the expression of the AHR binding partners ARNT and ARNT2: while ARNT was essentially co-regulated with AHR in all models, ARNT2 upregulation was less pronounced with the exception of the rCOC model, in which ARNT2, but no ARNT

upregulation was observed. As the differential roles of ARNT and ARNT2 on AHR signalling are incompletely understood [149], the relevance of this finding remains unknown.

We also had hypothesized, that the observed patterns of Notch/AhR/IL-22 axis gene expression in mice correlate with the respective gene expression found in corresponding human kidney disease. In fact, significant correlations, albeit with somewhat intermediate correlation strength, were observed for lupus nephritis and diabetic nephropathy. In the recent past, there has been considerable debate on the appropriateness of mouse models for the study of human disease, sometimes with diametral conclusions by different groups on the same data set (!) [150], [151]. Nevertheless, mouse research has led to therapeutic innovation in human disease, most recently with the advent of immune checkpoint blockade for various types of cancer [152].

Several issues have to be considered when valuing mice/men comparisons in general [153] as well as the correlations observed in this study:

1) issues of cross-platform comparison, as gene expression in mice was analyzed by means of RTqPCR, while in humans, gene expression values are based on microarray data; 2) issues of timing, as in the mouse model different time points can be easily assessed while all mice being matched for the respective time points, while human data are available only once a clinical decision for biopsy is made, which can vary greatly between patients (index biopsy after certain time points vs. newly diagnosed, active disease); 3) issues of treatment effects in humans, which virtually are all treated with some medication, while all mice in this study were therapy-naïve; 4) issues of genetic variability, as humans in the ERCB despite mostly being Caucasian are highly diverse, while all mice in this study are inbred, so genetic

variability is basically eliminated. All these differences render definitive statements based on the results of this work questionable. However, microarray data on the comparison between mice and men for lupus nephritis [154] and diabetic nephropathy [155] are available and generally show acceptable comparability. The analysis of the Notch-AhR-IL22 pathway in these datasets might be used to validate the findings of this work.

We had further hypothesized, that IL-22 exerts an active protective role during acute kidney injury as well as chronic kidney disease development rather than only being a biomarker for disease activity. Indeed, we did find biological effects of IL-22 in rAOC as well as UUO. Specifically, we were interested in the broader mode of action of IL-22 during kidney injury and regeneration, as available data yielded somewhat different conclusions: while one study described the function of IL-22 during ischemia-reperfusion injury mostly as a survival factor for renal tubular epithelial cells, ameliorating acute tubular cell death [122], the other study depicted IL-22 as a regeneration-promoting factor on tubular cells or renal progenitor cells, reinstituting tubular cell function after injury [92] . This study adds to the resolution of this question: 1) in humans, IL-22 acts on renal tubular epithelial cells, but not on renal progenitor cells. This finding is highly relevant, as very recently it has been shown that tubular regeneration is solely conferred by Pax2+ renal progenitors [156], but not by tubular epithelial cells, as previously thought [157]. Thus, the effect of IL-22 upon kidney injury is not mediated by progenitor cells and therefore most probably does not involve cell proliferation. 2) This study showed, that IL-22 maintains integrity of the tubular barrier and protects both from pressure-induced cell death in vivo as well as from crystal toxicity *in vitro* and *in vivo*. Interestingly, there was no significant difference in rAOC between $IL22^{+/+}$ and $IL22^{-/-}$ mice 24 hours after crystal administration. However, there was a significantly

increased mortality of IL22$^{-/-}$ compared to IL22$^{+/+}$ mice in the later phase of rAOC and the phenotype of wild-type mice could by ameliorated by the administration of exogenous Il-22. 3) This study excludes any effect of IL-22 on renal fibroblasts, as recent studies have shown IL-22 receptor expression in some extrarenal fibroblast populations [158-162]. This finding is important, as any effect of exogenously administered IL-22 on fibroblasts might trigger fibrosis, hence worsening the disease phenotype.

4.1 Limitations

Given the effect of IL-22 in rAOC as well as UUO, the study of the IL-22 knock-out in rCOC would have been most interesting. Of note, with genetic interventions the induction of nephrocalcinosis (i.e. the rCOC phenotype) in the knock-out mice needs to be carefully evaluated, as unexpected effect e.g. of the TNF-receptor on crystal formation have been observed [7]). Specifically, *Tnfr1-, Tnfr2-*, and *Tnfr1/2*-deficient mice do not develop nephrocalcinosis despite significant hyperoxaluria. Thus, the protection from nephrocalcinosis-related CKD is not due to an altered immune activation as in Nlrp3-deficient mice [44], but simply due to the absence of nephrocalcinosis. This finding is not trivial, as also in humans with the causative mutations for primary hyperoxaluria there is a variability of clinical manifestations [163], compatible with other genes regulating nephrocalcinosis development independent of oxalate levels. In line with this is the recent finding, that nephrocalcinosis development even differs between substrains of C57/BL6 mice [164]. As for this study the IL22 knock-out animals were on a Balb/c background, the induction of the rCOC could not be performed.

For the gene expression studies, obviously the methodological spectrum is limited. Except for IL-22, we did not validate our expression analyses results by a separate method. Also, a

better phenotypic characterization of cells expressing IL-22 within the tissues of acute and chronic disease animal models as well as a better evaluation of cell infiltration (only neutrophils and macrophages were characterized) could have been of value (e.g. by the co-immunofluorescence approach). Generally, changes in mRNA expression levels do not tell about gene functions in a given pathophysiological state. More in-depth studies (such as performed for rAOC and UUO) are required for such a conclusion. Thus, the data on all other models remain on a descriptive level.

The use of the UUO model, despite being well established for the study of CKD, has certain disadvantages: 1) as only one kidney is affected, serum retention parameters do not rise [165] and in general many of the hallmarks of CKD are not elicited (as opposed to the rCOC model), as the contralateral kidney fully compensates for the loss of function in the UUO kidney. Also, while reversible UUO has been described [50], this modification requires a second surgical intervention and introduces a lot of variability, as the degree of recanalization of the ureters varies between animals [51]. For theses reasons, the irreversible UUO model was used in this study, excluding the possibility to study effects of IL-22 during regeneration for chronic renal injury.

5 Abstract

IL-22 is a pro-regeneratory cytokine, that restores epithelial integrity upon injury in a wide array of tissues and diseases. IL-22 is exclusively produced by immune cells, while its receptor, IL22R, is specifically expressed on epithelial cells, making IL-22 a prototypic mediator of ‚immuno-epithelial' signaling. Among the upstream regulators of IL-22 are members of the Notch and Ahr signaling cascade, integrating important regulators of tissue homeostasis into downstream signaling of IL-22 through IL22R and STAT3.The present work aimed to determine the role of IL-22 in several different mouse models of glomerular and tubulointerstitial kidney disease and exploring its effects in chronic as well as acute kidney injury. We characterized the gene expression of the Notch/AhR/IL-22 axis in the models of acute and chronic oxalate nephropathy, unilateral ureteral obstruction, diabetic nephropathy, lupus nephritis, anti-GBM disease as well as adriamycin nephropathy and compared the gene expression patterns observed in the mouse models with the Notch/AhR/IL-22 axis gene expression in corresponding human kidney diseases to determine the relevance of the findings in the mouse model for the respective human disease. Finally, we employed IL22 knock-out mice as a tool to elucidate functional roles of IL-22 in acute oxalate nephropathy and progressive kidney fibrosis after unilateral ureteral obstruction. We found that Notch- and AhR-signaling were involved both in acute renal inflammation and chronic fibrosis with specific gene expression changes in each model. IL-22 was upregulated in acute inflammation, followed by a rapid downregulation during regeneration or, with the exception of unilateral ureteral obstruction, chronic injury. The gene expression patterns we found were mostly consistent between models of glomerular vs. tubulointerstitial disease as well as between mouse model and corresponding human

disease. In addition, IL-22 deficiency impaired the regeneration after acute oxalate crystallopathy leading to an excess mortality of IL22-defiencent animals during the regeneration phase, while exogenous IL-22 administration fastened regeneration upon injury. During chronic injury and progressive fibrosis, IL22-defiency further aggravated tubular injury and cell death, while no effect was seen on interstitial fibrosis. This effect was associated with less STAT3- and Akt- phosphorylation, but increased expression of the pro-apoptotic mediator Bad in obstructed kidneys of IL22-deficient mice compared to wild-type animals. Consistent with the findings in the mouse models, IL-22 improved human and mouse tubular epithelial cell survival and regeneration in several *in vitro* assays, while no effects of IL-22 on human or mouse fibroblasts were observed. Taken together, these findings indicate that IL-22 plays a role in several different mouse models of kidney disease and possibly also in the human counterparts of this model. The effect of IL-22 in the kidney is confined to tubular epithelial cells on which it acts both as a pro-survival and a pro-regenerative factor. More research is warranted to explore a potential role of IL-22 in kidney disease.

6 List of abbreviations

Ab	antibody
ADAM	a disintegrin and metalloprotease domain
AHR	aryl hydrocarbon receptor
AKI	acute kidney injury
AKIN	Acute Kidney Injury Network
ANOVA	analysis of variance
ARNT	aryl hydrocarbon receptor nuclear translocator
BSG	basigin
CaOx	calcium oxalate
CASP	caspase
cDNA	complementary desoxyribonucleic acid
CKD	chronic kidney disease
COL1A1	collagen
CYP	cytochrome p450
DLK	delta homolog
DLL	Delta-like
DMEM	Dulbecco's modified Eagle media
DN	diabetic nephropathy
ECIS	Epithelial barrier testing via electric cell–substrate impedance sensing
ERCB	European Renal cDNA bank
FADD	FAS-associated death domain
FDA	U.S. Food and Drug Administration
FSGS	focal segmental glomerulosclerosis
GBM	glomerular basement membrane
GFR	glomerular filtration rate
HES	hairy and enhancer of split-1
HEY	Hairy/enhancer-of-split related with YRPW motif
ICH	immunohistochemistry

IF	immunofluorescence
IL	interleukin
iTEX	induced tubular epithelial cells
JAG	jagged
KIM1	kidney injury molecule 1
LDH	lactate dehydrogenase
LN	lupus nephritis
MTT	3-(4,5-dimethylthiazol-2-yl)-2,5-diphenyltetrazolium bromide
NGAL	neutrophil gelatinase-associated lipocalin
OD	optical density
PAS	Periodic Acid Schiff Staining
PSEN	presenilin
qPCR	quantitative polymerase chain reaction
rAOC	renal acute oxalate crystallopathy
RBP-J	Recombining binding protein suppressor of hairless
rCOC	renal chronic oxalate crystallopathy
rIRI	renal ischemia-reperfusion injury
RNA	ribonucleic acid
RPC	renal progenitor cells
RPGN	rapidly progressive glomerulonephritis
RT	reverse transcription
SSeCKs	src suppressed C kinase substrate
STAT	signal transducer and activator of transcription
THP	Tamm-Horsfall protein
TIMP	tissue inhibitor of matrix metalloproteinase

7 References

1. Eckardt, K.U., et al., *Evolving importance of kidney disease: from subspecialty to global health burden.* Lancet, 2013. **382**(9887): p. 158-69.
2. Bruck, K., et al., *CKD Prevalence Varies across the European General Population.* J Am Soc Nephrol, 2016. **27**(7): p. 2135-47.
3. Coresh, J., et al., *Prevalence of chronic kidney disease in the United States.* JAMA, 2007. **298**(17): p. 2038-47.
4. Verband Deutsche Nierenzentren (DN), e.V. 2015 [cited 2018 August 14th]; Available from: http://www.die-nephrologen.de/index.php?id=fakten.
5. Kerr, M., et al., *Estimating the financial cost of chronic kidney disease to the NHS in England.* Nephrol Dial Transplant, 2012. **27 Suppl 3**: p. iii73-80.
6. Chertow, G.M., et al., *Acute kidney injury, mortality, length of stay, and costs in hospitalized patients.* J Am Soc Nephrol, 2005. **16**(11): p. 3365-70.
7. Mulay, S.R., et al., *Hyperoxaluria Requires TNF Receptors to Initiate Crystal Adhesion and Kidney Stone Disease.* J Am Soc Nephrol, 2017. **28**(3): p. 761-768.
8. Palevsky, P.M., *Chronic-on-acute kidney injury.* Kidney Int, 2012. **81**(5): p. 430-1.
9. Bucaloiu, I.D., et al., *Increased risk of death and de novo chronic kidney disease following reversible acute kidney injury.* Kidney Int, 2012. **81**(5): p. 477-85.
10. Rosner, M.H. and M.A. Perazella, *Acute Kidney Injury in Patients with Cancer.* N Engl J Med, 2017. **376**(18): p. 1770-1781.
11. Ferenbach, D.A. and J.V. Bonventre, *Mechanisms of maladaptive repair after AKI leading to accelerated kidney ageing and CKD.* Nat Rev Nephrol, 2015. **11**(5): p. 264-76.
12. Mehta, R.L., et al., *Acute Kidney Injury Network: report of an initiative to improve outcomes in acute kidney injury.* Crit Care, 2007. **11**(2): p. R31.
13. O'Riordan, P., P.E. Stevens, and E.J. Lamb, *Estimated glomerular filtration rate.* BMJ, 2014. **348**: p. g264.
14. Ferguson, T.W., P. Komenda, and N. Tangri, *Cystatin C as a biomarker for estimating glomerular filtration rate.* Curr Opin Nephrol Hypertens, 2015. **24**(3): p. 295-300.
15. Alge, J.L. and J.M. Arthur, *Biomarkers of AKI: a review of mechanistic relevance and potential therapeutic implications.* Clin J Am Soc Nephrol, 2015. **10**(1): p. 147-55.
16. Vijayan, A., et al., *Clinical Use of the Urine Biomarker [TIMP-2] x [IGFBP7] for Acute Kidney Injury Risk Assessment.* Am J Kidney Dis, 2016. **68**(1): p. 19-28.
17. *Notice.* Kidney International Supplements, 2012. **2**(1): p. 1.
18. Jang, H.R. and H. Rabb, *Immune cells in experimental acute kidney injury.* Nat Rev Nephrol, 2015. **11**(2): p. 88-101.
19. Linkermann, A., et al., *Regulated cell death in AKI.* J Am Soc Nephrol, 2014. **25**(12): p. 2689-701.
20. Romagnani, P., *Toward the identification of a "renopoietic system"?* Stem Cells, 2009. **27**(9): p. 2247-53.
21. Romagnani, P., L. Lasagni, and G. Remuzzi, *Renal progenitors: an evolutionary conserved strategy for kidney regeneration.* Nat Rev Nephrol, 2013. **9**(3): p. 137-46.
22. Mulay, S.R. and H.J. Anders, *Crystallopathies.* N Engl J Med, 2016. **374**(25): p. 2465-76.

23. Anders, H.J., *Immune system modulation of kidney regeneration--mechanisms and implications.* Nat Rev Nephrol, 2014. **10**(6): p. 347-58.
24. Levey, A.S., et al., *Definition and classification of chronic kidney disease: a position statement from Kidney Disease: Improving Global Outcomes (KDIGO).* Kidney Int, 2005. **67**(6): p. 2089-100.
25. Romagnani, P., et al., *Chronic kidney disease.* Nat Rev Dis Primers, 2017. **3**: p. 17088.
26. Nastase, M.V., et al., *Targeting renal fibrosis: Mechanisms and drug delivery systems.* Adv Drug Deliv Rev, 2018. **129**: p. 295-307.
27. Allinovi, M., et al., *Anti-fibrotic treatments: A review of clinical evidence.* Matrix Biol, 2018. **68-69**: p. 333-354.
28. Allam, R., et al., *Histones from dying renal cells aggravate kidney injury via TLR2 and TLR4.* J Am Soc Nephrol, 2012. **23**(8): p. 1375-88.
29. Lech, M., et al., *Macrophage phenotype controls long-term AKI outcomes--kidney regeneration versus atrophy.* J Am Soc Nephrol, 2014. **25**(2): p. 292-304.
30. Anders, H.J., et al., *The macrophage phenotype and inflammasome component NLRP3 contributes to nephrocalcinosis-related chronic kidney disease independent from IL-1-mediated tissue injury.* Kidney Int, 2018. **93**(3): p. 656-669.
31. Eltzschig, H.K. and T. Eckle, *Ischemia and reperfusion--from mechanism to translation.* Nat Med, 2011. **17**(11): p. 1391-401.
32. Cavaille-Coll, M., et al., *Summary of FDA workshop on ischemia reperfusion injury in kidney transplantation.* Am J Transplant, 2013. **13**(5): p. 1134-48.
33. El Sabbahy, M. and V.S. Vaidya, *Ischemic kidney injury and mechanisms of tissue repair.* Wiley Interdiscip Rev Syst Biol Med, 2011. **3**(5): p. 606-18.
34. Bonventre, J.V. and A. Zuk, *Ischemic acute renal failure: an inflammatory disease?* Kidney Int, 2004. **66**(2): p. 480-5.
35. Chouchani, E.T., et al., *Ischaemic accumulation of succinate controls reperfusion injury through mitochondrial ROS.* Nature, 2014. **515**(7527): p. 431-435.
36. Mulay, S.R., et al., *How Kidney Cell Death Induces Renal Necroinflammation.* Semin Nephrol, 2016. **36**(3): p. 162-73.
37. Linkermann, A., et al., *Regulated cell death and inflammation: an auto-amplification loop causes organ failure.* Nat Rev Immunol, 2014. **14**(11): p. 759-67.
38. Schofield, Z.V., et al., *Neutrophils--a key component of ischemia-reperfusion injury.* Shock, 2013. **40**(6): p. 463-70.
39. McMartin, K., *Are calcium oxalate crystals involved in the mechanism of acute renal failure in ethylene glycol poisoning?* Clin Toxicol (Phila), 2009. **47**(9): p. 859-69.
40. Mulay, S.R., et al., *Calcium oxalate crystals induce renal inflammation by NLRP3-mediated IL-1beta secretion.* J Clin Invest, 2013. **123**(1): p. 236-46.
41. Mulay, S.R., et al., *Cytotoxicity of crystals involves RIPK3-MLKL-mediated necroptosis.* Nat Commun, 2016. **7**: p. 10274.
42. Watts, R.W., *Primary hyperoxaluria type I.* QJM, 1994. **87**(10): p. 593-600.
43. Latta, K. and J. Brodehl, *Primary hyperoxaluria type I.* Eur J Pediatr, 1990. **149**(8): p. 518-22.
44. Knauf, F., et al., *NALP3-mediated inflammation is a principal cause of progressive renal failure in oxalate nephropathy.* Kidney Int, 2013. **84**(5): p. 895-901.
45. Mulay, S.R., et al., *Oxalate-induced chronic kidney disease with its uremic and cardiovascular complications in C57BL/6 mice.* Am J Physiol Renal Physiol, 2016. **310**(8): p. F785-F795.

46. Lorenz, G., M.N. Darisipudi, and H.J. Anders, *Canonical and non-canonical effects of the NLRP3 inflammasome in kidney inflammation and fibrosis.* Nephrol Dial Transplant, 2014. **29**(1): p. 41-8.
47. Steiger, S., et al., *Anti-Transforming Growth Factor beta IgG Elicits a Dual Effect on Calcium Oxalate Crystallization and Progressive Nephrocalcinosis-Related Chronic Kidney Disease.* Front Immunol, 2018. **9**: p. 619.
48. Wahlberg, J., *The renal response to ureteral obstruction.* Scand J Urol Nephrol Suppl, 1983. **73**: p. 1-30.
49. Higgins, D.F., et al., *Hypoxia promotes fibrogenesis in vivo via HIF-1 stimulation of epithelial-to-mesenchymal transition.* J Clin Invest, 2007. **117**(12): p. 3810-20.
50. Cochrane, A.L., et al., *Renal structural and functional repair in a mouse model of reversal of ureteral obstruction.* J Am Soc Nephrol, 2005. **16**(12): p. 3623-30.
51. Chaabane, W., et al., *Renal functional decline and glomerulotubular injury are arrested but not restored by release of unilateral ureteral obstruction (UUO).* Am J Physiol Renal Physiol, 2013. **304**(4): p. F432-9.
52. Wendt, T., et al., *Glucose, glycation, and RAGE: implications for amplification of cellular dysfunction in diabetic nephropathy.* J Am Soc Nephrol, 2003. **14**(5): p. 1383-95.
53. Gugliucci, A. and T. Menini, *The axis AGE-RAGE-soluble RAGE and oxidative stress in chronic kidney disease.* Adv Exp Med Biol, 2014. **824**: p. 191-208.
54. Reidy, K., et al., *Molecular mechanisms of diabetic kidney disease.* J Clin Invest, 2014. **124**(6): p. 2333-40.
55. Komala, M.G., et al., *Sodium glucose cotransporter 2 and the diabetic kidney.* Curr Opin Nephrol Hypertens, 2013. **22**(1): p. 113-9.
56. Ferrannini, E. and W.C. Cushman, *Diabetes and hypertension: the bad companions.* Lancet, 2012. **380**(9841): p. 601-10.
57. Anders, H.J., J.M. Davis, and K. Thurau, *Nephron Protection in Diabetic Kidney Disease.* N Engl J Med, 2016. **375**(21): p. 2096-2098.
58. Ninichuk, V., et al., *Tubular atrophy, interstitial fibrosis, and inflammation in type 2 diabetic db/db mice. An accelerated model of advanced diabetic nephropathy.* Eur J Med Res, 2007. **12**(8): p. 351-5.
59. Vallon, V., et al., *SGLT2 inhibitor empagliflozin reduces renal growth and albuminuria in proportion to hyperglycemia and prevents glomerular hyperfiltration in diabetic Akita mice.* Am J Physiol Renal Physiol, 2014. **306**(2): p. F194-204.
60. Wanner, C., et al., *Empagliflozin and Progression of Kidney Disease in Type 2 Diabetes.* N Engl J Med, 2016. **375**(4): p. 323-34.
61. Ghodke-Puranik, Y. and T.B. Niewold, *Immunogenetics of systemic lupus erythematosus: A comprehensive review.* J Autoimmun, 2015. **64**: p. 125-36.
62. Andrews, B.S., et al., *Spontaneous murine lupus-like syndromes. Clinical and immunopathological manifestations in several strains.* J Exp Med, 1978. **148**(5): p. 1198-215.
63. Watanabe-Fukunaga, R., et al., *Lymphoproliferation disorder in mice explained by defects in Fas antigen that mediates apoptosis.* Nature, 1992. **356**(6367): p. 314-7.
64. Reap, E.A., et al., *Apoptosis abnormalities of splenic lymphocytes in autoimmune lpr and gld mice.* J Immunol, 1995. **154**(2): p. 936-43.
65. Izui, S., et al., *Induction of various autoantibodies by mutant gene lpr in several strains of mice.* J Immunol, 1984. **133**(1): p. 227-33.

66. Liu, Z. and A. Davidson, *Taming lupus-a new understanding of pathogenesis is leading to clinical advances.* Nat Med, 2012. **18**(6): p. 871-82.
67. Lech, M. and H.J. Anders, *The pathogenesis of lupus nephritis.* J Am Soc Nephrol, 2013. **24**(9): p. 1357-66.
68. Muhammad, S., *Nephrotoxic nephritis and glomerulonephritis: animal model versus human disease.* Br J Biomed Sci, 2014. **71**(4): p. 168-71.
69. Hoppe, J.M. and V. Vielhauer, *Induction and analysis of nephrotoxic serum nephritis in mice.* Methods Mol Biol, 2014. **1169**: p. 159-74.
70. Kumar, S.V., et al., *Neutrophil Extracellular Trap-Related Extracellular Histones Cause Vascular Necrosis in Severe GN.* J Am Soc Nephrol, 2015. **26**(10): p. 2399-413.
71. Unanue, E.R. and F.J. Dixon, *Experimental Glomerulonephritis. Vi. The Autologous Phase of Nephrotoxic Serum Nephritis.* J Exp Med, 1965. **121**: p. 715-25.
72. Bideak, A., et al., *The atypical chemokine receptor 2 limits renal inflammation and fibrosis in murine progressive immune complex glomerulonephritis.* Kidney Int, 2018. **93**(4): p. 826-841.
73. Jefferson, J.A. and S.J. Shankland, *The pathogenesis of focal segmental glomerulosclerosis.* Adv Chronic Kidney Dis, 2014. **21**(5): p. 408-16.
74. Fogo, A.B., *Causes and pathogenesis of focal segmental glomerulosclerosis.* Nat Rev Nephrol, 2015. **11**(2): p. 76-87.
75. Kopp, J.B. and C.A. Winkler, *Genetics, Genomics, and Precision Medicine in End-Stage Kidney Disease.* Semin Nephrol, 2018. **38**(4): p. 317-324.
76. Yang, J.W., et al., *Recent advances of animal model of focal segmental glomerulosclerosis.* Clin Exp Nephrol, 2018. **22**(4): p. 752-763.
77. Pereira Wde, F., et al., *The experimental model of nephrotic syndrome induced by Doxorubicin in rodents: an update.* Inflamm Res, 2015. **64**(5): p. 287-301.
78. Lee, V.W., et al., *Adriamycin nephropathy in severe combined immunodeficient (SCID) mice.* Nephrol Dial Transplant, 2006. **21**(11): p. 3293-8.
79. Wang, Y., et al., *Depletion of CD4(+) T cells aggravates glomerular and interstitial injury in murine adriamycin nephropathy.* Kidney Int, 2001. **59**(3): p. 975-84.
80. Pippin, J.W., et al., *Inducible rodent models of acquired podocyte diseases.* Am J Physiol Renal Physiol, 2009. **296**(2): p. F213-29.
81. Weidenbusch, M., S. Rodler, and H.J. Anders, *Interleukin-22 in kidney injury and regeneration.* Am J Physiol Renal Physiol, 2015. **308**(10): p. F1041-6.
82. Dudakov, J.A., A.M. Hanash, and M.R. van den Brink, *Interleukin-22: immunobiology and pathology.* Annu Rev Immunol, 2015. **33**: p. 747-85.
83. Nikoopour, E., S.M. Bellemore, and B. Singh, *IL-22, cell regeneration and autoimmunity.* Cytokine, 2015. **74**(1): p. 35-42.
84. Sonnenberg, G.F., L.A. Fouser, and D. Artis, *Border patrol: regulation of immunity, inflammation and tissue homeostasis at barrier surfaces by IL-22.* Nat Immunol, 2011. **12**(5): p. 383-90.
85. Nikoopour, E., S.M. Bellemore, and B. Singh, *IL-22, cell regeneration and autoimmunity.* Cytokine, 2014.
86. Wolk, K., et al., *Biology of interleukin-22.* Semin Immunopathol, 2010. **32**(1): p. 17-31.
87. Wolk, K. and R. Sabat, *Interleukin-22: a novel T- and NK-cell derived cytokine that regulates the biology of tissue cells.* Cytokine Growth Factor Rev, 2006. **17**(5): p. 367-80.
88. Nagem, R.A., et al., *Crystal structure of recombinant human interleukin-22.* Structure, 2002. **10**(8): p. 1051-62.

89. Wolk, K., et al., *IL-22 increases the innate immunity of tissues.* Immunity, 2004. **21**(2): p. 241-54.
90. Tachiiri, A., et al., *Genomic structure and inducible expression of the IL-22 receptor alpha chain in mice.* Genes Immun, 2003. **4**(2): p. 153-9.
91. Spits, H., et al., *Innate lymphoid cells--a proposal for uniform nomenclature.* Nat Rev Immunol, 2013. **13**(2): p. 145-9.
92. Kulkarni, O.P., et al., *Toll-like receptor 4-induced IL-22 accelerates kidney regeneration.* J Am Soc Nephrol, 2014. **25**(5): p. 978-89.
93. Zheng, Y., et al., *Interleukin-22 mediates early host defense against attaching and effacing bacterial pathogens.* Nat Med, 2008. **14**(3): p. 282-9.
94. Eyerich, S., et al., *IL-17 and IL-22: siblings, not twins.* Trends Immunol, 2010. **31**(9): p. 354-61.
95. Mezrich, J.D., et al., *An interaction between kynurenine and the aryl hydrocarbon receptor can generate regulatory T cells.* J Immunol, 2010. **185**(6): p. 3190-8.
96. Ema, M., et al., *Dioxin binding activities of polymorphic forms of mouse and human arylhydrocarbon receptors.* J Biol Chem, 1994. **269**(44): p. 27337-43.
97. Veldhoen, M., et al., *The aryl hydrocarbon receptor links TH17-cell-mediated autoimmunity to environmental toxins.* Nature, 2008. **453**(7191): p. 106-9.
98. Zheng, Y., et al., *Interleukin-22, a T(H)17 cytokine, mediates IL-23-induced dermal inflammation and acanthosis.* Nature, 2007. **445**(7128): p. 648-51.
99. Tominaga, A., et al., *Autonomous cure of damaged human intestinal epithelial cells by TLR2 and TLR4-dependent production of IL-22 in response to Spirulina polysaccharides.* Int Immunopharmacol, 2013. **17**(4): p. 1009-19.
100. Lee, J.S., et al., *AHR drives the development of gut ILC22 cells and postnatal lymphoid tissues via pathways dependent on and independent of Notch.* Nat Immunol, 2011. **13**(2): p. 144-51.
101. Alam, M.S., et al., *Notch signaling drives IL-22 secretion in CD4+ T cells by stimulating the aryl hydrocarbon receptor.* Proc Natl Acad Sci U S A, 2010. **107**(13): p. 5943-8.
102. Liu, Z., et al., *Aryl hydrocarbon receptor activation maintained the intestinal epithelial barrier function through Notch1 dependent signaling pathway.* Int J Mol Med, 2018. **41**(3): p. 1560-1572.
103. Kotenko, S.V., et al., *Identification of the functional interleukin-22 (IL-22) receptor complex: the IL-10R2 chain (IL-10Rbeta) is a common chain of both the IL-10 and IL-22 (IL-10-related T cell-derived inducible factor, IL-TIF) receptor complexes.* J Biol Chem, 2001. **276**(4): p. 2725-32.
104. He, M. and P. Liang, *IL-24 transgenic mice: in vivo evidence of overlapping functions for IL-20, IL-22, and IL-24 in the epidermis.* J Immunol, 2010. **184**(4): p. 1793-8.
105. Lejeune, D., et al., *Interleukin-22 (IL-22) activates the JAK/STAT, ERK, JNK, and p38 MAP kinase pathways in a rat hepatoma cell line. Pathways that are shared with and distinct from IL-10.* J Biol Chem, 2002. **277**(37): p. 33676-82.
106. Pickert, G., et al., *STAT3 links IL-22 signaling in intestinal epithelial cells to mucosal wound healing.* J Exp Med, 2009. **206**(7): p. 1465-72.
107. Weber, G.F., et al., *IL-22-mediated tumor growth reduction correlates with inhibition of ERK1/2 and AKT phosphorylation and induction of cell cycle arrest in the G2-M phase.* J Immunol, 2006. **177**(11): p. 8266-72.
108. Mitra, A., S.K. Raychaudhuri, and S.P. Raychaudhuri, *IL-22 induced cell proliferation is regulated by PI3K/Akt/mTOR signaling cascade.* Cytokine, 2012. **60**(1): p. 38-42.

109. Wolk, K., et al., *The Th17 cytokine IL-22 induces IL-20 production in keratinocytes: a novel immunological cascade with potential relevance in psoriasis.* Eur J Immunol, 2009. **39**(12): p. 3570-81.
110. Lerman, G., et al., *The crosstalk between IL-22 signaling and miR-197 in human keratinocytes.* PLoS One, 2014. **9**(9): p. e107467.
111. Kotenko, S.V., et al., *Identification, cloning, and characterization of a novel soluble receptor that binds IL-22 and neutralizes its activity.* J Immunol, 2001. **166**(12): p. 7096-103.
112. Dumoutier, L., et al., *Cloning and characterization of IL-22 binding protein, a natural antagonist of IL-10-related T cell-derived inducible factor/IL-22.* J Immunol, 2001. **166**(12): p. 7090-5.
113. Weiss, B., et al., *Cloning of murine IL-22 receptor alpha 2 and comparison with its human counterpart.* Genes Immun, 2004. **5**(5): p. 330-6.
114. Martin, J.C., et al., *Interleukin-22 binding protein (IL-22BP) is constitutively expressed by a subset of conventional dendritic cells and is strongly induced by retinoic acid.* Mucosal Immunol, 2014. **7**(1): p. 101-13.
115. Huber, S., et al., *IL-22BP is regulated by the inflammasome and modulates tumorigenesis in the intestine.* Nature, 2012. **491**(7423): p. 259-63.
116. Sabat, R., W. Ouyang, and K. Wolk, *Therapeutic opportunities of the IL-22-IL-22R1 system.* Nat Rev Drug Discov, 2014. **13**(1): p. 21-38.
117. Wolk, K., et al., *IL-22 regulates the expression of genes responsible for antimicrobial defense, cellular differentiation, and mobility in keratinocytes: a potential role in psoriasis.* Eur J Immunol, 2006. **36**(5): p. 1309-23.
118. Sugimoto, K., et al., *IL-22 ameliorates intestinal inflammation in a mouse model of ulcerative colitis.* J Clin Invest, 2008. **118**(2): p. 534-44.
119. Eyerich, S., et al., *IL-22 and TNF-alpha represent a key cytokine combination for epidermal integrity during infection with Candida albicans.* Eur J Immunol, 2011. **41**(7): p. 1894-901.
120. Hill, T., et al., *The involvement of interleukin-22 in the expression of pancreatic beta cell regenerative Reg genes.* Cell Regen (Lond), 2013. **2**(1): p. 2.
121. Feng, D., et al., *Interleukin-22 promotes proliferation of liver stem/progenitor cells in mice and patients with chronic hepatitis B virus infection.* Gastroenterology, 2012. **143**(1): p. 188-98 e7.
122. Xu, M.J., et al., *IL-22 ameliorates renal ischemia-reperfusion injury by targeting proximal tubule epithelium.* J Am Soc Nephrol, 2014. **25**(5): p. 967-77.
123. Radaeva, S., et al., *Interleukin 22 (IL-22) plays a protective role in T cell-mediated murine hepatitis: IL-22 is a survival factor for hepatocytes via STAT3 activation.* Hepatology, 2004. **39**(5): p. 1332-42.
124. Liang, S.C., et al., *IL-22 induces an acute-phase response.* J Immunol, 2010. **185**(9): p. 5531-8.
125. Bachmann, M., et al., *IFNalpha converts IL-22 into a cytokine efficiently activating STAT1 and its downstream targets.* Biochem Pharmacol, 2013. **85**(3): p. 396-403.
126. Wolk, K., et al., *IL-22 and IL-20 are key mediators of the epidermal alterations in psoriasis while IL-17 and IFN-gamma are not.* J Mol Med (Berl), 2009. **87**(5): p. 523-36.
127. Aujla, S.J., et al., *IL-22 mediates mucosal host defense against Gram-negative bacterial pneumonia.* Nat Med, 2008. **14**(3): p. 275-81.

128. Sestito, R., et al., *STAT3-dependent effects of IL-22 in human keratinocytes are counterregulated by sirtuin 1 through a direct inhibition of STAT3 acetylation.* FASEB J, 2011. **25**(3): p. 916-27.
129. Brand, S., et al., *IL-22-mediated liver cell regeneration is abrogated by SOCS-1/3 overexpression in vitro.* Am J Physiol Gastrointest Liver Physiol, 2007. **292**(4): p. G1019-28.
130. Xu, A.T., et al., *High Suppressor of Cytokine Signaling-3 Expression Impairs STAT3-dependent Protective Effects of Interleukin-22 in Ulcerative Colitis in Remission.* Inflamm Bowel Dis, 2014.
131. Weathington, N.M., et al., *Glycogen synthase kinase-3beta stabilizes the interleukin (IL)-22 receptor from proteasomal degradation in murine lung epithelia.* J Biol Chem, 2014. **289**(25): p. 17610-9.
132. Marschner, J.A., et al., *Optimizing Mouse Surgery with Online Rectal Temperature Monitoring and Preoperative Heat Supply. Effects on Post-Ischemic Acute Kidney Injury.* PLoS One, 2016. **11**(2): p. e0149489.
133. Vielhauer, V., et al., *Obstructive nephropathy in the mouse: progressive fibrosis correlates with tubulointerstitial chemokine expression and accumulation of CC chemokine receptor 2- and 5-positive leukocytes.* J Am Soc Nephrol, 2001. **12**(6): p. 1173-87.
134. Tato, M., et al., *Cathepsin S inhibition combines control of systemic and peripheral pathomechanisms of autoimmune tissue injury.* Sci Rep, 2017. **7**(1): p. 2775.
135. Darisipudi, M.N., et al., *Dual blockade of the homeostatic chemokine CXCL12 and the proinflammatory chemokine CCL2 has additive protective effects on diabetic kidney disease.* Am J Pathol, 2011. **179**(1): p. 116-24.
136. Mulay, S.R., et al., *Podocyte loss involves MDM2-driven mitotic catastrophe.* J Pathol, 2013. **230**(3): p. 322-35.
137. Cohen, C.D. and M. Kretzler, *[Gene expression analyses of kidney biopsies: the European renal cDNA bank--Kroner-Fresenius biopsy bank].* Pathologe, 2009. **30**(2): p. 101-4.
138. Cohen, C.D., et al., *Quantitative gene expression analysis in renal biopsies: a novel protocol for a high-throughput multicenter application.* Kidney Int, 2002. **61**(1): p. 133-40.
139. Hochberg, Y. and Y. Benjamini, *More powerful procedures for multiple significance testing.* Stat Med, 1990. **9**(7): p. 811-8.
140. Wang, S., et al., *Interleukin-22 ameliorated renal injury and fibrosis in diabetic nephropathy through inhibition of NLRP3 inflammasome activation.* Cell Death Dis, 2017. **8**(7): p. e2937.
141. Chow, B.S. and T.J. Allen, *Mouse Models for Studying Diabetic Nephropathy.* Curr Protoc Mouse Biol, 2015. **5**(2): p. 85-94.
142. Peters, V. and C.P. Schmitt, *Murine models of diabetic nephropathy.* Exp Clin Endocrinol Diabetes, 2012. **120**(4): p. 191-3.
143. Pesic, M. and F.R. Greten, *Inflammation and cancer: tissue regeneration gone awry.* Curr Opin Cell Biol, 2016. **43**: p. 55-61.
144. Yuan, X., et al., *Notch signaling: an emerging therapeutic target for cancer treatment.* Cancer Lett, 2015. **369**(1): p. 20-7.
145. Rizzo, P., et al., *Rational targeting of Notch signaling in cancer.* Oncogene, 2008. **27**(38): p. 5124-31.

146. Zhong, Z., et al., *Relationship between DLK1 gene promoter region DNA methylation and non-small cell lung cancer biological behavior.* Oncol Lett, 2017. **13**(6): p. 4123-4126.
147. Nueda, M.L., et al., *Different expression levels of DLK1 inversely modulate the oncogenic potential of human MDA-MB-231 breast cancer cells through inhibition of NOTCH1 signaling.* FASEB J, 2017. **31**(8): p. 3484-3496.
148. Nueda, M.L., et al., *The proteins DLK1 and DLK2 modulate NOTCH1-dependent proliferation and oncogenic potential of human SK-MEL-2 melanoma cells.* Biochim Biophys Acta, 2014. **1843**(11): p. 2674-84.
149. Dougherty, E.J. and R.S. Pollenz, *Analysis of Ah receptor-ARNT and Ah receptor-ARNT2 complexes in vitro and in cell culture.* Toxicol Sci, 2008. **103**(1): p. 191-206.
150. Seok, J., et al., *Genomic responses in mouse models poorly mimic human inflammatory diseases.* Proc Natl Acad Sci U S A, 2013. **110**(9): p. 3507-12.
151. Takao, K. and T. Miyakawa, *Genomic responses in mouse models greatly mimic human inflammatory diseases.* Proc Natl Acad Sci U S A, 2015. **112**(4): p. 1167-72.
152. Pardoll, D.M., *The blockade of immune checkpoints in cancer immunotherapy.* Nat Rev Cancer, 2012. **12**(4): p. 252-64.
153. Shay, T., J.A. Lederer, and C. Benoist, *Genomic responses to inflammation in mouse models mimic humans: we concur, apples to oranges comparisons won't do.* Proc Natl Acad Sci U S A, 2015. **112**(4): p. E346.
154. Berthier, C.C., et al., *Cross-species transcriptional network analysis defines shared inflammatory responses in murine and human lupus nephritis.* J Immunol, 2012. **189**(2): p. 988-1001.
155. Hodgin, J.B., et al., *Identification of cross-species shared transcriptional networks of diabetic nephropathy in human and mouse glomeruli.* Diabetes, 2013. **62**(1): p. 299-308.
156. Lazzeri, E., et al., *Endocycle-related tubular cell hypertrophy and progenitor proliferation recover renal function after acute kidney injury.* Nat Commun, 2018. **9**(1): p. 1344.
157. Humphreys, B.D., et al., *Repair of injured proximal tubule does not involve specialized progenitors.* Proc Natl Acad Sci U S A, 2011. **108**(22): p. 9226-31.
158. Andoh, A., et al., *Interleukin-22, a member of the IL-10 subfamily, induces inflammatory responses in colonic subepithelial myofibroblasts.* Gastroenterology, 2005. **129**(3): p. 969-84.
159. Hosokawa, Y., et al., *IL-22 enhances CCL20 production in IL-1beta-stimulated human gingival fibroblasts.* Inflammation, 2014. **37**(6): p. 2062-6.
160. Ikeuchi, H., et al., *Expression of interleukin-22 in rheumatoid arthritis: potential role as a proinflammatory cytokine.* Arthritis Rheum, 2005. **52**(4): p. 1037-46.
161. McGee, H.M., et al., *IL-22 promotes fibroblast-mediated wound repair in the skin.* J Invest Dermatol, 2013. **133**(5): p. 1321-9.
162. Kong, X., et al., *Interleukin-22 induces hepatic stellate cell senescence and restricts liver fibrosis in mice.* Hepatology, 2012. **56**(3): p. 1150-9.
163. Harambat, J., et al., *Genotype-phenotype correlation in primary hyperoxaluria type 1: the p.Gly170Arg AGXT mutation is associated with a better outcome.* Kidney Int, 2010. **77**(5): p. 443-9.
164. Usami, M., et al., *Genetic differences in C57BL/6 mouse substrains affect kidney crystal deposition.* Urolithiasis, 2018.

165. Puri, T.S., et al., *Chronic kidney disease induced in mice by reversible unilateral ureteral obstruction is dependent on genetic background.* Am J Physiol Renal Physiol, 2010. **298**(4): p. F1024-32.

8 Acknowledgement

I'd like to thank my thesis supervisor and great expert on IL-22 biology, Prof. Dr. Carsten Schmidt-Weber, my co-supervisor and long-term mentor Prof. Dr. Hans-Joachim Anders as well as my thesis committee member and valuable scientific advisor Prof. Dr. Dirk Busch.

I'd like to thank the PhD program staff at the TUM Medical Graduate Center, namely its managing director Dr. Katrin Offe, its co-coordinators Desislava Zlatanova, Dr. Nicole Abbrederis and Bettina Kratzer for their kind support and seemingly endless patience.

I'd like to thank all teachers of the PhD program, for their enthusiasm and the open door to their labs for the bench courses as well as all my fellow PhD students for the nice, warm and collegial atmosphere.

I also wish to express my gratitude to our external collaboration partners, namely PD Dr. Sebastian Kobold for the provision of IL-22 knock-out mice, as well as PD Dr. Clemens Cohen and PD Dr. Maja Lindenmeyer for the provision of data from the ERCB.

I'd like to give special thanks to all members of my lab, for the helping hands, for great discussions during journal clubs and progress reports and for a nice sense of community also on bad days. I'd like to especially acknowledge the skilled help of Dr. Takamasa Iwakura, who performed the ECIS experiments, and of Janina Mandelbaum and Dan Draganovici, who performed the histological stainings.

This work would not have been possible without the continued support of all my friends and especially my family. Thank you guys for always being there for me!

My most personal „Thank you" goes out to my beloved wife Ghena, for every day, and for the greatest gift of life: love.